2018

Discovering Novel Hearing Loss Genes: Roles For Esrp1 And Gas2 In Inner Ear Development And Auditory Function

Alex Martin Rohacek
University of Pennsylvania, alexmroh@gmail.com

Discovering Novel Hearing Loss Genes: Roles For Esrp1 And Gas2 In Inner Ear Development And Auditory Function

Abstract
Hearing loss is the most common form of congenital birth defect, affecting an estimated 35 million children worldwide. To date, nearly 100 genes have been identified which contribute to a deafness phenotype in humans, however, many cases remain in which a causative mutation has yet to be found. In addition, the exact mechanism by which hearing loss occurs in the presence of many of these mutations is still not understood. This is due, in part, to the complex nature of the development and function of the cochlear duct, the organ of hearing. The cochlea undergoes an intricate morphogenetic development and requires the proper specification and maintenance of dozens of different cell types in order to function correctly. In the mature duct, an interplay between mechanotransducing sensory hair cells, supporting pillar and Dieters' cells, and generation of electrochemical potential by the stria vascularis are necessary to respond to sound stimuli. We utilized exome and RNA-sequencing experiments combined with mouse genetics in order to discover novel genes that play roles in cochlear development and function. Exome sequencing of families with profound hearing loss uncovered mutations in Epithelial Splicing Regulatory Protein 1 (ESRP1), a critical regulator of alternative mRNA splicing. Analysis of Esrp1 mutant mice revealed a shortened cochlear duct, delay in hair cell differentiation and maturation, and loss of the stria vascularis due to inappropriate Fgf ligand usage, stemming from an alternatively spliced receptor, in these cells. To identify additional regulators of inner ear development we performed an RNA-seq experiment comparing the gene expression profiles of control and Smoecko otic vesicles, which lack a cochlear duct. This generated a dataset of hundreds of cochlear enriched transcripts including Growth Arrest Specific 2 (Gas2) a cytoskeletal binding protein with the potential to act as a regulator of cochlear development. We generated a Gas2 null mouse line and discovered that these animals have severe hearing impairment likely due to defects in microtubule organization in the

pillar cells. Taken together, these studies implicate Esrp1 and Gas2 as novel hearing loss genes that regulate aspects of cochlear development and function.

Degree Type
Dissertation

Degree Name
Doctor of Philosophy (PhD)

Graduate Group
Cell & Molecular Biology

First Advisor
Douglas J. Epstein

Keywords
Alternative Splicing, Cytoskeleton, FGF Signaling, Hearing loss, Inner Ear

Subject Categories
Cell Biology | Developmental Biology | Molecular Biology

DISCOVERING NOVEL HEARING LOSS GENES: ROLES FOR *ESRP1* AND *GAS2* IN INNER EAR DEVELOPMENT AND AUDITORY FUNCTION

Alex M. Rohacek

A DISSERTATION

in

Cell and Molecular Biology

Presented to the Faculties of the University of Pennsylvania

in

Partial Fulfillment of the Requirements for the

Degree of Doctor of Philosophy

2018

Supervisor of Dissertation

_____

Douglas J. Epstein, Ph.D., Professor of Genetics

Graduate Group Chairperson

_____

Daniel S. Kessler, Ph.D., Associate Professor of Cell and Developmental Biology

Dissertation Committee

Stewart A Anderson, M.D., Professor of Psychiatry

Russ P. Carstens, M.D., Associate Professor of Medicine

Christopher J. Lengner, Ph.D., Associate Professor of Cell and Developmental Biology

Stephen A. Liebhaber, M.D., Professor of Genetics

DISCOVERING NOVEL HEARING LOSS GENES: ROLES FOR *ESRP1* AND *GAS2* IN INNER EAR DEVELOPMENT AND AUDITORY FUNCTION

Dedication page

This work is dedicated to my family: my Mother, who is my most vocal supporter and my greatest source of advice; my Father, who always pushes me to do the things I think are impossible; my Sister, who is always my friend and ally; and our pets (both here and who have gone), who were always there to bring me a smile. I couldn't have done it without all of you.

ACKNOWLEDGMENT

This work would not have been possible without the help from many people who I'd like to take the time to thank. My advisor, Doug Epstein, for seeing me through my graduate work with the equal measures of pressure and guidance that I needed. My undergraduate advisors Bryant Buchannan and Sharon Wise who encouraged me to apply to graduate school and gave me my start in science. My lab mates who provided me with advice and friendship over the years. And, all of my collaborators who helped my along the way with experiments and contributed to this body of work.

ABSTRACT

DISCOVERING NOVEL HEARING LOSS GENES: ROLES FOR *ESRP1* AND *GAS2* IN INNER EAR DEVELOPMENT AND AUDITORY FUNCTION

Alex M Rohacek

Douglas J Epstein

Hearing loss is the most common form of congenital birth defect, affecting an estimated 35 million children worldwide. To date, nearly 100 genes have been identified which contribute to a deafness phenotype in humans, however, many cases remain in which a causative mutation has yet to be found. In addition, the exact mechanism by which hearing loss occurs in the presence of many of these mutations is still not understood. This is due, in part, to the complex nature of the development and function of the cochlear duct, the organ of hearing. The cochlea undergoes an intricate morphogenetic development and requires the proper specification and maintenance of dozens of different cell types in order to function correctly. In the mature duct, an interplay between mechanotransducing sensory hair cells, supporting pillar and Dieters' cells, and generation of electrochemical potential by the stria vascularis are necessary to respond to sound stimuli. We utilized exome and RNA-sequencing experiments combined with mouse genetics in order to discover novel genes that play roles in cochlear development and function. Exome sequencing of families with profound hearing loss uncovered mutations in *Epithelial Splicing Regulatory Protein 1* (*ESRP1*), a critical regulator of alternative mRNA splicing. Analysis of *Esrp1* mutant mice revealed a shortened cochlear duct, delay in hair cell differentiation and maturation, and loss of the stria vascularis due to inappropriate Fgf ligand usage, stemming from an alternatively spliced receptor, in these cells. To identify additional regulators of inner ear development we performed an

RNA-seq experiment comparing the gene expression profiles of control and *Smo*^{ecko} otic vesicles, which lack a cochlear duct. This generated a dataset of hundreds of cochlear enriched transcripts including *Growth Arrest Specific 2* (*Gas2*) a cytoskeletal binding protein with the potential to act as a regulator of cochlear development. We generated a *Gas2* null mouse line and discovered that these animals have severe hearing impairment likely due to defects in microtubule organization in the pillar cells. Taken together, these studies implicate *Esrp1* and *Gas2* as novel hearing loss genes that regulate aspects of cochlear development and function.

TABLE OF CONTENTS

LIST OF TABLES

LIST OF ILLUSTRATIONS

Chapter 1: Introduction

The inner ear

The inner ear is a multifunctional organ embedded in the temporal bone of the skull (Fig. 1.1A). The dorsal structures of the inner ear comprise the vestibular apparatus, a set of three semicircular canals (SCCs) and associated crista ampullaris that function in the detection of three-dimensional orientation of the head, while the utricle and saccule sense horizontal and vertical linear acceleration respectively (Fig.1.1B). The ventral structure of the inner ear is the coiled cochlear duct which functions in the sensing and translation of sound (Fig. 1.1B).

Induction and patterning of the inner ear

The intricate structures of the inner ear arise from a simple, common otic precursor and undergo a complex series of morphological changes throughout embryogenesis (Cantos et al., 2000; Kopecky et al., 2012). Inner ear development begins with the specification of a pair of ectodermally derived placodes that form on either side of the neural tube at the level of the hindbrain between rhombomeres 4 and 6 (Kopecky et al., 2012; Noramly and Grainger, 2002; Solomon and Fritz, 2002; Fig. 1.2A). Induction of otic placodes is first observed at Carnegie stage 9 (CS9; ~20 days post fertilization) in humans and embryonic day 8 (E8.0) in the mouse (Arnold and Lang, 2001; Kikuchi and Hilding, 1965; Morsli et al., 1998; Toyoda et al., 2015). Experiments in the mouse and chicken have implicated members of the fibroblast growth factor (Fgf) signaling family as the initiators of otic development. Mouse knockouts of *Fgf3* and *10* or *Fgf3* and *8* demonstrate a complete failure in otic development, a phenotype recapitulated by loss of hindbrain *Fgf3* in the chick (Alvarez et al., 2003; Ladher et al.,

2005; Urness et al., 2010; Wright and Mansour, 2003; Yang et al., 2013; Zelarayan et al., 2007). An arrest of early inner ear morphogenesis is also seen in mouse mutants for *Fgfr2*, the receptor for Fgf3 and 10 (Pirvola et al., 2000). Conversely, ectopic expression of FGF ligands 3 and 10 in transgenic mice, or with *Fgf8* and *19* soaked beads in chicken, leads to formation of additional, ectopic, otic placodes (Alvarez et al., 2003; Ladher et al., 2005). These findings reveal that FGF ligands 3, 8 and 10 (mouse) or 19 (chick) emanating from the underlying mesenchyme and neural tube are critically required for otic placode formation. Induction of an otic fate causes the ectoderm to alter its gene expression profile. The activation of a number of transcription factors such as *Eya1*, *Gata3*, and *Pax2* as well as signaling factors including *Bmp7* have been observed to be some of the earliest definitive markers of otic identity (Lawoko-Kerali et al., 2002; Oh et al., 1996; Xu et al., 1999).

After induction, the otic placodes form as epithelial sheets. These sheets then invaginate to form a cup shape and finally close at the dorsal surface to become a spherical vesicle, termed the otic vesicle, by CS13 in humans and E9.5 in mice (Arnold and Lang, 2001; Morsli et al., 1998; Toyoda et al., 2015; Fig. 1.2B). The otic vesicle is subsequently patterned across its dorsal-ventral (DV) and medial-lateral (ML) axes to create gene expression territories that will specify the adult structures of the inner ear (Fig. 1.2C-D).

A multitude of experiments in mouse and chick have implicated signals emanating from the developing hindbrain as the primary effectors of DV pattering. The dorsal neural tube expresses ligands of the Wnt family while Sonic hedgehog (Shh) emanates from the ventral neural tube and notochord. The position of these morphogens medially to the otic vesicle places them in optimal range to function as patterning

mediators. In chick embryos in which the hindbrain has been ablated after otic induction, the final inner ear structure resembles a simple vesicle with no apparent patterning, revealing the critical requirement for the hindbrain in inner ear morphogenesis (Bok et al., 2005; Fig. 1.2C-D). Mice lacking both *Wnt1* and *Wnt3a* demonstrate a lack of expression of dorsally restricted genes such as *Dlx5* and *6* and *Gbx2* (Riccomagno et al., 2005). Subsequently these mice fail to form any recognizable dorsal structures and lack a defined vestibular apparatus. A similar phenotype is observed in mouse mutants for these transcription factors with *Dlx5*, *Dlx5/6* double, and *Gbx2* mutants all displaying SCC morphogenesis defects (Acampora et al., 1999; Lin et al., 2005; Merlo et al., 2002; Robledo and Lufkin, 2006). Taken together, these results demonstrate the critical requirement of Wnt signaling in vestibular specification.

In explant experiments in chick, excision and dorsal rotation of the hindbrain abolishes the expression of dorsal otic genes while simultaneously promoting expansion of ventrally restricted genes, such as *Six1*, into dorsal territories (Bok et al., 2005). A similar phenomenon is seen in transgenic mouse (*ShhP1*) and chick embryos where Shh is ectopically expressed in the dorsal otic vesicle. In *ShhP1* embryos the inner ear is malformed, lacking most vestibular structures, and, in both these and *Shh* transfected chick embryos, ventrally restricted genes become expressed in the dorsal otic vesicle (Ohta et al., 2016; Riccomagno et al., 2002). This suggests that the ventral hindbrain specifies ventral fates, likely through Shh signaling, and that the otocyst at the vesicle stage is still largely plastic and not yet committed to its final patterning.

Shh null mice demonstrate a nearly complete failure of otic development beyond the vesicle stage with the inner ear lacking most of its defining structure or gene expression profiles (Riccomagno et al., 2002). This extreme phenotype is thought to

largely be due to the combinatorial effects of Shh loss and an expansion of the Wnt signaling domain, which is normally restricted by Shh signaling within the neural tube. More sophisticated genetic approaches have revealed further roles for Shh signaling in inner ear development. Combinatorial deletion of the Gli family transcription factors, the downstream mediators of Shh signaling, results in shortened cochlear ducts with reduced expression of ventrally restricted genes such as *Pax2* and *Otx1* and *2* (Bok et al., 2007). Conditional deletion of the obligate Shh transducer Smoothened (*Smo*) within the otic vesicle leads to a complete failure in cochlear morphogenesis and loss of expression for almost all ventrally expressed genes (Brown and Epstein, 2011). This is phenocopied in chick experiments in which hybridoma cells expressing Shh neutralizing antibodies are injected near the hindbrain (Bok et al., 2005). Of note, in both of these cases the dorsal vestibular structures are largely normal and suffer no direct consequences from the loss of Shh signaling. These studies confirm that Shh signaling is required for the specification of the ventral otic vesicle and subsequent development of the cochlear duct.

Morphogenesis of the vestibular apparatus and cochlear duct

Following its initial patterning, the inner ear undergoes a complex series of morphogenetic events to arrive at the adult structure. The vestibular apparatus develops rapidly beginning at mouse E10.5 and human CS14 with the expansion and evagination of the dorsal otic epithelium to form the vertical and horizontal canal pouches. The three SCCs are sculpted from these pouches, the anterior and posterior SCCs from the vertical pouch and the lateral SCC from the horizontal, by a process of cell movements, apoptosis and resorption (Martin and Swanson, 1993). Proliferation of the surrounding mesenchyme forces the epithelium at the center of the pouch together where the cells

intercalate to form a single layered fusion plate (Haddon and Lewis, 1991; Pirvola et al., 2004). The cells of the fusion plate then undergo apoptosis or are integrated into the lateral rim of remaining epithelium to form the final canal structure (Fekete et al., 1997; Martin and Swanson, 1993; Rakowiecki and Epstein, 2013). The resulting vestibular structure will undergo many days or weeks of refinement but is recognizably in its complete morphology by E14.5 or CS19.

The formation of the SCCs is governed by a host of intrinsic and extrinsic factors. Expression of the laminin-related protein netrin 1 (*Ntn1*) at the fusion plate instructs these cells to undergo apoptosis and be resorbed. *Ntn1* mutant mice demonstrate an excess of dorsal otic epithelium and an inability to form SCCs (Nishitani et al., 2017; Salminen et al., 2000). Wnt signaling has been implicated in canal morphogenesis through the regulation of *Dlx5* and *Ntn1* (Rakowiecki and Epstein, 2013). Inactivating canonical Wnt signaling in the ear through conditional deletion of the downstream transcriptional effecter β-catenin, after initial patterning, results in loss of *Dlx5* expression and an expansion of *Ntn1* throughout the canal epithelium. The expansion of *Ntn1* leads to a loss of the anterior and posterior SCCs due to complete resorption of the vestibular epithelium. This implicates Wnt signaling maintaining *Dlx5* as the instructive cue for cell maintenance in the presumptive horizontal and vertical SCCs. Mutants for the transmembrane protein Lrig3 show a complete resorption of the horizontal pouch and, thus, loss of the lateral SCC (Abraira et al., 2008). As *Lrig3* expression in this canal is complementary to *Ntn1*, similar to *Dlx5* in the horizontal and vertical pouches, it can be concluded that this factor is acting to maintain the cells that will give rise to the final SCC.

Extracellular signaling molecules of the bone morphogenic protein (Bmp), and Fgf families have also been shown to be critical for SCC morphogenesis. A number of Bmp ligands are expressed in the developing cristae of the SCCs including *Bmp2*, *4* and *7*. In experiments in chicken embryos, expression of exogenous *Noggin*, a potent Bmp antagonist, results in a failure of SCC formation (Chang et al., 2004a). Mice with inner ear specific deletion of *Bmp4* also present with absent vestibular organs, demonstrating that Bmps are required for canal development (Chang et al., 2008). Fgfs have also been shown to influence canal morphogenesis through signaling to the surrounding mesenchyme. Mouse knockouts for *Fgf9* display expanded vestibular pouches that fail to resorb into SCCs (Pirvola et al., 2004). This is due in large part to a defect in proliferation of the surrounding mesenchymal cells which leads to a failure to form a fusion plate. This failure to resorb phenotype is also seen in chick embryos treated with the Fgfr inhibitor SU5402, demonstrating the critical role for Fgf signaling in the canal sculpting process (Chang et al., 2004b).

The morphogenesis of the cochlear duct is more prolonged than its vestibular counterpart, completing postnatally in mouse and by gestational week 18-20 in humans. The duct arises from a ventral evagination of the otic vesicle at E10.5 or CS14. The initiation and outgrowth of the cochlea is dependent on Shh signaling emanated from the ventral hindbrain, as described previously, as well as the expression of *Eya1*, *Six1*, and *Pax2* within the otic epithelium (Brown and Epstein, 2011; Ozaki et al., 2004; Riccomagno et al., 2002; Xu et al., 1999; Zheng et al., 2003; Zou et al., 2006). *Eya1* and *Six1* function cooperatively as a transcriptional coactivator complex required for maintaining patterning and cell survival within the otic vesicle. Mouse mutants for these genes display strikingly similar phenotypes with arrest of otic development at the vesicle

stage and large-scale apoptosis of the inner ear epithelium (Ozaki et al., 2004; Xu et al., 1999; Zheng et al., 2003). *Pax2* is required for maintenance of cochlear outgrowth post-initiation as evidenced by mouse knockouts that present with dramatically shortened cochleae due to apoptosis of *Pax2* expressing cells during elongation (Burton et al., 2004). Interestingly, experiments in which compound *Eya1/Six1/Pax2* heterozygous animals were generated demonstrate that these factors function cooperatively in cochlear outgrowth with increasingly severe phenotypes seen with decreasing gene dosage (Zou et al., 2006). It remains unclear, however, if these interactions are direct or how they might interplay with other regulators of cochlear outgrowth, such as Shh signaling.

The mature cochlear duct contains one and one-half turns in the mouse and two and one-half turns in the human. Following its initial outgrowth from the otic vesicle the developing cochlea extends medially, towards the neural tube, then loops in the anterior direction and begins to coil around the central spiral ganglia neurons between E12.5 and E18.5 (Cantos et al., 2000; Kopecky et al., 2012). These stages of cochlear elongation are dependent on convergent extension movements of sensory cells within the epithelium and will be discussed in detail in following sections.

The structures of hearing

The internal organization of the cochlear duct is highly complex and specialized to allow for the sensation and transmission of sound information. In cross section, the duct is a hollow tube divided into three fluid filled chambers, from lateral to medial: the scala vestibuli, scala media and scala tympani, separated by epithelial membranes. The scala vestibuli and tympani contain perilymph, a fluid of low ionic concentration that

buffers the scala media. Within the scala media are the primary structures and cell types, as well as endolymph fluid, required for hearing (Fig. 1.3A).

Lining the medial wall of the scala media is the organ of Corti which contains the mechanosensory hair and underlying support cells which sit upon the basilar membrane and function in the transduction of sound (Pritchard, 1878; Fig. 1.3B). The hair cells develop from epithelial progenitors and take on neuronal properties allowing them to act as the sensors of sound. In mammals, the hair cells are organized into 4 stereotyped rows along the length of the cochlear duct. At the interior of the spiral a single row of inner hair cells (IHCs) act as the primary sound transducers while the more circumferentially located rows of outer hair cells (OHCs) function to intensify reception of low amplitude sound. A number of actin based microvilli like projections, referred to as stereocilia, coat the luminal surface of each hair cell in a chevron pattern. The stereocilia are connected to each other by specialized proteins at their tips and link to mechanically gated ion channels that open upon sound stimulation (Kachar et al., 2000; Fig. 1.5D).

Underlying and adjacent to the hair cells are a set of specialized cells, collectively called support cells, that have additional, likely indirect, roles in hearing (Fig. 1.3A-B). Sitting between the inner and first row of outer hair cells are a pair of pillar cells. The pillar cells are large, column shaped, microtubule rich, cells that form the sides of an open triangle, called the tunnel of Corti, that runs the length of the cochlea. The inner pillar cell (IPC) sits immediately adjacent to the row of IHCs and extends a “head” across the tunnel to connect to OHC row one. The outer pillar cell body lies adjacent to OHC row one, while its head underlies and supports that of the IPC and extends a process to connect with OHC row two. In the adult, the pillar cells are thought to act as structural supports for the tunnel of Corti given that the movement of the basilar membrane and

outer hair cells occurs at this point. Supporting this idea, the pillar cells are known to be rich in acetylated- and detyrosinated-tubulin, signs of highly stable microtubules, and display increased cellular stiffness when compared to neighboring hair cells (Arima et al., 1986; Slepecky et al., 1995; Szarama et al., 2012a; Tannenbaum and Slepecky, 1997; Tolomeo and Holley, 1997). Experiments in gerbil cochlear explants and mechanical modeling have shown that the pillar cells move dynamically upon sound stimulation, likely placing these cells under shear and torsion stresses that must be endured for proper functioning (Chan and Hudspeth, 2005; Karavitaki and Mountain, 2007; Nam and Fettiplace, 2010; Ni et al., 2016).

Sitting below the OHCs are three rows of Deiters' cells, morphologically complex cells that cup each OHC and send a long projection towards the luminal surface to create a barrier between the OHCs, preventing the diffusion of ions from the endolymph. Laterally to the OHCs and Deiters' cells are the Hensen's and Claudius cells. These simple, cuboidal epithelial cells function to recycle cations from the hair cells during mechanotransduction and preserve the ionic concentration of the endolymph. The entire organ of Corti sits between two acellular, gel-like, membranes, the basilar and tectorial membranes, which are comprised primarily of collagen and glycoproteins. The basilar membrane underlies the organ of Corti and bends in response to sound waves. The tectorial membrane extends from the greater epithelial ridge and lays on top of the hair cells providing the surface on which the stereocilia are deflected.

The lateral wall of the cochlear duct is comprised of Reissner's membrane, an epithelial sheet separating the scala media and vestibuli, and the stria vascularis (sv), a multilayered wall of cells responsible for generating the ionic concentrations in the endolymph (Locher et al., 2015; Patuzzi, 2011; Salt et al., 1987; Smith, 1957; Tasaki and

Spyropoulos, 1959; Fig. 1.3A,C). The stria vascularis is comprised of three layers, the outermost basal layer interacts with cells of the spiral ligament, sharing gap junctions claudin 11 (*Cldn11*) and Connexin 26 (*Cx26*), which bring potassium ions (K^+) from the Hensen's and Claudius cells back into the epithelium (Kitajiri et al., 2004; Xia et al., 1999). The central, intermediate layer, contains capillaries surrounded by specialized melanocytes and the intrastitial fluid rich in chloride, potassium, and sodium ions. Cl^- and Na^+ diffuse from the blood while K^+ is pumped in from the melanocytes through Kir4.1 channels (Hibino et al., 1997). The inner most marginal layer lines the lumen of the cochlea and contains the rectifying ion channels, Barttin (*Bsnd*), sodium-potassium co-transporter (*Atp1A1*), and sodium–potassium–chloride co-transporter (*Nkcc1*) on their basal and potassium voltage-gated channel subfamily Q member 1 (*Kcnq1*) on their luminal surface (Birkenhäger et al., 2001; Flagella et al., 1999; Neyroud et al., 1997; Xia et al., 1999; Fig. 1.3C). Atp1A1 and Nkcc1 draw K^+, Na^+ and Cl^- from the intrastitial fluid into the cells. Atp1A1 and Barttin then balance and remove Na^+ and Cl^- from the marginal cells while Kcnq1 pumps K^+ into the endolymph. This complicated orchestra of ion movements ultimately maintains the positive potential charge within the cochlear duct required for hearing (Fig. 1.3C).

Development of cochlear sensory structures

The complex sensory and nonsensory structures of the cochlear duct arise from simple epithelial progenitors in the otic vesicle. The organ of Corti arises from the medial wall of the vesicle. Early sensory progenitors can be described as early as E10.5 as a buildup of cells in the medial wall epithelium that express the transcription factor Sox2 and notch signaling components jagged (*Jag1*) and lunatic fringe (*Lfng*) (Kiernan et al., 2005, 2006; Morsli et al., 1998; Pan et al., 2010; Fig. 1.4A). Mouse knockouts for *Jag1*

display a dramatic reduction in sensory cells while loss of *Sox2* results in a complete absence of the organ of Corti (Kiernan et al., 2005, 2006). Furthermore, ectopic activation of these factors, particularly *Sox2*, has been shown to drive otic progenitors into a sensory fate (Liu et al., 2012a; Pan et al., 2013; Savoy-Burke et al., 2014). These experiments demonstrate both the necessity and requirement of these genes in sensory specification.

Following their specification and expansion, prosensory progenitors must exit the cell cycle in order to differentiate. Starting around E12.5, expression of $p27^{kip1}$ beings in the sensory cells at the apical most extent of the cochlea and progresses towards the base, finishing around E14.5 (Chen and Segil, 1999; Kanzaki et al., 2006; Lee et al., 2006; Fig. 1.4A). Timely initiation of $p27^{kip1}$ expression is required for proper patterning of the organ of Corti as mouse knockouts demonstrate an overabundance of hair and support cells, as expected for the loss of a regulator of mitosis. Interestingly, hair and support cells do arise in these mutants and do appear to exit the cell cycle, albeit much delayed from WT counterparts, suggesting that timely expression of $p27^{kip1}$ is required for generating proper cell numbers but not the ultimate differentiation of these cells. The factors governing the timing of cell cycle exit remain elusive, however, recent work has identified the RNA-binding protein Lin28b and microRNA (miRNA) *let-7* as regulators of $p27^{kip1}$ expression (Golden et al., 2015). In transgenic mice, overexpression of *Lin28b* results in a failure to express $p27^{kip1}$ in a timely manner. The opposing phenotype, a more rapid cell cycle exit, is seen when *let-7*, a target for Lin28b repression, is overexpressed. This suggests that a critical timing window of expression for *Lin28b* and *let-7* plays a key role in governing cell cycle exit in the cochlea, however, additional

factors must also be contributing as these models do not completely abrogate *p27^{kip1}* expression or sensory differentiation.

Once the sensory progenitors have exited the cell cycle they rapidly begin to express differentiation markers and become specified as hair and support cells (Fig. 1.4A). The expression of the basic helix-loop-helix (bHLH) transcription factor Atonal1 *Atoh1* (*Math1*) *is* the earliest marker of sensory differentiation and also progresses in a wave like manner along the length of the cochlear duct (Bermingham et al., 1999; Chen and Segil, 1999). Fascinatingly, this expression follows in inverse pattern to cell cycle exit, beginning in cells at the base around E14.5 and progressing apically until E16.5. Similarly to *Sox2*, *Atoh1* knockout animals lack an organ of Corti as sensory cells fails to differentiate (Bermingham et al., 1999; Pan et al., 2011). Further, overexpression of *Atoh1* is sufficient to drive presumptive support cells and cells expressing *Sox2*, such as in the greater epithelial ridge, into a hair cell fate (Kawamoto et al., 2003; Woods et al., 2004; Zheng and Gao, 2000).

How *Atoh1* expression is activated in a graded fashion in the cochlea has been a widely researched topic given its critical role in hair cell development (Fig. 1.4B). Experiments with inactivation and ectopic expression of *Sox2* have shown that it is both necessary and sufficient for *Atoh1* expression (Ahmed et al., 2012; Dabdoub et al., 2008; Kempfle et al., 2016; Kiernan et al., 2005; Neves et al., 2012; Pan et al., 2013; Puligilla and Kelley, 2016). After its initial activation, *Atoh1* becomes autoregulatory, binding its own promoter and activating its own transcription while becoming inhibitory to *Sox2* (Helms et al., 2000). This incoherent feedback loop is required to generate a proper compliment of hair cells as it has been found that continued expression of *Sox2* also negatively regulates *Atoh1*. In a number of transgenic overexpression studies, *Sox2*

must be inactivated in order for hair cells to terminally differentiate as it inactivates downstream factors, such as *Pou4F3*, and prevents *Atoh1* autoregulation (Ahmed et al., 2012; Dabdoub et al., 2008; Kempfle et al., 2016; Puligilla and Kelley, 2016). The inhibitory role of Sox2 on *Atoh1* is thought to be through the activation of Hey family transcription factors *Hey1* and *2*, which negatively regulate *Atoh1*. Mouse double knockouts for *Hey1* and *2* exhibit a premature hair cell differentiation phenotype and recent work has shown these factors bind directly to the *Atoh1* promoter element, repressing its transcriptional activity (Abdolazimi et al., 2016; Benito-Gonzalez and Doetzlhofer, 2014).

Additional experiments have also implicated extracellular signaling from Shh and insulin-like growth factor (Igf) in *Atoh1* regulation (Fig. 1.4B). Inactivation of Shh signaling after otic patterning, through deletion of *Shh* in the spiral ganglia neurons or *Smo* in the cochlear duct at E12.5, leads to premature hair cell differentiation (Bok et al., 2013; Tateya et al., 2013). A similar phenotype is observed in animals that express a truncated, repressor form, of Gli3 which present with an expanded sensory epithelium and ectopic hair cells (Driver et al., 2008). Ectopic activation of Shh signaling through the use of a constitutively active Smoothened allele (*SmoM2*) or treating explants with Shh ligand results in the reverse phenotype of delayed differentiation (Driver et al., 2008; Tateya et al., 2013). In these transgenic experiments, as well as cochlear explants treated with Shh, activation of *Hey1* and *2* was found, suggesting that Shh signaling is acting to repress *Atoh1* by maintaining expression of its antagonists (Benito-Gonzalez and Doetzlhofer, 2014; Tateya et al., 2013). In addition to Shh, inhibition of Igf signaling, through deletion of its receptor, *Igfr1*, or pharmacological inhibition, also results in delayed hair cell differentiation and *Atoh1* expression (Okano et al., 2011). In these

studies, it was discovered that *Sox2* was significantly upregulated, likely impairing *Atoh1* expression, however a direct link between the Igf signaling pathway and *Sox2* has yet to be described.

Downstream of *Atoh1*, additional transcription factors, such as *Brn3C/Pou4F1* and *Gfi1* are activated specifically in the hair cells to further their differentiation, maturation and are required for their survival (Erkman et al., 1996; Wallis et al., 2003; Xiang et al., 1997). Mature hair cells express a number of specialized proteins such as the non-muscle myosins, Myosin VI (Myo6) and Myosin VIIa (Myo7a), and tip link proteins connecting the stereocilia, protocadherin 15 and cadherin 23 (Avraham et al., 1995, 1997; Hasson et al., 1995; Kazmierczak et al., 2007; Siemens et al., 2004). The timing of hair cell maturation in humans is estimated to complete by gestational week 20, coinciding with onset of hearing function, and postnatally in mice, which begin to hear at approximately 2 weeks of age.

Support cells are specified from a subset of the Atoh1 expressing sensory cells and begin a separate developmental trajectory starting around E15.5. Future hair cells will begin to express notch signaling ligands *Jag2* and Delta 1 (*Dll1*) which activates Notch 1 and downstream targets *Hes1* and *5* in the neighboring cells (Lanford et al., 1999; Zine et al., 2000; Fig. 1.4A). Deletion of *Jag2*, *Dll1*, *Notch1*, *Hes1*, and *Hes5* lead to varying degrees, depending on the combination of factors, of hair cell overproduction at the expense of the support cells (Lanford et al., 1999; Tateya et al., 2011; Zheng et al., 2000; Zine and de Ribaupierre, 2002; Zine et al., 2000, 2001). This process of lateral inhibition, through Notch signaling, generates an alternating, “checkerboard”, pattern of presumptive hair and support cells. The Notch activated support cells then begin to express the transcription factor Prospero Homeobox 1 *(Prox1*) (Bermingham-McDonogh

et al., 2006). Interestingly, *Prox1* mutants display only mild disruption of hair cell organization and support cell development, suggesting it is not absolutely required for their development (Fritzsch et al., 2010). Evidence from viral transduction experiments in cochlear explants revealed that ectopic expression of *Prox1* led to a repression of *Atoh1* and *Gfi1* and subsequent degeneration of OHCs (Kirjavainen et al., 2008). These data support a role for *Prox1* as a repressor of hair cell fate rather than as an activator of the support cell lineage.

Differentiation of support cell progenitors into pillar and Deiters' cells has been shown to be dependent on Fgf signaling. Mouse knockouts for *Fgf8*, normally expressed in the IHC, and *Fgfr3*, expressed in the support cells, demonstrate similar phenotypes with a lack of support cell differentiation (Hayashi et al., 2007; Jacques et al., 2007a; Mueller et al., 2002). Interestingly, the *Fgfr3* knockout animals also show a fate switch of the outer pillar cell into a Deiters' cell, likely due to loss of responsiveness to additional Fgf ligands, such as Fgf10 expressed from the greater epithelial ridge, and demonstrates the strict requirement for exacting levels of Fgf signaling in support cell fate determination (Hayashi et al., 2007; Mueller et al., 2002). Further support for this is seen in mutants for Sprouty 2 (*Spry2*), an antagonist of Fgf signaling, and Fgfr3P224R, an activating mutation in *Fgfr3* that renders it responsive to additional ligands (Mansour et al., 2009, 2013; Shim et al., 2005). These mutants result in an increased response to Fgf signaling and the transformation of Deiters' cells into ectopic pillar cells. Strikingly, these phenotypes can be rescued by simply decreasing the amount of Fgf signaling through deletion of specific ligands, *Fgf8* and *Spry2* or *Fgf10* and Fgfr3P224R in combination. Pillar cells continue to develop and mature until just before hearing onset, reaching their final morphology postnatally in mouse at approximately P7-10. The

complex arrays of microtubules that provide structural support for these cells begin to form early postnatally and extend in dynamic fashion from organizing centers at the apical and basal surfaces of the cells (Henderson et al., 1994, 1995; Mogensen et al., 1997; Tucker et al., 1992, 1995). The acquisition of this microtubule network is associated with alterations in the mechanical properties of these cells, such that, their stiffness is increased over time (Szarama et al., 2012a, 2012b; Tolomeo and Holley, 1997; Zetes et al., 2012). Finally, the tunnel of Corti opens between P10 and P12, just before hearing onset, and the pillar cells achieve their final morphology (Ito et al., 1995; Kraus and Aulbach-Kraus, 1981).

Concomitant with their differentiation, hair and support cells undergo complex movements to arrive at their final positions and influence the extension of the cochlear duct. The most well studied of these movements require components of the planar cell polarity (PCP) pathway which polarizes cells and orients them against the plane of tissue extension. PCP components localize to the membrane of hair cells, Van Gogh-Like 2 (*Vangl2*) is found on the proximal side of the cell while Cadherin EGF LAG Seven-Pass G-Type Receptor 1 (*Celsr1)* and Disheveled (*Dvl*) line the distal wall, and function to orient the stereociliary bundles (Etheridge et al., 2008; Montcouquiol et al., 2003, 2006; Torban et al., 2008; Wang et al., 2005, 2006). Recent work has also implicated an interaction between G-protein coupled signaling and orientation of the kinocilium regulated by the actions of *Lgn*, *Bbs8*, *Itf29*, and *Daple* to localize the cilium, as well as PCP and other signaling components (Bhonker et al., 2016; May-Simera et al., 2015; Siletti et al., 2017). Mutants for these genes exhibit similar phenotypes with misoriented hair cells and a shortened cochlear duct that contains a buildup of hair cells at the apical turn. This buildup of hair cells has long been attributed to defects in convergent

extension, a process by which cells migrate and reconfigure their junctions within the plane of elongation to drive the outgrowth of a tissue. Prosensory cells initially form as a multilayered, pseudostratified epithelium which resolves over time into the bilayered organ of Corti. Recent work has described how prosensory cells remodel their cell junctions into rosettes that resolve along the axis of elongation and that cell adhesion proteins of the cadherin family, E-cadherin, N-cadherin and P120-Catenin, are involved in both convergent extension and PCP (Chacon-Heszele et al., 2012; Driver et al., 2017). Live cell imaging techniques have also found that hair and support cells undergo dynamic movements, extending long processes and crawling along the basement membrane, and that their apical migration is dependent on the cellular myosin motor, Myosin II (Driver et al., 2017). These results paint a complex picture of sensory development and cochlear elongation where PCP and convergent extension interact, and potentially regulate each other, to generate the adult structure.

Development of the cochlear lateral wall

Despite the critical requirement of the stria vascularis and Reissner's membrane to hearing function, much less is known about their development when compared to the organ of Corti. Proper maintenance of endocochlear potential through sv function has been shown to be critical for both the sense of hearing as well as hair cell survival, with nearly all the sv mutants described here demonstrating degeneration of the organ of Corti (Ohlemiller et al., 2016; Neyroud et al., 1997; Rickheit et al., 2008; Tasaki and Spyropoulos, 1959; Salt et al., 1987). The three layers of the sv arise from unique origins and come together to form this complex tissue (Locher et al., 2015; Smith, 1957). The marginal layer is derived from otic epithelium along the lateral cochlear duct and is marked at around E15.5 by the expression of the nuclear receptor, Estrogen-related

receptor β (*ERR-β*; *Nr3b2*) (Chen and Nathans, 2007). *Nr3b2* ear specific knockouts display defects in marginal cell differentiation and abnormal intermediate layers that fail to express critical ion channels, demonstrating that this factor is required for sv development but not its early specification. The intermediate cell layer is comprised primarily of neural crest derived melanocytes that interdigitate with the marginal cells and surround the intermingled capillaries to form an osmotic barrier (Freyer et al., 2011; Hilding and Ginzberg, 1977; Locher et al., 2015; Steel and Barkway, 1989). The exact timing of melanocyte recruitment has not been described but is known to be dependent on hepatocyte growth factor (*Hgf*) signaling through receptor tyrosine kinase, c-MET (Shibata et al., 2016). Loss of *Hgf* expression from the presumptive sv results in a failure to incorporate melanocytes into the intermediate cell layer. Mouse mutants for genes that regulate melanocyte development, such as Melanogenesis Associated Transcription Factor (*MITF*) and *Pax3*, as well as naturally occurring albino animals, also demonstrate breakdown in sv development and function from a lack of melanocytes (Tachibana, 2001; Cable et al., 1992; Steel and Barkway, 1989; Tachibana et al., 1992; Kim et al., 2014; Steel and Barkway, 1989). Finally, the basal cell layer develops from the surrounding periotic mesenchyme which condenses and takes on epithelial properties, eventually expressing gap junction proteins shared with the spiral ligament and ion transporters of the intermediate layer.

Reissner's membrane develops from a thin layer of epithelial cells on the cochlear lateral wall, immediately adjacent and lying between the organ of Corti and the sv. Mouse knockouts for *Fgf10* display a complete absence of Reissner's membrane with little effects on other regions of the cochlea, demonstrating a critical requirement for signaling from this Fgf ligand in Reissner's development (Urness et al., 2015). A similar

failure to develop Reissner's membrane is found in inner ear specific knockouts for the transcription factor *Otx2*, one of the earliest expressed genes on the cochlear lateral wall (Vendrell et al., 2015). Interestingly, ear specific *Otx2* mutants also display profound defects in cochlear duct patterning with a duplicated, mirror image, organ of Corti and an expanded sv in the domain once occupied by Reissner's membrane. Based on these data, it remains uncertain if *Otx2* is required to specify Reissner's membrane or if the loss of Reissner's in these mutants is secondary to the failure to repress the domains of the sv and sensory cells.

The sense of hearing and hearing loss

Sounds, at their core, are simply pressure waves that the ear detects and translates into electrical information that is transmitted to the brain. We measure sound by its amplitude, or loudness, in decibels (dB) and its frequency, or tone, in hertz (Hz). Humans can hear over a wide range of frequencies and intensities, from soft breathing at ~10Hz and 0dB to a loud siren at ~10kHz and 120dB. Interestingly, the hair cells at each region of the cochlear duct respond only to specific frequencies, with low frequency sound detected by cells at the apex and high frequency sound at the base, creating a tonotopic map along the length of the duct (Fig. 1.5B). The establishment of tonotopy is not entirely understood but is thought to arise from a combination of the properties of the sound waves themselves, with lower frequency sound traveling further along the cochlea, as well as increases in the length of OHC stereocilia and in the thickness and width of the basilar membrane towards the apex of the duct.

Sound waves are collected by the outer ear and vibrate the tympanic membrane, colloquially called the ear drum, which translates the sound mechanically through the three middle ear bones, the incus, malleus, and stapes (Fig. 1.5A). The vibration of the

tympanic membrane moves the stapes in and out of the oval window, a small opening at the base of the cochlear duct, and causes pressure waves to resonate through the perilymph fluid, transmitting the sound into the cochlea. As the sound waves travel through the cochlea they displace the perilymph fluid and cause the basilar membrane to oscillate into the scala media (Fig. 1.5C). The oscillation of the basement membrane causes the hair cell stereocilia to push against the tectorial membrane, deflecting them and opening mechanically gated ion channels (Kazmierczak and Müller, 2012; Fig. 1.5D). This results in an influx of K+ into the hair cell, depolarizing it and stimulating the release of neurotransmitter that signals to connecting neurons of the 8th cranial nerve.

Hearing impairment and deafness are the most common forms of sensory deficit in the developed world. Loss of hearing function can arise in a multitude of ways. Exposure to loud noise, above 120dB, direct damage and infection, normal aging and genetic perturbations can all result in hearing loss (Furness, 2015; Venkatesh et al., 2015). Congenital hearing impairment affects 1 in 500 newborns with approximately half of all cases in developed countries having a genetic etiology. Single gene mutations in over 100 different loci have been identified thus far (http://hereditaryhearingloss.org). Mutations in the majority of these genes result in nonsyndromic sensorineural hearing loss (SNHL), where abnormal inner ear function is the only diagnostic feature. These mutations affect nearly every aspect of hearing function from development of sensory cells (*EYA1*, *POU4F3*), hair cell function (*MYO6*, *MYO7A*), to maintenance of endocochlear potential (*BSND*, *GJB2*) (Atik et al., 2015; Raviv et al., 2010; Shearer et al., 1993; Weil et al., 1995). However, despite the large number of identified hearing loss genes, the cause of inherited SNHL remains uncertain in many cases (Mehta et al., 2016; Sloan-Heggen and Smith, 2016). Thus, it is critical to continue to expand our

knowledge of inner ear development to better understand the factors that contribute to hearing and how their dysfunction may impact the form and function of this structure.

Figures

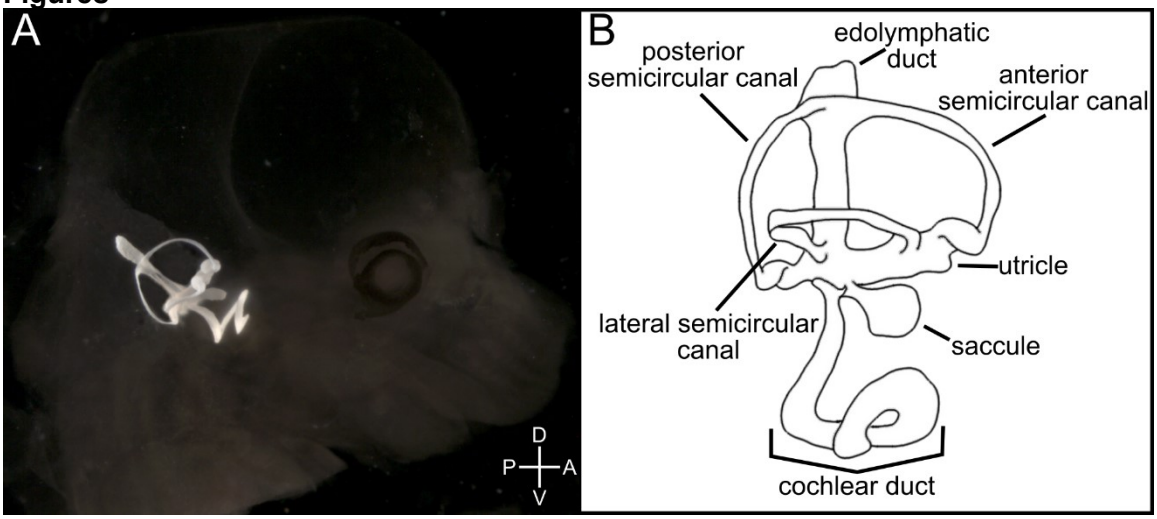

Figure 1.1. The structures of the inner ear. (A) Paint fill of an E14.5 mouse embryo displaying the anatomy and location of the inner ear within the temporal bone of the skull. (B) Diagram of an inner ear as viewed from the posterior side with the anatomical structures labeled. Abbreviations: D (dorsal), V (ventral), P (posterior), A (anterior).

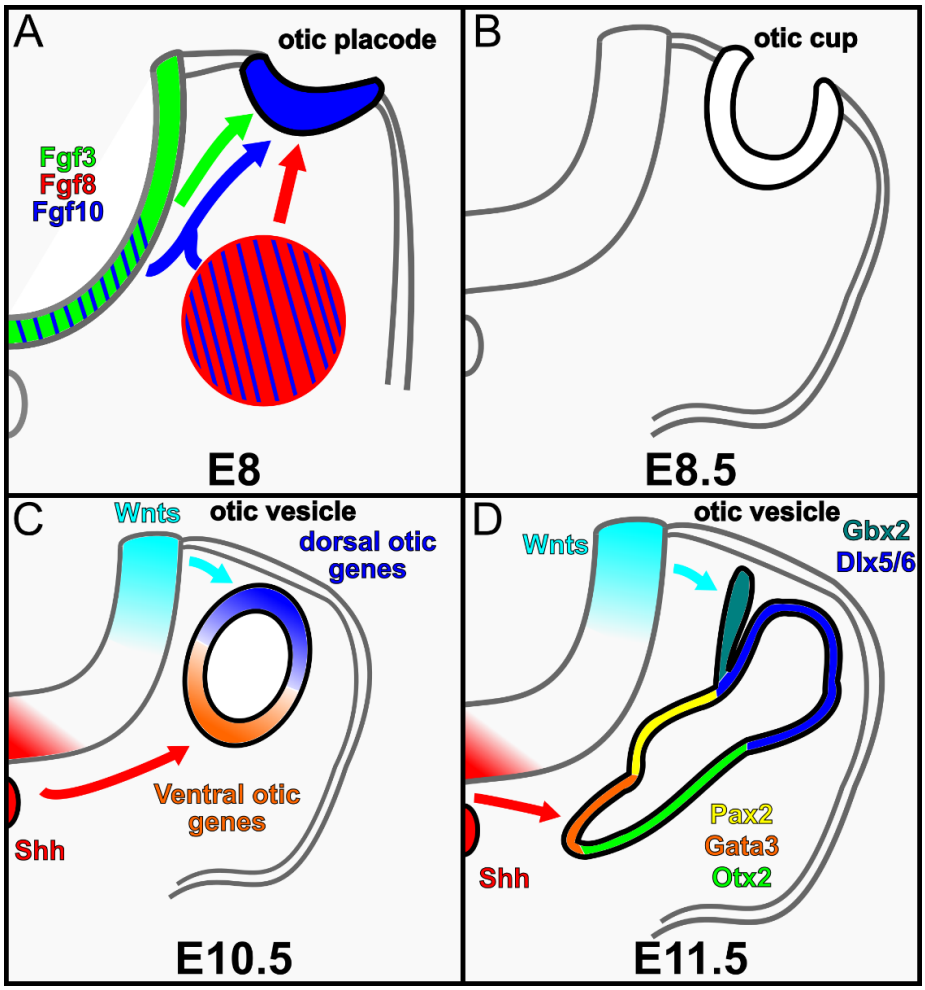

Figure 1.2. Inner ear morphogenesis and patterning. (A-D) Diagrams of mouse inner ear development as seen on transverse section through the hindbrain at indicated stages. (A) At E8.0 Fgf signals from the hindbrain and mesenchyme induce otic placode formation. (B) By E8.5 the placode invaginates to form an otic cup. (C) By E10.5, the otic cup closes at its dorsal surface and pinches off from the ectoderm to form an otic vesicle. Hindbrain Wnt and Shh signals pattern the vesicle into dorsal and ventral gene expression domains respectively. (D) Between E10.5 and E11.5 the otic vesicle begins to undergo a complex series of morphogenetic changes and alterations in gene expression that will give rise to the final, mature, inner ear structures.

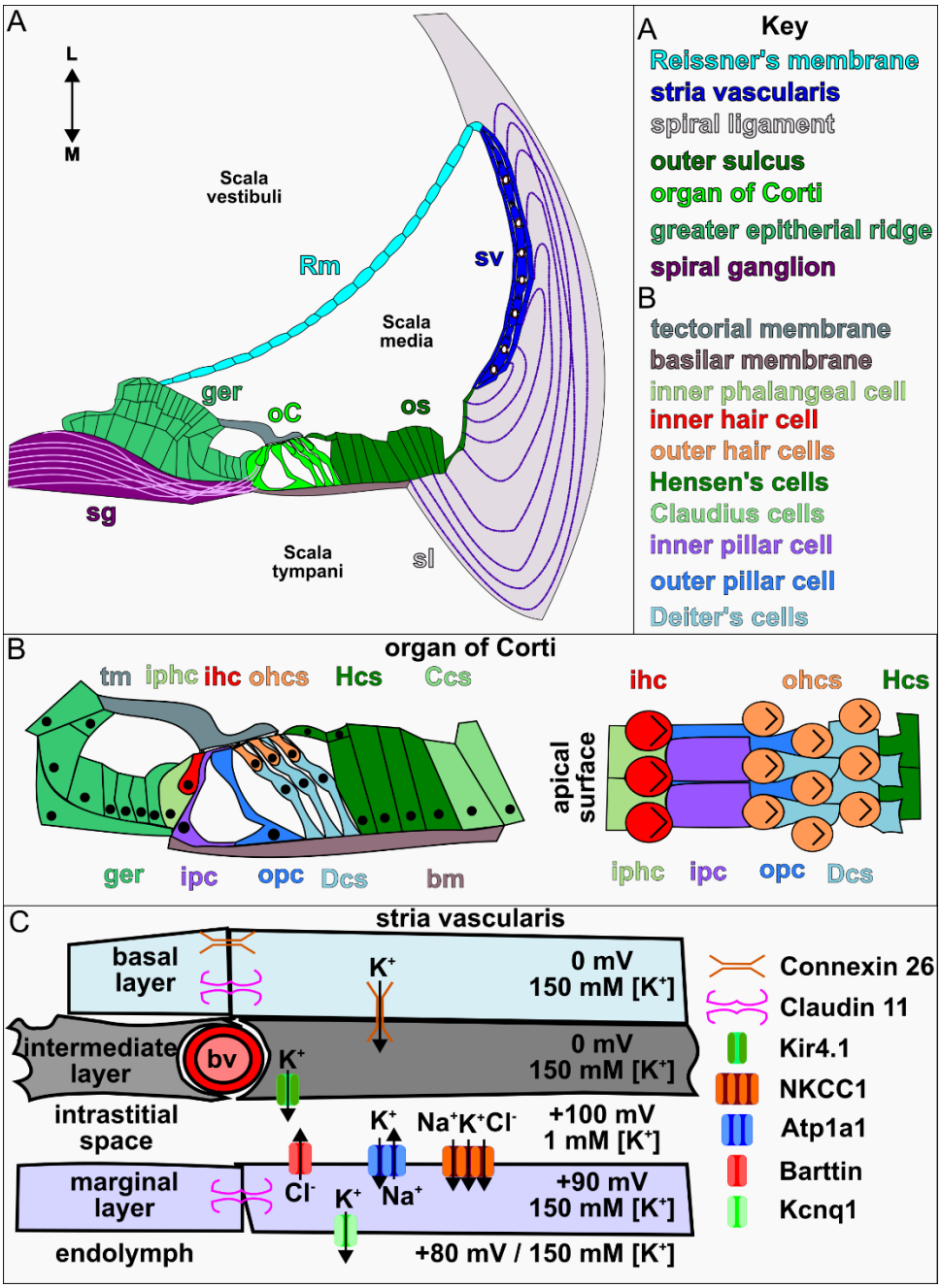

Figure 1.3. The structure and cell types of the cochlear duct. (A) Diagram of a representative transverse view of an adult cochlear duct. (B). Schematic of the organ of Corti. (C) Schematic representation of the stria vascularis. Abbreviations: L (lateral), M (medial), Bv (blood vessel) and included Key.

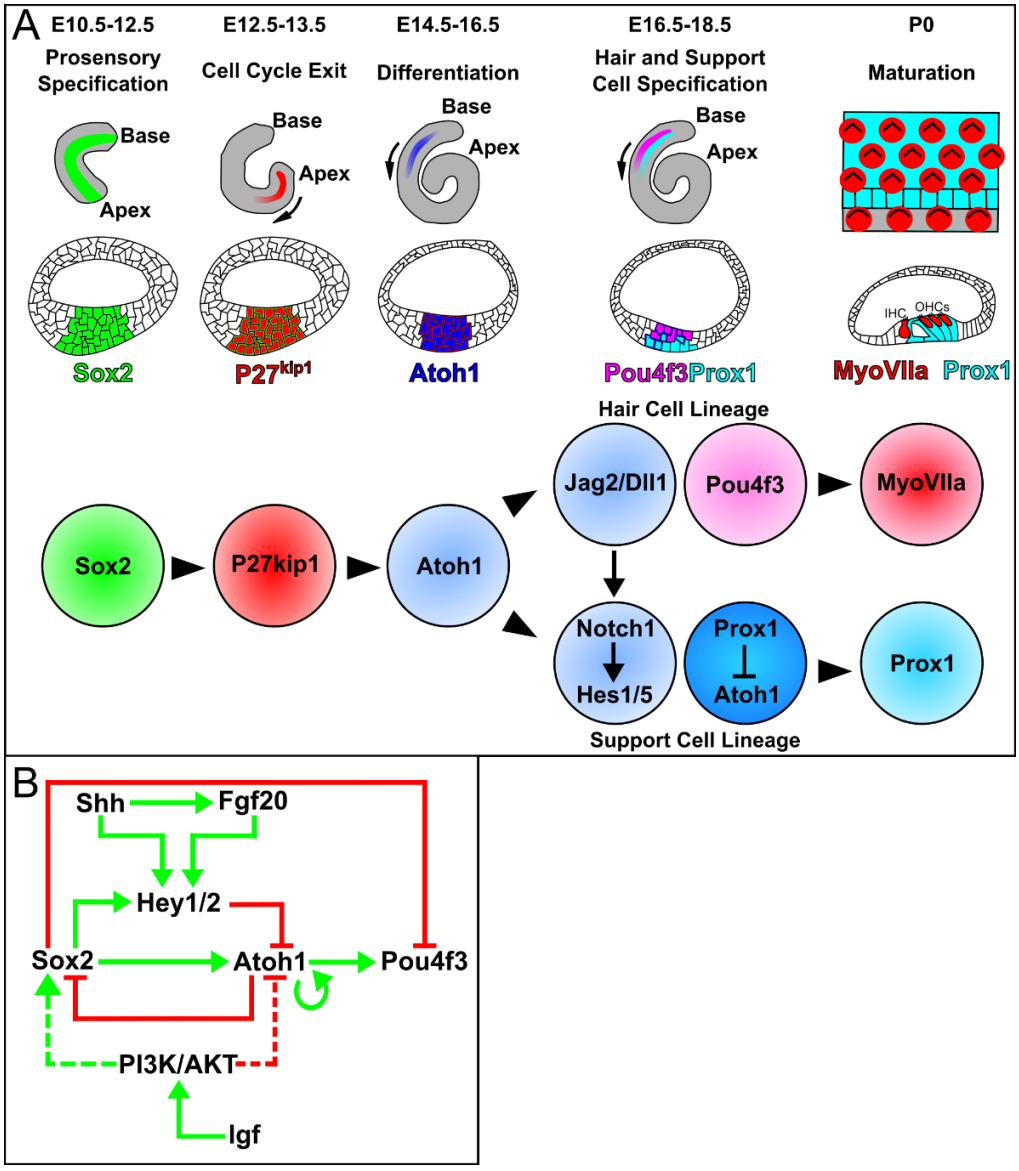

Figure 1.4. Timing and regulation of factors critical for the development of the organ of Corti. (A) Diagrams of sensory development represented on an apical view of the cochlear duct and in transverse section. Colored circles represent sensory cells at the indicated time points along with genetic interactions. (B) Schematic of the gene regulatory network controlling hair cell differentiation. Dashed lines represent potentially indirect or unclear regulation. Abbreviations: inner hair cell (ihc), outer hair cells (ohc).

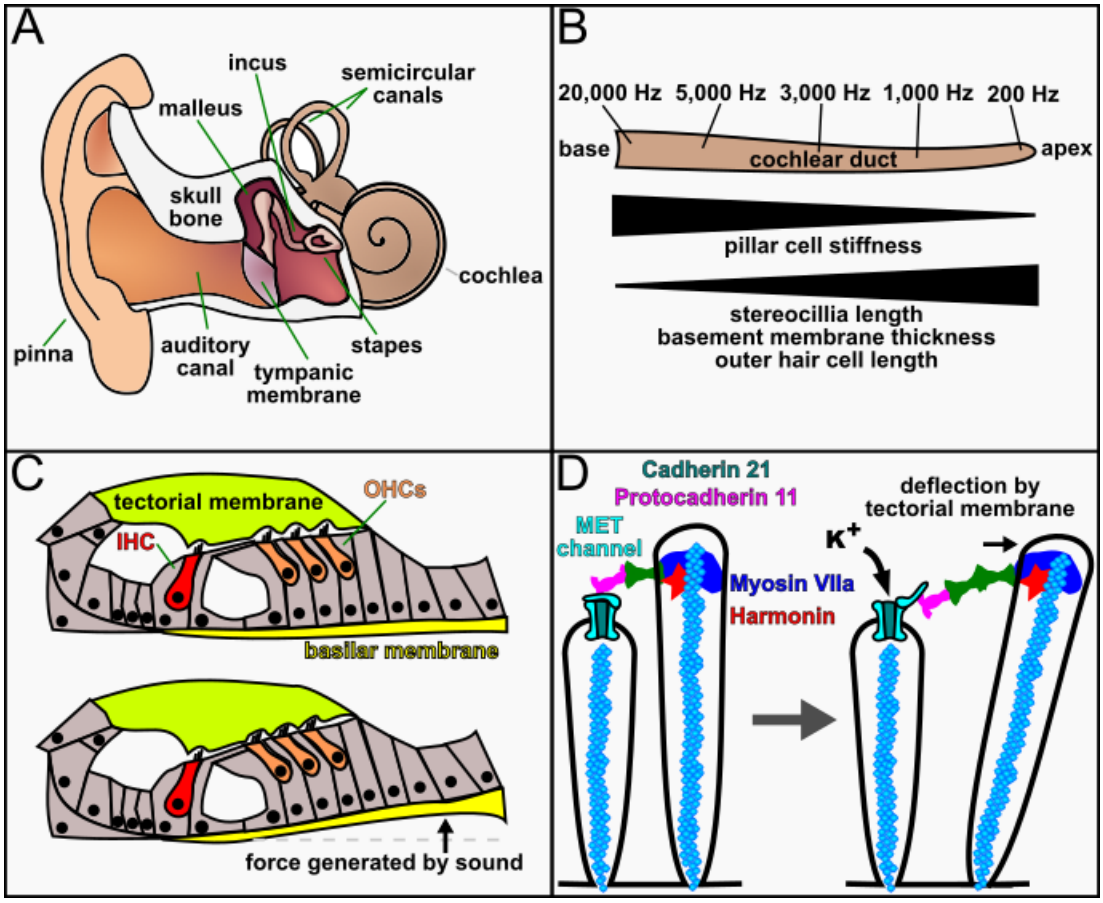

Figure 1.5. The structures and mechanisms of hearing. (A) Diagram of the human external and internal auditory system. (B) Representative schematic of the cochlear duct displaying the range and localization of human hearing response. Changes in cell morphology and physiology that correlate with sound frequency response are indicated below. (C) Transverse view of the organ of Corti at rest and during movement of the basilar membrane by sound transduction. (D) Schematic of hair cell stereocilia before and during mechanical stimulation. Tip link proteins attached to the actin cytoskeleton (blue spheres) of the taller stereocilia connect to the MET channels and force them open upon deflection. Abbreviations: Hz (hertz), IHC (inner hair cell), OHC (outer hair cell), MET (mechanoelectrical transducer).

Chapter 2: *ESRP1* mutations cause hearing loss due to defects in alternative splicing that disrupt cochlear development

Introduction

Alternative Splicing

While the genomic DNA encodes nearly all of the information required for the function of an organism it must be transcribed into a messenger RNA (mRNA) and subsequently translated into a protein in order to enact its coded function. The direct product of transcription is a pre-mRNA transcript which contains not only the protein coding information, exons, but also additional stretches of intervening base pairs, introns. To form a mature mRNA that can be translated into protein the introns must be removed via splicing and the exons joined. Alternative splicing is an additional posttranscriptional process that alters the exons which are retained between the pre- and mature mRNA. The multiple types of alternative splicing events can be roughly categorized as: cassette exons, where one or more exons are included or skipped, mutually exclusive exons, where neighboring exons are unique to separate transcripts, alternative 5' or 3' splice sites which extend the length of exons, and retained introns (Fig. 2.1B). These events allow for a single locus to encode for multiple RNAs and proteins, vastly increasing the complexity of a finite genome (Chen and Manley, 2009; Fu and Ares, 2014). Recent work has discovered that ~95% of all human multi-exon genes are alternatively spliced in a regulated manner, demonstrating that this is a nearly ubiquitous property of protein coding genes (Pan et al., 2008; Wang et al., 2008).

The process of alternative splicing revolves around the formation of the spliceosome, a large complex of small nuclear ribonucleoprotein particles (snRNPs) and

proteins that bind the pre-mRNA transcript at specific sequences and catalyze the splicing reaction (Barabino et al., 1990; Berglund et al., 1997; Bindereif and Green, 1987; Black, 2003; Matlin and Moore, 2007; Zamore and Green, 1989). The reaction begins with the binding of the U1 snRNP to the 5' splice site, splicing factor 1 (SF1) to the nucleotide which will provide the free hydroxyl group for the reaction and U2AF to the 3' splice site. SF1 is then replaced by U2 and the U4/U6–U5 tri-snRNP complex is recruited to complete the spliceosome (Fig. 2.1A). Due to the relatively small size of exons compared to introns, ~150-200bp versus thousands respectively, the binding of these factors results in creating an exon definition where the sequence between U1 and U2 is the intron to be spliced out (Wang et al., 2012). Long distance interaction between the 5' and 3' splice site brings them into close proximity and the spliceosome complex catalyzes the splicing reaction to remove the intervening sequence and join the exons.

Alternative splicing generally occurs when factors enhance or interfere with the binding of U1 or U2 to their splice sites. Specialized RNA binding proteins are thought to be the primary mediators of the inclusion or exclusion of alternatively spliced exons based on their recruitment to cis acting elements in target transcripts (Bourgeois et al., 1999; Chen and Manley, 2009; Fu and Ares, 2014). Alternative splicing regulators commonly contain at least one RNA recognition motif (RRM) that binds to specific sequences in the exons or flanking introns of target pre-mRNA transcripts. The binding of these factors can both enhance and inhibit splicing in a context dependent manner. Inhibition can occur through the binding of RRM containing proteins to the splice recognition site, hampering the spliceosome complex by steric hindrance of U1 or U2 or by direct inhibition its formation or function (Tange et al., 2001; Zhou and Lou, 2008). Enhancing splicing can be accomplished in a similar fashion, RNA binding proteins can

direct the spliceosome to specific sites or facilitate formation and function of the complex (Graveley et al., 2001; Wu and Maniatis, 1993). Additionally, binding of splice regulators can have position dependent effects where binding upstream of an exon represses its inclusion and binding downstream enhances inclusion.

Epithelial Splicing Regulatory Proteins

Epithelial Splicing Regulatory Proteins (Esrp) are a family of RNA binding proteins, containing 3 RRMs, that are conserved from humans to *C. elegans* (Fig. 2.1C). Mammals possess two highly homologous *Esrp* genes, *Esrp1* and *Esrp2*, which share 80-90% sequence similarity in their RRM domains. The *Esrps* were originally characterized in a cell-based screen for regulators of an *FGFR2* splicing event (Warzecha et al., 2009a, 2009b). *FGFR2* has two primary isoforms, driven by the inclusion of the mutually exclusive IIIB or IIIC exons, which are expressed in a cell type specific manner and confer ligand binding preferences to the extracellular domain. Expression of *ESRP1* or *2* cDNA in mesenchymal cells drove a switch from the IIIC to IIIB isoform of *FGFR2*, demonstrating the requirement for these genes in alternative splicing (Fig. 2.1D; Warzecha et al., 2009a, 2009b). Since their initial identification, additional genome wide studies in cell lines and mice have identified hundreds of Esrp dependent splicing targets (Bebee et al., 2015, 2016; Cieply et al., 2016; Dittmar et al., 2012; Fagoonee et al., 2013). Esrp1 and 2 have been found to be partially functionally redundant, with many splicing events show a dose dependent response to loss of individual alleles of each gene (Bebee et al., 2015). These proteins bind to 6-mers of GU rich sequences in their target RNAs and both promote and repress splicing of all known event types in a position dependent manner (Bebee et al., 2015; Dittmar et al., 2012). Interestingly, the Esrps have also become a model for cell type specific splicing events

as their expression is restricted to epithelial tissues throughout development and adulthood (Bebee et al., 2015; Warzecha et al., 2009a, 2009b).

Due to their restricted expression, the Esrps have been heavily studied in the context of epithelial-to-mesenchymal (EMT) transition. Cells undergoing EMT drastically alter their morphology and gene expression profiles to accommodate their new identity. Recent work has found that *Esrps* are downregulated during EMT which promotes a switch to mesenchymal isoforms of alternatively spliced transcripts. In cell lines, knockdown of *Esrp*s results in a mesenchymal like expression pattern but not a complete EMT and overexpression drives only a partial epithelial isoform splicing pattern (Göttgens et al., 2016; Warzecha and Carstens, 2012; Yang et al., 2016). Thus, it remains unclear if Esrps are drivers of EMT or an accessory pathway to assist in the transition. Esrp function has also been studied in the context of cancer given the contribution of an EMT component to tumor metastasis. *ESRP1* was found to be downregulated in colorectal cancer samples and mutations have been found in patients with colitis and inflammatory bowel disease (Deloria et al., 2016; Jeong et al., 2017; Mager et al., 2017). Several studies have also suggested that ESRP1 can act as a tumor suppressor by inhibiting EMT and metastasis in pancreatic cancer, oral squamous cell and non-small cell lung carcinomas (Hayakawa et al., 2017; Ishii et al., 2014; Shapiro et al., 2011). The level of *ESRPs* must be tightly regulated, however, as overexpression of this gene has also been reported to increase the metastatic properties of breast and colorectal cancer cell lines and correlates with poor survival of breast and gastric cancer patients (Hayakawa et al., 2017).

Esrps, and the splicing programs they regulate, are also required during development. Loss of *Esrp1* in mouse results in a fully penetrant cleft-lip and palate

phenotype and defects in kidney development that manifest as a spectrum from decreases in uretic branching and nephrons to complete kidney aplasia (Bebee et al., 2015, 2016). *Esrp2* is dispensable for development on its own, likely due to functional redundancy with *Esrp1* (Bebee et al., 2015). Double knockouts for *Esrp1* and *2* present with developmental defects in multiple organ systems in addition to the cleft-lip, palate and kidney defects seen in the single mutants (Bebee et al., 2015). These mice are severely reduced in size and weight and various epithelial organs are aplastic, including the lungs and salivary glands, and the thymus is severely reduced in size. Additionally, *Esrp1/2* knockouts display forelimb agenesis with loss of multiple digits, the humerus and radius and a skin specific deletion shows barrier defects associated with reduced epidermal thickness and developmental defects.

Rationale

Many mammalian tissues show cell type and stage specific expression of alternatively spliced transcripts that often fit into biologically coherent pathways (Bebee et al., 2015; Fu and Ares, 2014; Raj and Blencowe, 2015; Traunmüller et al., 2016; Ule et al., 2005; Vuong et al., 2016; Yang et al., 2016; Zhang et al., 2016). Consequently, mutations that disrupt either the cis or trans regulators of alternative splicing contribute significantly to human disease (Cieply and Carstens, 2015; Xiong et al., 2015), as well as hearing loss in mice (Moayedi et al., 2014; Nakano et al., 2012). While many of the key transcriptional regulators of cochlear development are known, the role that posttranscriptional events play in the formation of inner ear structures and cell types is less clear. A more comprehensive approach to the study of gene expression dynamics that integrates transcriptional and posttranscriptional mechanisms is likely to improve our fundamental understanding of inner ear biology and hearing loss.

In the current study, we performed whole exome sequencing in individuals with profound bilateral SNHL and identified biallelic pathogenic mutations in *ESRP1*. Patient derived induced pluripotent stem cells (iPSCs) showed alterations in alternative splicing, consistent with a loss of ESRP1 function. To understand how mutations in *ESRP1* might cause hearing loss we evaluated *Esrp1*$^{-/-}$ mouse embryos and uncovered defects in inner ear morphogenesis, auditory hair cell differentiation and cell fate specification along the lateral wall of the cochlear epithelium. RNA-seq analysis revealed impaired expression and splicing of genes associated with cochlear development and auditory function that explain several aspects of the inner ear phenotypes in *Esrp1*$^{-/-}$ embryos. In particular, aberrant splicing of Fgfr2 from the IIIb (epithelial) to IIIc (mesenchymal) isoforms compromised the identity of cells along the cochlear lateral wall due to improper Fgf9 ligand usage. Surprisingly, ectopic Fgf9/Fgfr2-IIIc signaling also compensated for the loss of Fgfr2-IIIB to promote cochlear duct morphogenesis in *Esrp1*$^{-/-}$ mutants. These findings implicate mutations in *ESRP1* as a novel cause of SNHL and demonstrate the complex interplay between alternative splicing, inner ear development, and auditory function.

Results

Exome sequencing reveals *ESRP1* mutations in a family with SNHL

An eight-year-old female with congenital profound bilateral SNHL, born to healthy non-consanguineous parents, was evaluated at the Division of Otolaryngology at the Children's Hospital of Philadelphia (Fig. 2.2A). A temporal bone CT scan of the proband showed no abnormalities in cochlear morphology. However, an unusual vestibular dysplasia was revealed, consisting of a rudimentary lateral semicircular canal deficient in its central bony island that took on a cystic appearance (Fig. 2.3A-D). A 14-year-old

brother was also diagnosed with severe to profound bilateral SNHL from birth, and showed the same vestibular dysplasia as his sister (Fig. 2.3E-F). Despite the abnormal vestibular findings, neither child presented with balance or movement disorders. Four other healthy siblings, including the proband's twin brother, have normal hearing (Fig. 2.2A). No other family history of hearing loss was reported.

To identify damaging mutations associated with the inner ear phenotypes in this pedigree we performed whole exome sequencing on DNA isolated from peripheral blood of the parents, proband, affected brother and unaffected siblings. Coding region and splice site variants that segregated in an autosomal recessive inheritance pattern and that occurred with a population frequency less than 3% in the 1000 Genomes Project Database and Exome Sequencing Project Exome Variant Server were selected for further analysis. No pathogenic mutations in known SNHL genes were found using this approach. However, compound heterozygous mutations were identified in a novel candidate hearing loss gene, *ESRP1,* that segregated with SNHL in this family (Fig. 2.2A and Fig. 2.3G). The two children with SNHL inherited different *ESRP1* mutations from each parent, while the unaffected siblings had either one or no mutations (Fig. 2.2A, Fig. 2.3G). The paternal *ESRP1* mutation harbors a 19 bp deletion in exon 7 (c.665_683 del) that is predicted to cause a frame shift at codon Asp222 resulting in premature termination of translation 31 amino acids downstream (p.Asp222Glyfs*32). The maternal *ESRP1* mutation contains a missense variant in exon 8 (c.775C>G) that results in the substitution of leucine for valine (p.Leu259Val) at a highly conserved residue within the principle RNA recognition motif (Fig. 2.3G,H). An additional cohort of 144 probands with bilateral SNHL was screened for mutations in *ESRP1* and *ESRP2* by Sanger sequencing. While no homozygous or compound heterozygous variants were identified

in these genes, rare heterozygous missense substitutions in *ESRP1* were found in three samples (Fig. 2.3I).

To determine the impact of *ESRP1* mutations on alternative splicing we derived three independent iPSC lines from lymphoblastoid cells obtained from the parents and affected children in the pedigree (Fig. 2.2A). We first assessed the abundance of ESRP1 and found it to be reduced by 50% at both the transcript and protein level in the father and affected children, compared to the mother (Fig. 2.2B,D). No differences in *ESRP2* expression were observed across individuals (Fig. 2.2B). The *ESRP1* mRNA encoded by the mutant paternal allele is likely subject to nonsense-mediated decay due to the presence of a premature stop codon, accounting for its reduced expression. The paternal *ESRP1* mutation is also predicted to be non-functional since it would lead to out-of-frame translation prior to the essential RRM domains (Fig. 2.2A).

We interrogated the effects of the paternal *ESRP1* (c.665_683 del) allele in iPSCs from the proband by genetically repairing the mutation with the CRISPR-Cas9 system. A guide RNA specific to the mutant paternal *ESRP1* allele was cloned into the pX330 expression vector and electroporated into iPSCs from the proband along with a single-stranded oligodeoxynucleotide (ssODN) template that was used to correct the paternal mutation by homology directed repair (Fig. 2.2C). Three independent iPSC clones were identified with the corrected *ESRP1* paternal allele as assessed by Sanger sequencing (Fig. 2.2C). ESRP1 mRNA and protein levels were significantly increased in the genetically repaired iPSCs from the proband compared to the uncorrected iPSCs, and were similar to the unaffected mother (Fig. 2.2D,E). These results confirm the damaging effect of the paternal *ESRP1* (c.665_683 del) mutation on its expression in iPSCs.

The alternative splicing patterns of several known ESRP dependent events were evaluated in patient derived iPSCs by RT-PCR. The level of exon inclusion, quantified as percent spliced in (PSI), was significantly reduced for *ENAH*, *NF2* and *RALGPS2* and increased for *ARHGEF11* in iPSCs from both affected children, compared to either parent (Fig. 2.2F-I). These alterations in alternative splicing were restored in the genetically repaired iPSCs from the proband, indicating their dependency on ESRP1. Not all ESRP dependent exons showed significant differences in splicing (e.g. *SCRIB, MACF1, GRHL1*), implying that some events are less sensitive to the loss of ESRP1 than others (data not shown). The presence of *ESRP2* in iPSCs is likely to explain the partial, and in some cases nonexistent, splicing switches in the affected children, consistent with the recent finding in mice that Esrp2 is able to compensate for the loss of Esrp1 in the splicing of some, but not all, regulated transcripts (Bebee et al., 2015). In support of this premise, we observed similar splicing switches in mouse embryonic stem cells with a targeted disruption in *Esrp1* compared to iPSCs from the affected children (Fig. 2.2J).

To investigate the nature of the maternal *ESRP1* (c.775C>G) mutation, we performed retroviral transduction of wild type and mutant cDNAs into the MDA-MB 231 breast cancer cell line that does not express endogenous ESRP1 or ESRP2. Inclusion of the epithelial ENAH exon and skipping of the OSBPL3 exon was significantly increased in the presence of wild type ESRP1 compared to the maternal missense allele (Fig. 2.2K,L). These findings further support the hypomorphic nature of the *ESRP1* (c.775C>G) mutation.

Defects in inner ear morphogenesis and auditory hair cell differentiation in *Esrp1*$^{-/-}$ mouse mutants

Our finding that human mutations in *ESRP1* segregate with congenital hearing loss prompted us to investigate the role of Esrp1 during mouse inner ear development. *Esrp1* is broadly expressed throughout the epithelium of the otic vesicle (E10.5) and is notably absent from the surrounding mesenchyme (Fig. 2.4A). *Esrp1* continues to show unrestricted expression in sensory and nonsensory epithelial progenitors during cochlear and vestibular morphogenesis, although the level is weaker at later stages of inner ear development (Fig. 2.4B-E).

We evaluated *Esrp1*$^{-/-}$ embryos for defects in inner ear morphology using the paint fill technique. Alterations in the formation of cochlear and vestibular structures were observed in *Esrp1*$^{-/-}$ embryos compared to control littermates at E14.5, including a significant shortening and widening of the cochlear duct, as well as dysgenesis of the lateral semicircular canal and common crus due to incomplete resorption of the vestibular epithelium (Fig. 2.5A-D). This vestibular defect is similar to that described in children with *ESRP1* mutations (Fig. 2.3A-F). A more severe inner ear phenotype consisting of fluid filled cysts with no vestibular or cochlear outgrowth was also observed at low penetrance in *Esrp1*$^{-/-}$ embryos (16%, 23/138) and will be discussed further below (Fig. 2.15A,B).

We next determined whether the loss of Esrp1 affects sensory development within the inner ear. The cochlear sensory epithelium was isolated from *Esrp1*$^{-/-}$ and control embryos at E18.5 and co-stained by whole mount for actin (phalloidin) to visualize stereocilliary bundles, and Myosin VIIa (Myo7a), a hair cell marker. *Esrp1*$^{-/-}$ embryos displayed a 25% decrease in total hair cell number that was primarily

accounted for by a near complete absence of hair cells at the apex of the cochlear duct (Fig. 2.5E-M and Fig. 2.6A,B,E-G). Prosensory progenitors marked by Sox2 were present in the requisite number at the apex of the cochlear duct of *Esrp1*$^{-/-}$ embryos at E18.5, indicating that the missing hair cells in this region are not explained by an absence of sensory progenitors (Fig. 2.7A-C).

Hair cells at the base and middle turn of *Esrp1*$^{-/-}$ embryos showed an immature morphology compared to control littermates as seen by the reduced complexity of stereociliary bundles (Fig. 2.4E-H). Support cells marked by Sox2 and Prox1 revealed a normal compliment of pillar and Dieter cells at the basal turn of *Esrp1*$^{-/-}$ embryos (Fig. 2.5D-I). Moreover, vestibular sensory structures (maculae and cristae) were less affected by the loss of Esrp1 with only slight alterations in size, organization and innervation at E18.5 (Fig. 2.5J,K). These data reveal an intriguing cochlear phenotype in *Esrp1*$^{-/-}$ mutants consisting of a truncated cochlear duct with immature or absent hair cells.

We evaluated *Esrp1*$^{-/-}$ embryos one day later at postnatal day 0 (P0) to determine whether the hair cell phenotype was due to an arrest or delay in sensory development (Fig. 2.5N-V and Fig. 2.6C,D). Hair cell morphology at the base and middle turns of *Esrp1*$^{-/-}$ mutants appeared more advanced at P0 than at E18.5, with a notable improvement in stereocilia bundle morphology that was comparable to control pups at this stage (Fig. 2.5N-Q). Whereas the total number of hair cells was reduced in *Esrp1*$^{-/-}$ compared to control embryos after normalizing for cochlear duct length at E18.5, this difference was no longer apparent at P0 (Fig. 2.6H). This finding may be explained by the continued differentiation of Myosin VIIa positive hair cells at the apex of the cochlear duct of *Esrp1*$^{-/-}$ mutants between E18.5 and P0 (Fig. 2.5I,J,M,R,S,V), which occurred in

the absence of further elongation of the cochlear duct (Fig. 2.6C-H). Unfortunately, *Esrp1*$^{-/-}$ mutants die soon after birth due to complications from cleft lip and palate defects, preventing their analysis at later postnatal ages (Bebee et al., 2015). These data suggest that the sensory phenotype in *Esrp1*$^{-/-}$ mutants is due, in part, to a temporal delay in auditory hair cell development.

Esrp1 regulates the timing of hair cell differentiation

To identify gene expression networks that are disrupted in *Esrp1*$^{-/-}$ mutants we performed RNA-seq from purified cochlear epithelium at E16.5. Three biological replicates from *Esrp1*$^{-/-}$ and control littermates were sequenced to a depth of 40-60 million reads and mapped to the mouse genome. Our analysis revealed 751 genes (341 upregulated, 410 downregulated) that were differentially expressed between control and *Esrp1*$^{-/-}$ mutants (fold change ≥0.4, $p<0.05$, Fig. 2.8A). Gene ontology terms associated with inner ear morphogenesis, ion transport, sensory perception of sound, and auditory receptor cell differentiation showed a significant enrichment of differentially expressed genes as revealed by the DAVID 6.8 analysis tool (Fig. 2.8B; Huang et al., 2009).

We further grouped the list of differentially expressed genes into sensory and nonsensory categories based on their published expression patterns (Fig. 2.8C). Two of the sensory genes that were downregulated in *Esrp1*$^{-/-}$ embryos, *Atoh1* and *Pou4f3,* stood out because of their essential roles in regulating hair cell differentiation and maturation (Bermingham et al., 1999; Erkman et al., 1996; Xiang et al., 1997). *Atoh1* transcription initiated properly at the base and mid-base levels of the cochlea in *Esrp1*$^{-/-}$ embryos, but was delayed by approximately 48 hours at the apex (Fig. 2.9A-F; Fig. 2.10A-X; Table S2). On the other hand, Pou4f3 expression was delayed at all levels of

the cochlear duct in *Esrp1*$^{-/-}$ embryos by approximately 24 hours (Fig. 2.9G-L; Fig. 2.10Y-AP; and Table S2). No differences were observed in the expression of Sox2 or P27^{kip1} in prosensory progenitors along the cochlear duct of *Esrp1*$^{-/-}$ and control embryos, suggesting that the delay in hair cell differentiation was not associated with alterations in the specification or cell-cycle exit of sensory progenitors at earlier stages (Fig. 2.7L-O).

A previous study implicated the Hey family of bHLH transcription factors as negative regulators of Atoh1 (Benito-Gonzalez and Doetzlhofer, 2014). We examined *Hey1* and *Hey2* in sensory progenitors by in situ hybridization and observed a consistent upregulation in *Hey2* at the mid and apex regions of the cochlear duct of *Esrp1*$^{-/-}$ embryos at E16.5, a stage when *Hey2* transcription is typically downregulated (Fig. 2.9M-R). No obvious change in *Hey1* expression was detected (Fig. 2.10AQ and data not shown). Attempts to validate these results by qRT-PCR revealed a trend for increased expression of *Hey2* that did not reach statistical significance (Fig. 2.10AQ, Table S2). The discrepancy in these results might be explained by the dynamic and graded nature of *Hey2* expression along the developing cochlear duct at this stage. *Hey2* has also been shown to be modulated by Shh signaling (Benito-Gonzalez and Doetzlhofer, 2014). However, we found no changes in *Gli1* expression between *Esrp1*$^{-/-}$ and control embryos by in situ hybridization or qRT-PCR at E14.5 or E16.5, suggesting that elevated Shh signaling is unlikely to account for the increase in *Hey2* expression in *Esrp1*$^{-/-}$ embryos (Fig. 2.10AQ, Table S2, and data not shown).

We also observed a failure to downregulate Sox2 in *Esrp1*$^{-/-}$ hair cells at P0 (Fig. 2.9S-X), which is known to be associated with delays in sensory maturation (Puligilla and Kelley, 2016). These data suggest that an imbalance in the expression of negative

regulators of sensory development (Hey2 and Sox2) may underlie the delay in hair cell differentiation in *Esrp1*$^{-/-}$ embryos (Fig. 2.9Y). Although, the possibility also exists that the upregulation of Sox2 and Hey2 is a consequence rather than a cause of the sensory delay.

Esrp1 regulates the fate of nonsensory cells along the lateral cochlear wall

Genes in the nonsensory category displayed greater fold changes in expression between *Esrp1*$^{-/-}$ and control embryos than did the sensory genes (Fig. 2.8C). The most downregulated transcripts in the cochlea of *Esrp1*$^{-/-}$ mutants encode for ion channel subunits (Bsnd, Kcnq1) and the Estrogen related receptor beta (Nr3b2/Esrrβ) transcription factor that regulates their expression (Fig. 2.8C and Table S2). Each of these genes is expressed in marginal cells of the stria vascularis and cause hearing loss when mutated in humans and mice due to altered ion homeostasis in the endolymph (Chen and Nathans, 2007; Collin et al., 2008; Lee et al., 2000; Neyroud et al., 1997; Rickheit et al., 2008; Schlingmann et al., 2004). Of note, hearing loss genes were significantly enriched in the overall set of differentially expressed transcripts between *Esrp1*$^{-/-}$ and control embryos (Fig. 2.8D). These findings prompted us to investigate the integrity of the stria vascularis in *Esrp1*$^{-/-}$ embryos.

We stained the lateral wall of the cochlear epithelium with E-cadherin and observed a pronounced expansion of cells with a flattened epithelial morphology characteristic of Reissner's membrane, and a complete absence of cuboidal shaped marginal cells in *Esrp1*$^{-/-}$ compared to control embryos at E16.5 (Fig. 2.11A,D). Consistent with this change in epithelial morphology, we observed a three-fold increase in the number of cells expressing Otx2, a marker of Reissner's membrane, and a dramatic reduction of Nr3b2 positive marginal cells in *Esrp1*$^{-/-}$ compared to control

embryos (Fig. 2.11B,C,E-G). This phenotype resulted in a two-fold net gain in the number of cells within the lateral wall of the cochlear epithelium and likely explains the widened cochlear duct in *Esrp1*$^{-/-}$ embryos.

At E18.5, the lateral cochlear epithelium of *Esrp1*$^{-/-}$ embryos was highly dysmorphic compared to controls with an expanded and partially collapsed Reissner's membrane and no morphological evidence of marginal cells (Fig. 2.11H,O). Several key proteins marking distinct cell layers of the stria vascularis, including marginal cells (Kcnq1, Barttin), intermediate cells (Atp1a1, CD44), basal cells and fibrocytes (Atp1a1, Claudin-11, Connexin-26/GJB2) were reduced or absent in *Esrp1*$^{-/-}$ embryos (Fig. 2.11I-N,P-V). Taken together, these data suggest that the identity of cells along the lateral wall of the cochlear epithelium has been altered in *Esrp1*$^{-/-}$ mutants resulting in a gain in Reissner's membrane at the expense of marginal cells.

Altered splicing of *Fgfr2* is responsible for the lateral cochlear wall defects in *Esrp1* mutants

To define and quantify the differential splicing events between *Esrp1*$^{-/-}$ and control embryos that might explain unique aspects of the cochlear phenotype we analyzed the RNA-seq dataset from E16.5 cochlear epithelium using the MAJIQ algorithm (Vaquero-Garcia et al., 2016). This analysis uncovered 518 splicing alterations in mRNA transcripts from 490 different genes with a change in percent spliced in (ΔPSI) value of at least 10% (Fig. 2.12A and Table S1). Several of the genes that are dependent on Esrp1 for proper splicing have known roles in inner ear development and in some cases cause hearing loss in humans when mutated (Fig. 2.12B,C).

A switch in the epithelial to mesenchymal splicing pattern was confirmed by semi-quantitative RT-PCR analysis for 20 of these altered transcripts, consistent with the

premise that Esrp1 regulates an epithelial specific splicing program (Fig. 2.12D,E). *Fgfr2* exhibited the most dramatic change in PSI from 78% in control embryos to 7% in *Esrp1*$^{-/-}$ mutants (ΔPSI=71, Fig. 2.12B,C,F). Instead of expressing the Fgfr2-IIIb isoform typical of control cochlear epithelial cells, Esrp1 mutants inappropriately expressed the mesenchymal Fgfr2-IIIc isoform. This aberrant splicing switch in Fgfr2 is predicted to alter its binding specificity to Fgf ligands (Zhang et al., 2006).

The formation of Reissner's membrane is dependent on Fgf10, which normally signals through Fgfr2-IIIb (Urness et al., 2015). This raises the question of how Reissner's membrane might be expanded in *Esrp1*$^{-/-}$ mutants given the near complete replacement of Fgfr2-IIIb with Fgfr2-IIIc, an isoform that does not respond to Fgf10 (Zhang et al., 2006). It is unlikely that another Fgfr is compensating for the loss of Fgfr2-IIIb, since Fgfr1 and Fgfr3 predominantly express the IIIc isoform in the cochlear epithelium of wild type and *Esrp1*$^{-/-}$ embryos (Fig. 2.12F). Instead, we propose that ectopic signaling through a different Fgf ligand with affinity for Fgfr2-IIIc is mediating the expansion of Reissner's membrane and subsequent loss of the stria vascularis in *Esrp1*$^{-/-}$ mutants. Fgf9 is an excellent candidate to be fulfilling this role given its expression in lateral cochlear wall progenitors and its ability to signal through Fgfr2-IIIc in the periotic mesenchyme (Fig. 2.13A,B,E,F; Pirvola et al., 2004; Zhang et al., 2006). In support of this model, ectopic expression of Fgf signaling effectors, *Etv4* and *Etv5*, was observed along the lateral cochlear epithelium in *Esrp1*$^{-/-}$ embryos, concomitant with the expansion of Otx2 positive Reissner's membrane (Fig. 2.13C-N).

To test the hypothesis that aberrant expression of Fgfr2-IIIc in *Esrp1*$^{-/-}$ embryos causes a gain in Fgf9 signaling within the lateral cochlear epithelium, we generated *Esrp1*$^{-/-}$*; Fgf9*$^{+/-}$ compound mutants and observed a significant retraction of Reissner's

membrane (Otx2) and recovery of marginal (Nr3b2, Kcnq1, Barttin), intermediate (Cd44) and basal (Atp1a1) cell identities at E18.5 (Fig. 2.14A-V). *Esrp1*$^{-/-}$*; Fgf9*$^{+/-}$ compound mutants also showed a reduction in the ectopic expression of *Etv4* and *Etv5* (Fig. 2.13O-T). These results support our model that ectopic Fgf9 signaling through an aberrantly spliced Fgfr2-IIIc isoform is responsible for the cell fate switch between Reissner's membrane and marginal cells in *Esrp1*$^{-/-}$ mutants (Fig. 2.14W).

Ectopic Fgf9/Fgfr2-IIIc signaling compensates for the loss of Fgfr2-IIIb to promote cochlear morphogenesis in *Esrp1*$^{-/-}$ mutants

Surprisingly, 46% (6/13) of *Esrp1*$^{-/-}$*; Fgf9*$^{+/-}$ embryos also exhibited a cystic inner ear with no obvious vestibular or cochlear outgrowth (Fig. 2.15C). This phenotype is remarkably similar to that observed in 16% of *Esrp1*$^{-/-}$ mutants, as well as mouse embryos that specifically lack the *Fgfr2-IIIb* (epithelial) isoform (Fig. 2.15A-C; Pirvola et al., 2000). An important distinction between the *Fgfr2-IIIb* deletion line (De Moerlooze et al., 2000; Pirvola et al 2000) and *Esrp1*$^{-/-}$ mutants is that *Fgfr2* expression is altogether absent in the otic epithelium of *Fgfr2-IIIb* mutants, but is present in the otic epithelium of *Esrp1*$^{-/-}$ embryos, albeit as the Fgfr2-IIIc (mesenchymal) isoform. This finding raises the intriguing possibility that Fgf9/Fgfr2-IIIc signaling is also compensating for other Fgfr2-IIIb dependent functions at earlier stages of inner ear morphogenesis. Consistent with this premise, all *Esrp1*$^{-/-}$*; Fgf9*$^{-/-}$ double mutants examined (n=3) displayed cystic inner ears (Fig. 2.15D). Given that Fgf9 is normally dispensable for cochlear duct outgrowth (Pirvola et al., 2004), we attribute the fully penetrant cystic inner ear phenotype in *Esrp1*$^{-/-}$*; Fgf9*$^{-/-}$ mutants to the loss of ectopic Fgf9/Fgfr2-IIIc signaling at early stages of inner ear development.

Discussion

We performed whole exome sequencing and identified mutations in *ESRP1* that segregate with SNHL in a human pedigree. This finding represents the first known instance of mutations in a tissue specific regulator of alternative splicing being implicated in human deafness. Our analysis of inner ear phenotypes in *Esrp1*$^{-/-}$ mouse embryos revealed possible pathogenic mechanisms for hearing loss, including defects in cochlear duct morphogenesis, auditory hair cell differentiation and marginal cell fate specification. However, the phenotypes observed in *Esrp1*$^{-/-}$ mouse embryos may not all occur with the same severity in affected children from the pedigree given that one of their mutant *ESRP1* alleles (p.Leu259Val) is hypomorphic, as indicated by its reduced, but not absent, alternative splicing activity in patient derived iPSCs and other cell based assays. This residual ESRP1 function may have protected the affected children from cleft-lip and palate, which occurs in all *Esrp1*$^{-/-}$ newborn pups (Bebee et al., 2015). We therefore recommend that cases of congenital SNHL that are co-morbid with cleft-lip and palate be screened for mutations in *ESRP1*.

The most pronounced changes in gene expression within the cochlear duct of *Esrp1*$^{-/-}$ and control embryos were detected in nonsensory cells of the lateral cochlear epithelium. The expanded expression of Otx2 within Reissner's membrane, and the absence of Nr3b2 expression in marginal cells of the stria vascularis suggested that the identity of these cells had been severely compromised in *Esrp1*$^{-/-}$ embryos. This represents a unique phenotype in the inner ear as no other mutation has been described that completely abrogates formation of the stria vascularis. Nr3b2 is required for the expression of many ion channels and transporters that generate the high concentration of potassium ions in the endolymph, which is critical for hair cell mechanotransduction

(Chen and Nathans, 2007). Several of these Nr3b2 dependent genes cause hearing loss when mutated and are downregulated in *Esrp1*$^{-/-}$ embryos. Thus, the reduced expression of Nr3b2, or any one of its essential transcriptional targets, is expected to cause severe hearing impairment in humans with mutations in *ESRP1*.

Alterations in marginal cell identity may also explain some of the non-cell autonomous phenotypes observed in *Esrp1* mutants. Release of the Hepatocyte growth factor (Hgf) signal from marginal cells to its c-Met receptor on neural crest cell derived melanocytes is required for their recruitment to the intermediate cell layer of the stria vascularis (Shibata et al., 2016). Consequently, the loss of *Hgf* expression in *Esrp1*$^{-/-}$ embryos is likely responsible for the reduced number of intermediate cells.

Marginal cells are more severely affected in *Esrp1*$^{-/-}$ compared to *Nr3b2*$^{-/-}$ mutants, suggesting that other important determinants of their identity must also be misregulated in *Esrp1*$^{-/-}$ mutants. The expansion of Otx2 into the presumptive marginal cell territory in *Esrp1*$^{-/-}$ embryos represents the best explanation for why these cells failed to form. In wild type embryos, Otx2 is initially broadly expressed along the lateral wall of the cochlear duct at E13.5, including precursors of marginal cells and Reissner's membrane. Otx2 expression is then downregulated from the marginal cell territory by E15.5, coincident with the onset of Nr3b2, but continues to be expressed in Reissner's membrane. We propose that Otx2 regulates the timing of marginal cell development through a de-repression mechanism, whereby *Otx2* expression must be extinguished from marginal cell progenitors in order for their development to proceed. In agreement with this model, a recent study demonstrated that mice lacking Otx2 in the inner ear showed ectopic expression of marginal cell markers along the entire lateral wall of the cochlear duct (Vendrell et al., 2015). Moreover, reduction of ectopic Otx2 expression in

the marginal cell territory of *Esrp1*$^{-/-}$;*Fgf9*$^{+/-}$ embryos coincided with the recovery of the stria vascularis. These data indicate that the dynamic expression of Otx2 along the cochlear lateral wall is important for regulating the developmental fates of marginal cells and Reissner's membrane.

Reissner's membrane does not form in *Fgf10*$^{-/-}$ embryos (Urness et al. 2015). A similar phenotype might have been expected in *Esrp1*$^{-/-}$ mutants given the aberrant splicing of *Fgfr2*, which reduces the abundance of Fgfr2-IIIb, the high affinity Fgf10 receptor (Zhang et al., 2006). Surprisingly, Reissner's membrane still developed in *Esrp1*$^{-/-}$ embryos, albeit through an alternative signaling mechanism that benefitted from the ectopic expression of Fgfr2-IIIc in the cochlear epithelium and Fgf9, a ligand that normally signals to the otic mesenchyme and is mostly dispensable for cochlear but not vestibular development (Pirvola et al., 2004). However, a major consequence of utilizing Fgf9/Fgfr2-IIIc to compensate for Fgf10/Fgfr2-IIIb is the gain in signaling strength that results in expansion of Reissner's membrane at the expense of marginal cells. Our study adds to the list of genetic disorders (e.g. Apert syndrome, Muenke syndrome) caused by a gain in Fgf signaling that results from alterations in Fgfr ligand-binding interactions (Mansour et al., 2013; Yu et al., 2000).

Fgfr2-IIIb is also required at early stages of inner ear morphogenesis as evidenced by the cystic inner ear phenotype displayed by embryos in which the Fgfr2-IIIb isoform was selectively deleted (Pirvola et al., 2000). Fgf3 and Fgf10 are the ligands that signal predominantly through Fgfr2-IIIb to promote early aspects of inner ear development (Alvarez et al., 2003; Wright and Mansour, 2003). One might expect cystic inner ears to be more prevalent in *Esrp1*$^{-/-}$ mutants given the depletion of Fgfr2-IIIb, however, only 16% of these embryos showed this phenotype. This observation raised

the possibility that Fgf9/Fgfr2-IIIc signaling is also compensating for other Fgfr2-IIIb dependent functions at earlier stages of inner ear development in *Esrp1* mutants. In support of this hypothesis, the removal of an allele of *Fgf9* from the *Esrp1*$^{-/-}$ background (*Esrp1*$^{-/-}$*; Fgf9*$^{+/-}$) increased the penetrance of the cystic inner ear phenotype to almost 50%, whereas, 100% of *Esrp1*$^{-/-}$*; Fgf9*$^{-/-}$ double mutants displayed cystic inner ears. These results indicate that dose dependent signaling through Fgf9/Fgfr2-IIIc is able to compensate for the loss of Fgfr2-IIIb to promote inner ear morphogenesis in *Esrp1*$^{-/-}$ mutants. This remarkable example of genetic compensation highlights the tremendous flexibility in Fgf signaling activity brought about by alternative splicing of receptor isoforms and the numerous genetically encoded ligands that bind to them.

Esrp1$^{-/-}$ embryos also displayed a marked decrease in the number of differentiated hair cells at the apex of the cochlear duct. This phenotype was attributed to a 48-hour delay in the onset of *Atoh1* at the apical turn. Hair cell maturation was also delayed at the base and mid-base levels of the cochlear duct of *Esrp1*$^{-/-}$ embryos, but at a step downstream of Atoh1, as indicated by the 24-hour lag in Pou4f3 expression. Sensory progenitors depend on the input of multiple signaling pathways to coordinate the expression of a set of transcriptional activators and repressors, the balance of which dictates the timing of *Atoh1* transcription along the cochlear duct (Cai and Groves, 2015; Neves et al., 2013; Okano et al., 2011). The prevailing model stipulates that Sox2 functions through an incoherent feed forward loop to both directly activate *Atoh1* transcription but also to promote the expression of Atoh1 repressors, including *Hey1, Hey2* and *Id1-3* (Neves et al., 2013; Benito-Gonzalez and Doetzlhofer, 2014). Once Atoh1 accumulates to a point where it can maintain its own expression, Sox2 is downregulated, so that its blockade on Atoh1 and other downstream components of the

hair cell differentiation program can be released (Ahmed et al., 2012; Dabdoub et al., 2008; Neves et al., 2013; Puligilla and Kelley, 2016). Based on this model (Fig. 2.9Y), it is likely that the upregulation in *Hey2* mRNA and Sox2 protein that we observed in sensory progenitors and hair cells, respectively, impedes Atoh1 expression and transcriptional activity, causing the delay in hair cell differentiation in *Esrp1*$^{-/-}$ embryos. Alternatively, the altered expression of *Hey2* and Sox2 may be a secondary consequence of the delayed sensory development in *Esrp1*$^{-/-}$ embryos.

The aberrant splicing of one or more transcripts expressed within the sensory epithelium of the cochlear duct may contribute to the misregulation of *Hey2* and Sox2 in *Esrp1*$^{-/-}$ embryos, although the identity of these transcripts remains to be determined. Esrp1 has also been shown to antagonize Sox2 translation by limiting the available pool of *Sox2* transcripts for loading onto polysomes (Fagoonee et al., 2013). Future experiments will determine the precise mechanism responsible for the delay in hair cell differentiation in *Esrp1*$^{-/-}$ embryos and the consequence that this phenotype has on auditory function.

The work in this chapter is published as:

Rohacek A.M.*, Bebee T.W.*, Tilton R.K.*, Radens C.M., McDermott-Roe C., Peart N., Kaur M., Zaykaner M., Cieply B., Musunuru K., Barash Y., Germiller J.A., Krantz I.D., Russ P. Carstens R.P. and Epstein D.J. *ESRP1 mutations cause hearing loss due to defects in alternative splicing that disrupt cochlear development.* Developmental Cell (2017), https://doi.org/10.1016/j.devcel.2017.09.026

Author Contributions

Alex M. Rohacek[1,5], Thomas W. Bebee[2,5], Richard K. Tilton[4,5], Caleb M. Radens[1], Chris McDermott-Roe[2], Natoya Peart[2], Maninder Kaur[4], Michael Zaykaner[4], Benjamin Cieply[2], Kiran Musunuru[2], Yoseph Barash[1], John A. Germiller[3], Ian D. Krantz[1,4,6], Russ P. Carstens[2,6] and Douglas J. Epstein[1,6,7]

[1]Department of Genetics, Perelman School of Medicine, University of Pennsylvania, Philadelphia, Pennsylvania, USA. [2]Department of Medicine, Perelman School of Medicine, University of Pennsylvania, Philadelphia, Pennsylvania, USA. [3]Division of Pediatric Otolaryngology, The Children's Hospital of Philadelphia, Philadelphia, Pennsylvania, USA. [4]Division of Human Genetics, The Children's Hospital of Philadelphia, Philadelphia, Pennsylvania, USA. [5]These authors contributed equally. [6]Senior author. [7]Lead Contact

J.A.G, I.D.K, R.P.C. and D.J.E. conceived the study. J.A.G, R.K.T and I.D.K. characterized human clinical data. R.K.T, M.K., M.Z., and I.D.K. analyzed whole exome sequencing data and performed Sanger sequencing confirmation of *ESRP1* mutations. T.W.B., N.P., B.C. and R.P.C. designed and performed RT-PCR and splicing studies.

A.M.R and D.J.E designed and performed all mouse experiments. T.W.B. and A.M.R. generated and analyzed RNA-seq data. C.M.R. and Y.B. characterized alternative splicing data. C. M-R. and K.M. performed gene editing experiments in iPSCs. A.R.M, I.D.K, R.P.C and D.J.E, wrote the manuscript. All authors analyzed the data, discussed the results and commented on the manuscript.

Acknowledgements

We thank Dr. Jason Mills, Director of the iPSC Core at the Center for Advanced Retinal and Ocular Therapeutics (Perelman School of Medicine, University of Pennsylvania), for deriving iPSC lines used in this study. This work was funded by grants from the National Institutes of Health, R01 DC006254 (DJE), R01 DE024749 (RPC), U01 HG006546 (IDK), R01 AG046544 (YB). AMR was supported by the Predoctoral Training Program in Genetics (T32 GM008216) and an NRSA fellowship F31DC014647.

Figures

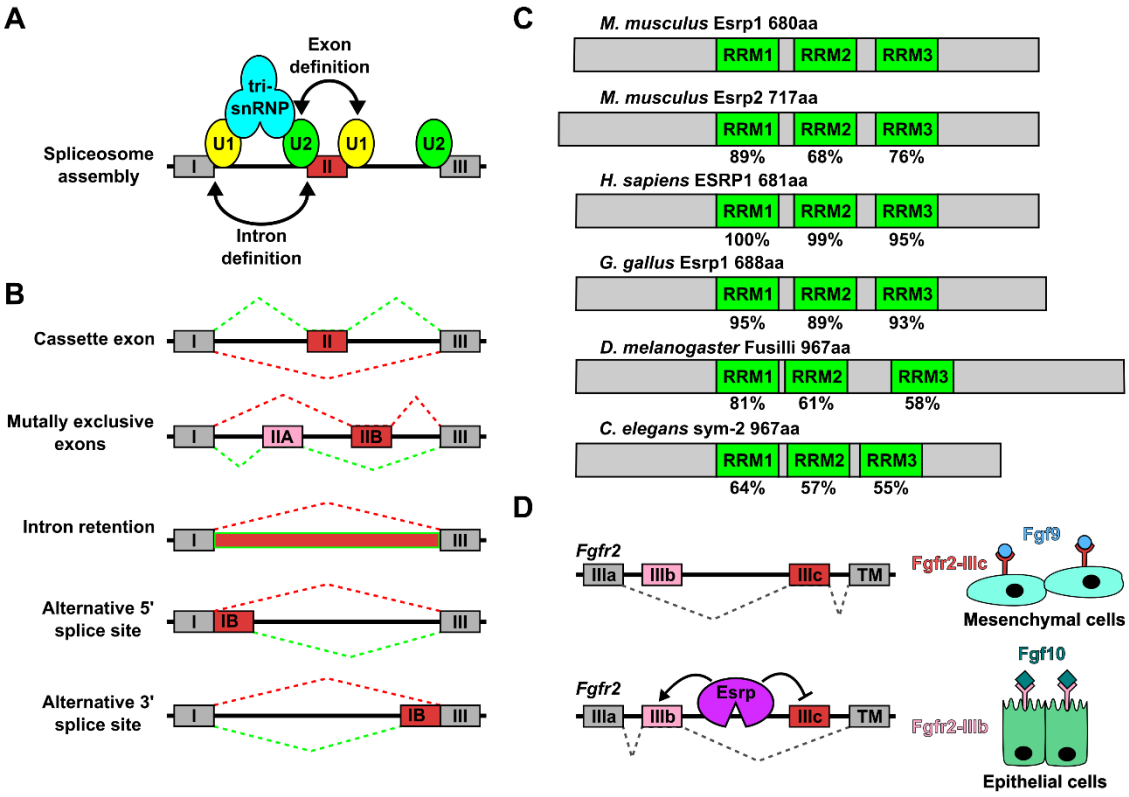

Figure 2.1. Alternative splicing and epithelial splice regulatory proteins. (A) Schematic of spliceosome assembly on an mRNA transcript. (B) Representations of possible alternative splicing events. (C) Diagrams of Esrp proteins in selected species, amino acid conservation of RNA recognition motifs (RRM) are listed below the respective domains. (D) Schematic of the *Fgfr2* splicing event directed by Esrp and resulting receptor-ligand interactions.

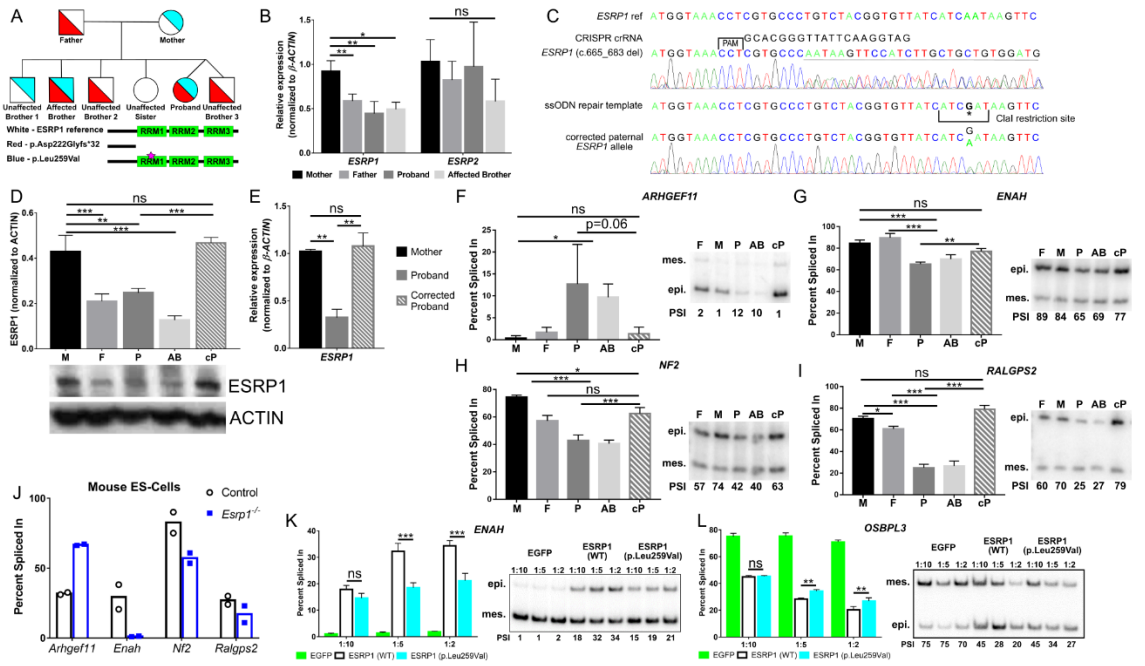

Figure 2.2. *ESRP1* mutations segregate with SNHL and disrupt alternative splicing.

(A) Pedigree with SNHL showing segregation of maternal (blue) and paternal (red) *ESRP1* mutations to affected (compound heterozygous) and unaffected offspring. The position of the *ESRP1* frameshift (p.Asp222Glyfs*32) and missense (p.Leu259Val) mutations is indicated. (B) Quantitative RT-PCR of *ESRP1* and *ESRP2* mRNAs from iPSCs derived from parents and affected children. (C) Schematic and sequencing tracks for CRISPR-Cas9 gene editing strategy to repair the paternal *ESRP1* (c.665_683 del) mutation. (D) Bar graph and gel image of western blot for ESRP1 from patient derived iPSCs and corrected proband (cP). (E) Quantitative RT-PCR of *ESRP1* mRNA from iPSCs comparing corrected to uncorrected proband and mother. (F-I) Bar graphs and gel images of radioactive RT-PCR results showing PSI values for ESRP1 dependent alternative splicing events in patient-derived iPSCs and corrected proband. (J) Graph of RT-PCR dependent alternative splicing events in mouse ESCs (Bar represents average

for two independent clones). (K,L) Bar graphs and gel images of radioactive RT-PCR results showing PSI values for ESRP1 dependent splicing events in MDA-MB-231 cells transduced with ESRP1 wild type (WT), ESRP1 mutant (p.Leu259Val) and EGFP cDNAs at three different titers. Abbreviations: Mother (M), Father (F), Proband (P), Affected brother (AB), CRISPR-Cas9 corrected Proband (cP), Percent Spliced In (PSI), epi (epithelial isoform), mes (mesenchymal isoform), ns (not significant). Graphs for B and E represent mean ± SE, D and F-I,K,L represent mean ± SD (* $P<0.05$, ** $P<0.001$; *** $P<0.0001$, (B,D-I) one-way ANOVA with Tukey's test, (K,L) 2-way ANOVA with Dunnet's test; n=3).

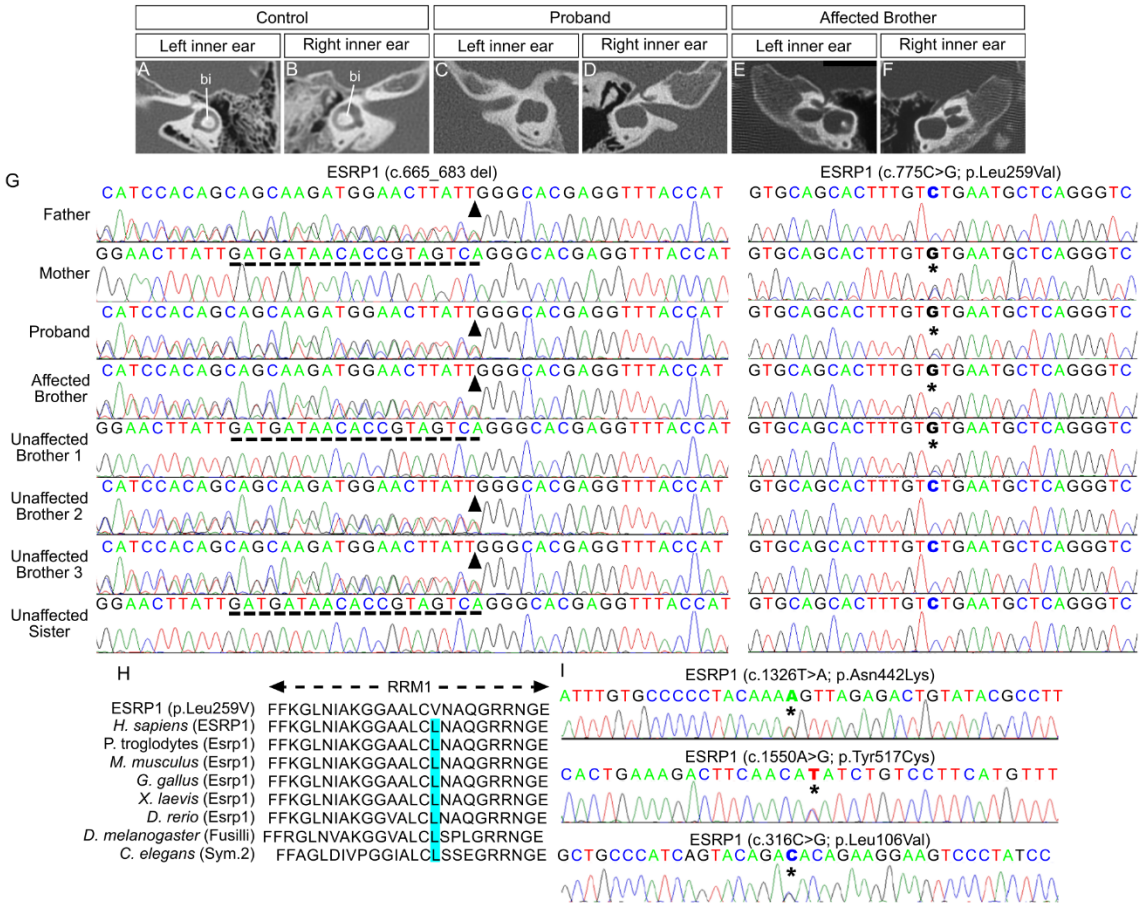

Figure 2.3. ESRP1 mutations in individuals with SNHL. (A-F) Axial CT scans of the lateral vestibule from control and affected children in pedigree with SNHL showing absence of bony island (bi) in (C-F). (G) Sanger sequencing tracks of *ESRP1* from individuals in pedigree with SNHL showing position of paternally inherited 19 bp deletion (arrowhead) corresponding to underlined sequence, and maternally inherited point mutation (asterisk). (H) Cross-species comparison of the first RNA recognition motif (RRM) in ESRP1 showing amino acid conservation at site of ESRP1 mutation (Leu259Val). (I) Sanger sequencing tracks of *ESRP1* from three isolated cases of SNHL showing position of point mutations (asterisk).

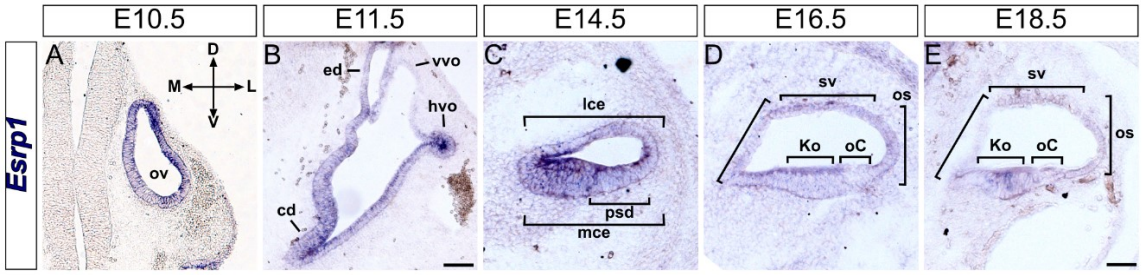

Figure 2.4. Esrp1 expression in the developing mouse cochlea. (A-E) Transverse sections through the otic vesicle (A,B) and cochlear duct (C-E) of wild type embryos over several developmental stages showing broad *Esrp1* expression in the otic epithelium. Scale bar = 100μm (A,B) and 50μm (C-E). Abbreviations: cochlear duct (cd), dorsal (D), endolymphatic duct (ed), horizontal vestibular outpouch (hvo), Kolliker's organ (Ko), lateral (L), lateral cochlear epithelium (lce), medial (M), medial cochlear epithelium (mce), , prosensory domain (psd), organ of Corti (oC), otic vesicle (ov), outer sulcus (os), Reissner's membrane (Rm), stria vascularis (sv), ventral (V), vertical vestibular outpouch (vvo).

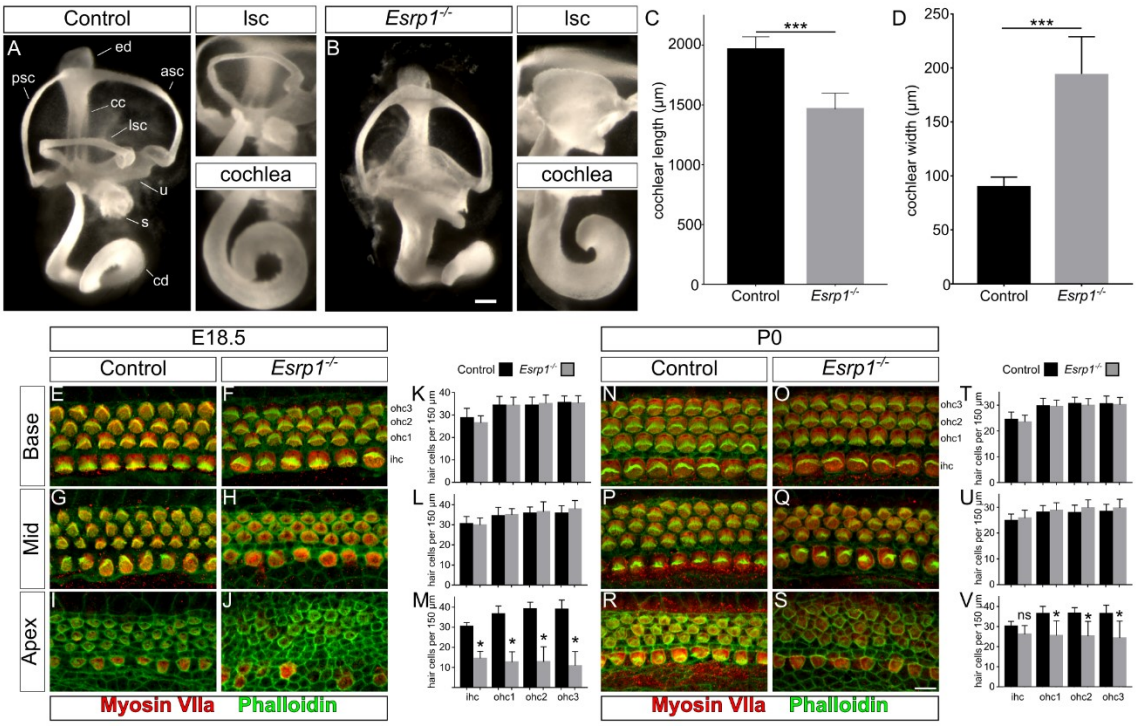

Figure 2.5. Inner ear morphogenesis and auditory hair cell differentiation are disrupted in *Esrp1*$^{-/-}$ mouse embryos. (A-B) Inner ear paint fills of control and *Esrp1*$^{-/-}$ embryos at E14.5. The lateral semicircular canal and apex of the cochlear duct are magnified in adjacent panels to reveal their dysmorphic features. Scale bar = 100μm. (C-D) Quantification of cochlear length and width from control and *Esrp1*$^{-/-}$ mutant embryos represented as mean ± SD (***P<0.001, unpaired t-test; n=8). (E-J, N-S) Whole mount preparations of control and *Esrp1*$^{-/-}$ cochlear sensory epithelium stained with markers of hair cells (Myosin VIIa) and actin/stereocilia (Phalloidin) at E18.5 (E-J) and P0 (N-S) at defined regions (base, mid and apex) of the cochlear duct. Scale bar = 10μm. (K-M, T-V) Quantification of inner and outer hair cells in control and *Esrp1*$^{-/-}$ embryos at E18.5 (K-M) and P0 (T-V) within a 150μm area from defined regions (base, mid and apex) of the cochlear duct represented as mean ± SD (*P<0.0001, one-way ANOVA with Tukey's

test; n=10). Abbreviations: anterior, posterior and lateral semicircular canals (asc, psc, lsc, respectively), cochlear duct (cd), common crus (cc), endolymphatic duct (ed), inner hair cell (ihc), outer hair cell (ohc), saccule (s), utricle (u).

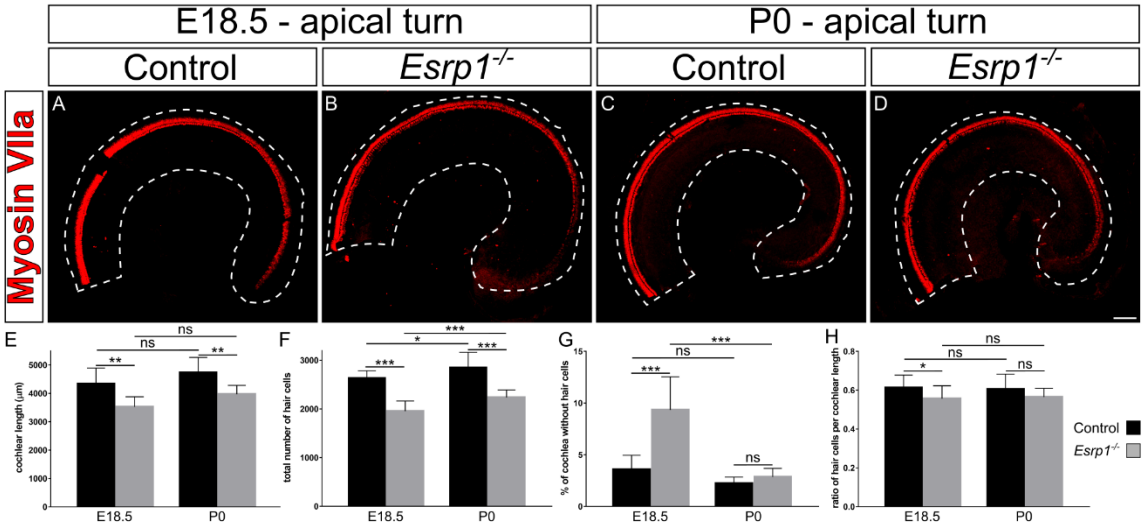

Figure 2.6. Hair cell differentiation is delayed at the apex of the cochlear duct in *Esrp1*$^{-/-}$ mutants. (A-D) Whole mount cochlear preparations from control and *Esrp1*$^{-/-}$ embryos immunostained for Myosin VIIa at E18.5 (A-B) and P0 (C-D). Scale bar = 100μm. (E-F) Quantification of cochlear length (E), total number of hair cells (F), percent of cochlea without hair cells (G), and ratio of hair cells per cochlear length (H) presented as mean ± SD (*P<0.05; ***P<0.0001, one-way ANOVA with Tukey's test, n=10).

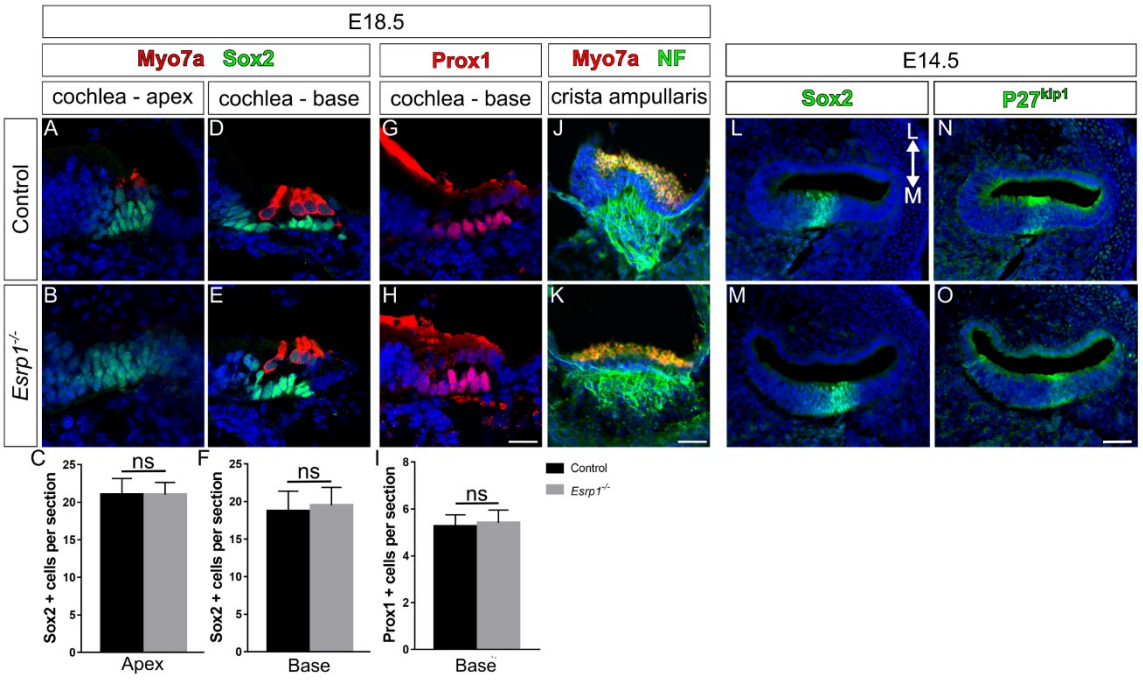

Figure 2.7. Specification of prosensory progenitors, support cells, vestibular hair cells and neurons is not compromised in *Esrp1*$^{-/-}$ embryos. (A-C) Sox2 staining reveals a normal pool of sensory progenitors at the apex of the cochlear duct of *Esrp1* mutants. (D-F) Sox2 and (G-I) Prox1 positive support cells are present in similar number and organization at the base of *Esrp1* mutants. Myo7a labels hair cells. All quantifications are presented as mean ± SD (ns, unpaired t-test). (J,K) Vestibular hair cells and neurons labeled with Myo7a and neurofilament (NF), respectively, are unaffected in *Esrp1* mutants. (L-O) The expression of Sox2 and P27^{kip1} in prosensory progenitors is not compromised in *Esrp1*$^{-/-}$ embryos. Scale bar = 10μm (A,B,D,E,G,H) and 50μm (J-O). n=5 for all panels. Abbreviations: L (lateral), M (medial).

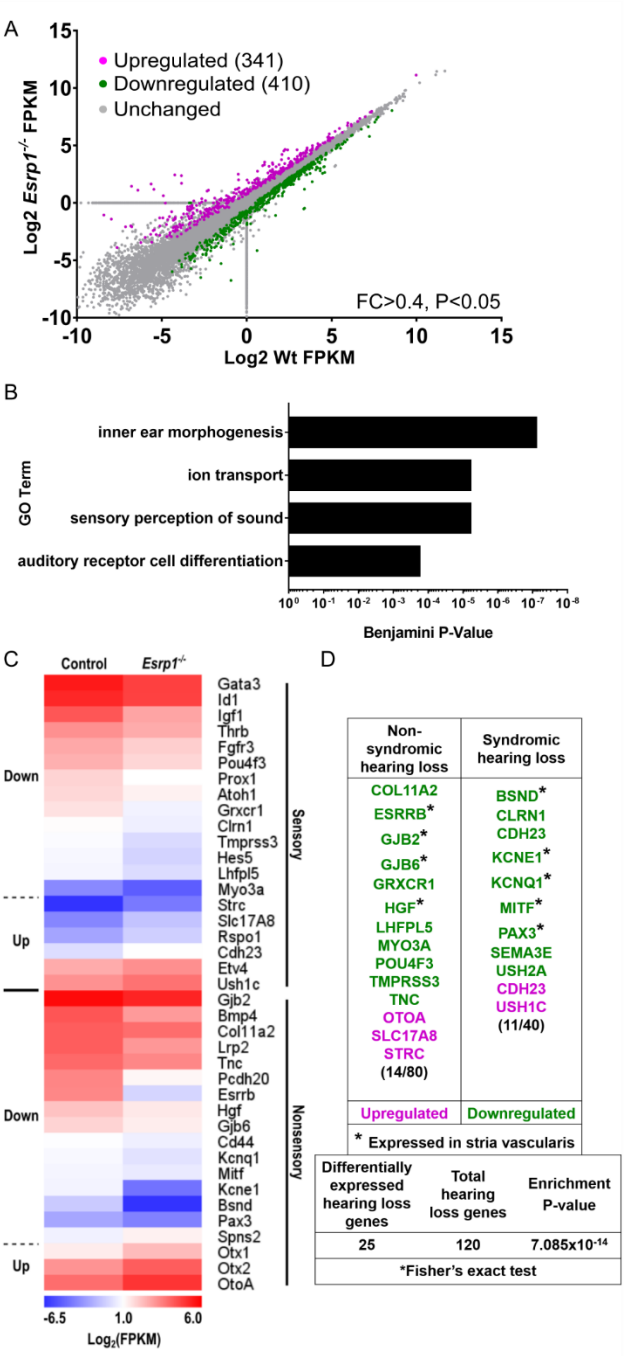

Figure 2.8. Sensory and nonsensory gene expression profiles are disrupted in the cochlear epithelium of *Esrp1*$^{-/-}$ embryos. (A) Plot of differentially expressed genes between wild type and *Esrp1*$^{-/-}$ cochlear epithelium at E16.5 with a fold change (FC) >

0.4 (n=3 replicates, P<0.05). (B) Gene Ontology term enrichment for differentially expressed genes between wild type and *Esrp1*$^{-/-}$ cochlear epithelium. (C) Heatmap of differentially expressed genes separated into sensory and nonsensory categories. (D) Hearing loss genes are significantly enriched in the set of differentially expressed transcripts between control and *Esrp1*$^{-/-}$ mutants. Genes expressed in the stria vascularis are marked with an asterisk.

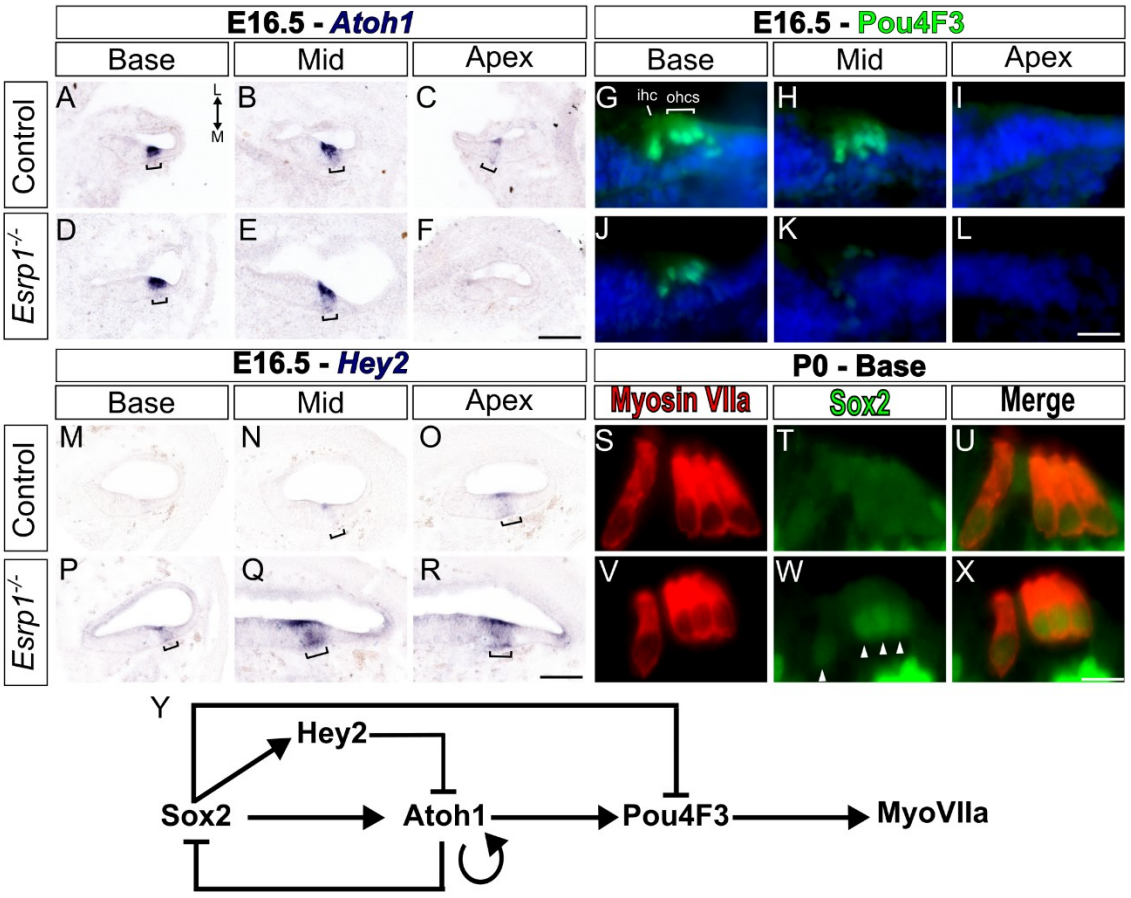

Figure 2.9. Hair cell differentiation is delayed in *Esrp1*$^{-/-}$ embryos. (A-X) Transverse sections through defined regions of the cochlear duct (Base, Mid, Apex) from control and *Esrp1*$^{-/-}$ embryos stained for *Atoh1* mRNA (A-F), Pou4F3 protein (G-L) and *Hey2* mRNA (M-R) at E16.5 (n=5 or 6). Staining in prosensory domain is marked with a bracket. Weak *Atoh1* expression at the apex of the cochlear duct in control embryos (C) is consistently absent in *Esrp1*$^{-/-}$ embryos at this stage. (S-X) Transverse sections through the organ of Corti of control and *Esrp1*$^{-/-}$ newborn pups (P0) stained for MyoVIIa and Sox2. Sox2 staining persists in hair cell nuclei of *Esrp1*$^{-/-}$ embryos (arrow heads in W). Scale bar = 100μm (A-F, M-R), 10μm (G-L) and 5μm (S-X). (Y) Schematic of the gene

regulatory network controlling hair cell differentiation. Abbreviations: inner hair cell (ihc), outer hair cells (ohc), medial (M), lateral (L).

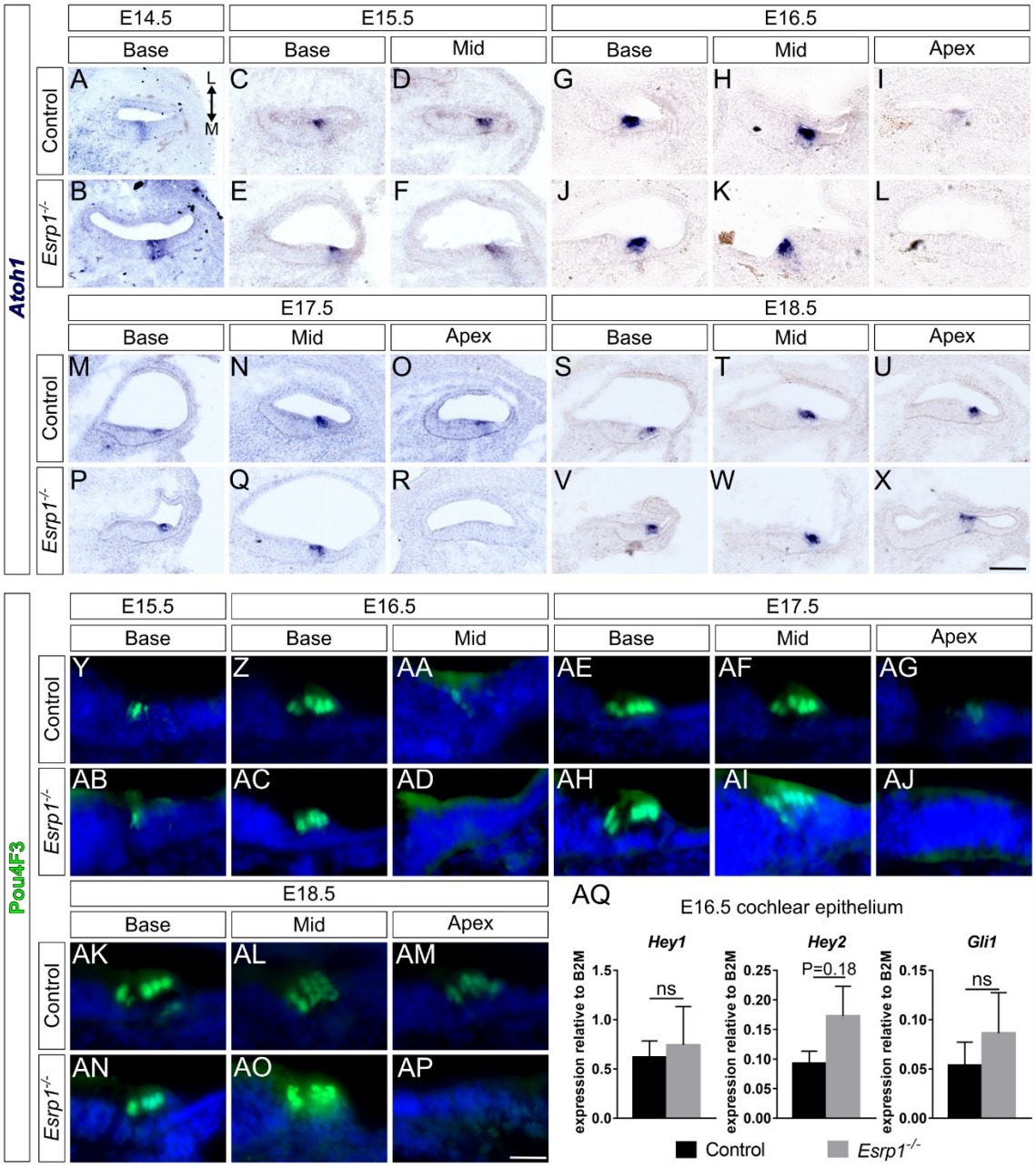

Figure 2.10. Hair cell differentiation and maturation is delayed in *Esrp1*$^{-/-}$ embryos.

(A-X) Transverse sections through the cochlear duct of control and *Esrp1*$^{-/-}$ embryos stained for *Atoh1* mRNA at progressively later stages of hair cell development. (Y-AP) Transverse sections through the cochlear duct of control and *Esrp1*$^{-/-}$ embryos

immunostained for Pou4F3 at progressively later stages of hair cell development. Scale bar = 100μm (A-X) and 10μm (Y-AP). (AQ) qRT-PCR of sensory markers on E16.5 cochlear epithelium represented as mean ± SD (ns, unpaired t-test). (A-AP) n=5, (AQ) n=6. Abbreviations: L (lateral), M (medial).

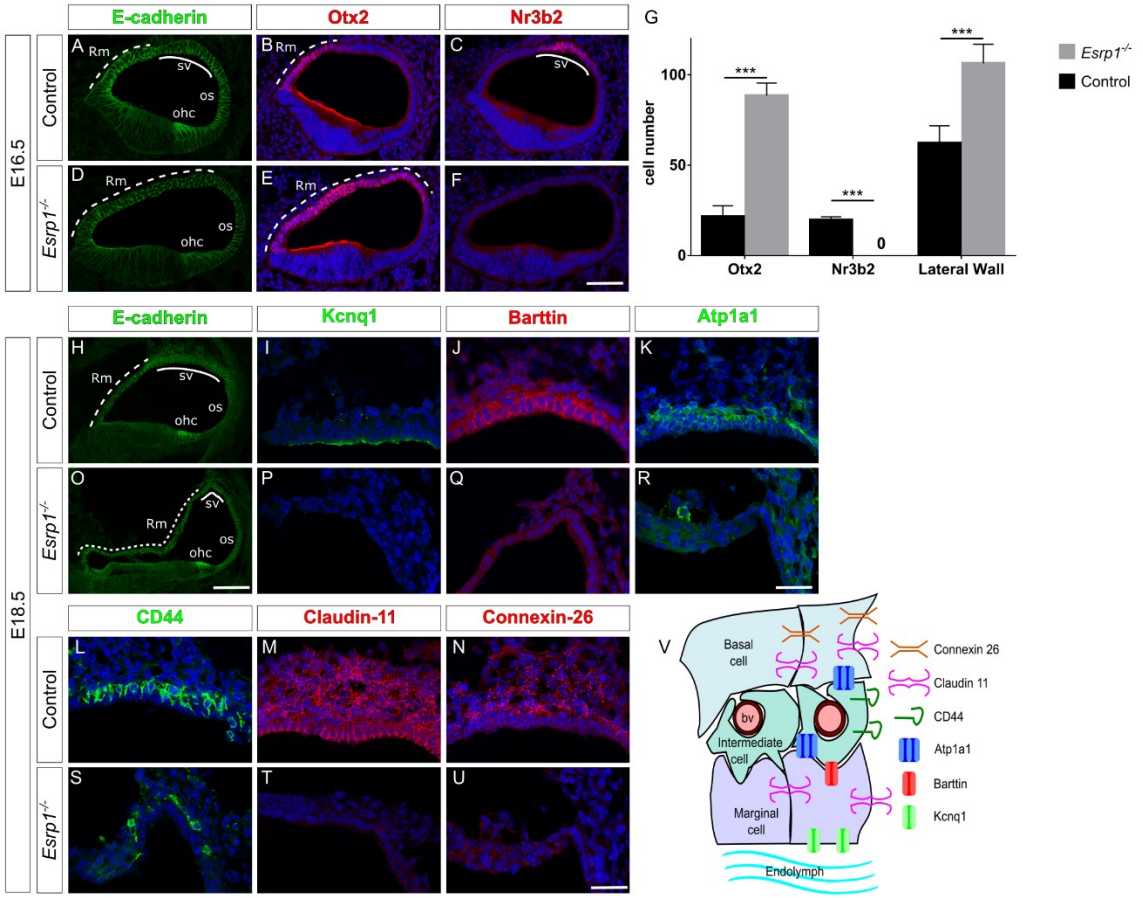

Figure 2.11. Esrp1 regulates the identity of nonsensory cells along the lateral cochlear wall. (A-F) Transverse sections through the cochlear duct of control (n=8) and *Esrp1*$^{-/-}$ (n=6) embryos at E16.5 immunostained for E-cadherin (A,D), Otx2 (B,E) and Nr3b2 (C,F). (G) Quantification of cells expressing Otx2, Nr3b2, as well as the total number of cells in the lateral cochlear epithelium represented as mean ± SD (***P<0.0001, Student's t-test). (H-U) Transverse sections through the cochlear duct of control (n=5) and *Esrp1*$^{-/-}$ (n=5) embryos at E18.5 immunostained for E-cadherin (H,O), and indicated cell type specific markers of the stria vascularis (I-N, P-U). Scale bar = 50μm (A-F, H,O) and 25μm (I-N, P-U). (V) Schematic of the stria vascularis displaying

cell types and markers analyzed in (H-U). Abbreviations: blood vessel (bv), outer hair cells (ohc), outer sulcus (os), Reissner's membrane (Rm) and stria vascularis (sv).

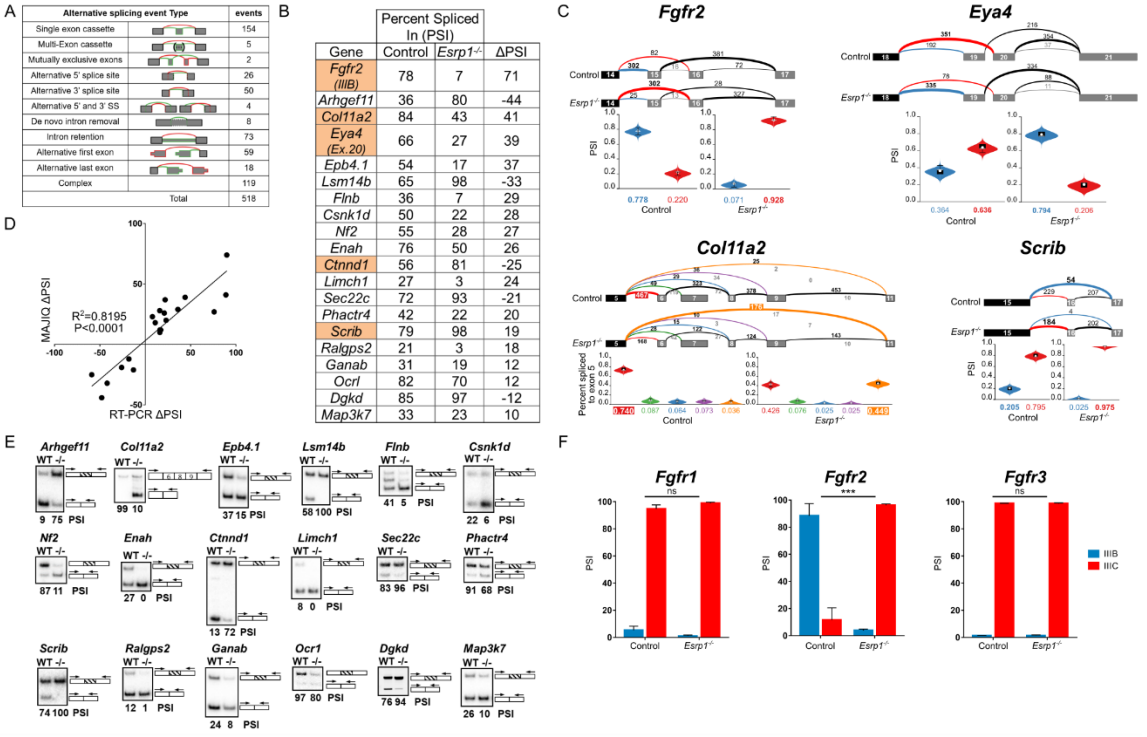

Figure 2.12. Alternative splicing is impaired in the cochlear epithelium of *Esrp1*$^{-/-}$ embryos. (A) Number and type of alternative splicing switches identified by MAJIQ between *Esrp1*$^{-/-}$ and control embryos in the cochlear epithelium at E16.5 (ΔPSI > 10%). (B) PSI (percent spliced in) values for selected genes with significant splicing differences between *Esrp1*$^{-/-}$ and control embryos determined by MAJIQ and subsequently validated by RT-PCR. The highlighted genes have known roles in inner ear development and/or auditory function. (C) Voila views (Vaquero-Garcia et al., 2016) of Esrp1 dependent alternative splicing events for four genes associated with hearing loss showing examples of mutually exclusive (*Fgfr2, Eya4*), complex (*Col11a2*) and single (*Scrib*) exon cassettes. Numbered exons for each gene are represented as rectangles. Numbers above splicing events indicate RNA-seq read counts. Violin plots represent PSI

estimates. (D) Correlation plot of alternative splicing switches predicted by MAJIQ and validated by RT-PCR. The Pearson's product-moment correlation and the line of best fit (least squares polynomial) were computed in R ($P<0.0001$). (E) Radioactive RT-PCR validation of differential splicing events in the cochlear epithelium of *Esrp1*$^{-/-}$ and control littermates at E16.5. (F) Comparison of PSI values for Fgfr1-3, exon III-b (epithelial) and exon III-c (mesenchymal) in cochlear epithelium from *Esrp1*$^{-/-}$ and control embryos as determined by RT-PCR (multiple t-test comparison, $P<0.0001$).

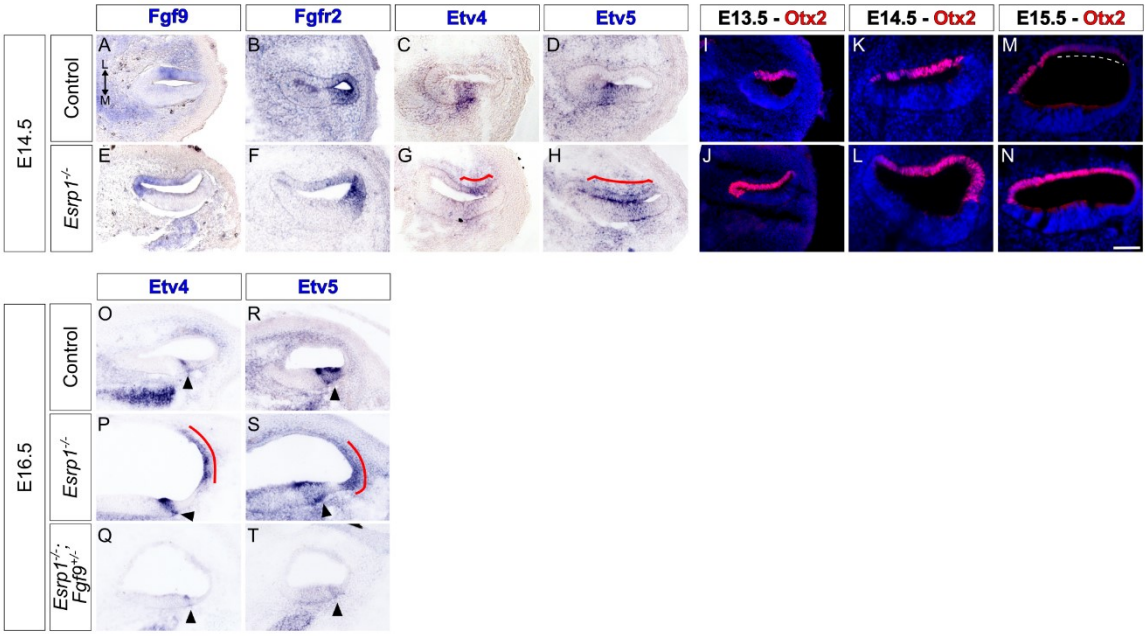

Figure 2.13. Fgf signaling is ectopically activated in the lateral cochlear epithelium of Esrp1 mutants. (A-H) Transverse sections through the cochlear duct of control and *Esrp1*$^{-/-}$ mutants at E14.5 stained with markers of Fgf signaling. Ectopic expression of *Fgf9*, *Etv4* and *Etv5* along the lateral cochlear epithelium is highlighted (red-bracket). (I-N) Otx2 is progressively restricted to Reissner's membrane in control embryos but remains broadly expressed throughout the lateral cochlear epithelium in *Esrp1* mutants. Otx2 repression from the stria vascularis is indicated (dashed line). (O-T) Transverse sections through the cochlear duct of control, *Esrp1*$^{-/-}$, and *Esrp1*$^{-/-}$;*Fgf9*$^{+/-}$ embryos at E16.5 stained for *Etv4* and *Etv5*. Ectopic expression of *Etv4* and *Etv5* along the lateral cochlear epithelium (red-bracket) and normal sensory expression (arrowhead) are highlighted. Scale bar = 50μm. n=4 for all panels. Abbreviations: L (lateral), M (medial).

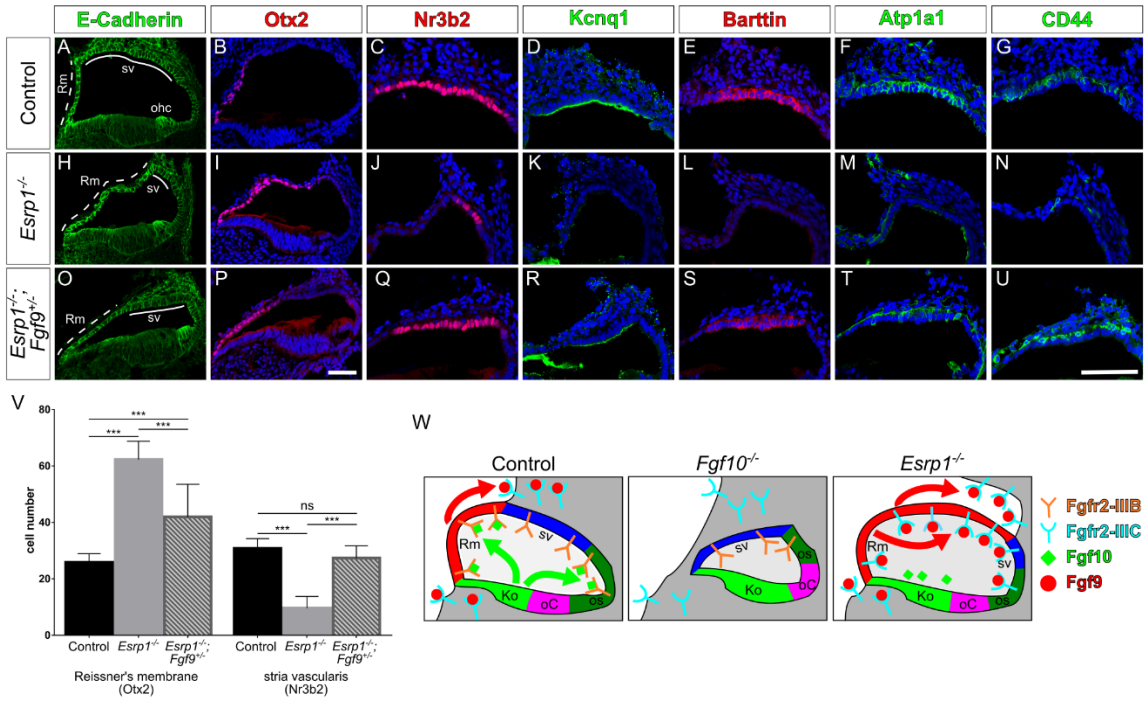

Figure 2.14. Ectopic signaling through Fgf9/Fgfr2-IIIc is responsible for the lateral cochlear wall defects in Esrp1 mutants. (A-U) Transverse sections through the cochlear duct of control (n=15), *Esrp1*$^{-/-}$ (n=7) and *Esrp1*$^{-/-}$;*Fgf9*$^{+/-}$ (n=6) embryos at E18.5 immunostained for E-cadherin (A,H,O), Otx2 (B,I,P) and cell type specific markers of the stria vascularis (C-G, J-N, Q-U). Scale bars = 50μm. (V) Quantification of cells expressing Otx2 and Nr3b2 represented as mean ± SD (***P<0.0001, ANOVA with Tukey's test). (W) Schematic representation of the lateral cochlear wall phenotypes manifesting from altered Fgf signaling in *Fgf10*$^{-/-}$ and *Esrp1*$^{-/-}$ mutants compared to a control embryo.

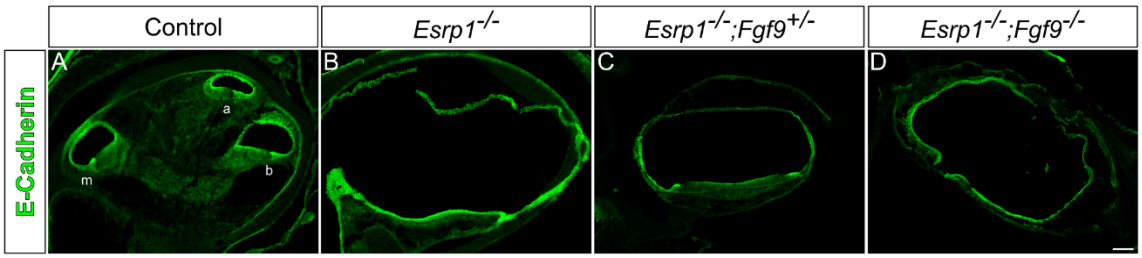

Figure 2.15. The cystic otic phenotype in *Esrp1*$^{-/-}$ embryos is exacerbated by the dose dependent loss of Fgf9. (A-D) Transverse sections through the cochlear ducts of control (n=6), *Esrp1*$^{-/-}$ (n=4), *Esrp1*$^{-/-}$*; Fgf9*$^{+/-}$ (n=4) and *Esrp1*$^{-/-}$*; Fgf9*$^{-/-}$ (n=3) embryos at E18.5 immunostained for E-cadherin. Scale bar=100μm. Abbreviations: apical turn (a), basal turn (b), medial turn (m).

Materials and Methods

Mice

Generation of *Esrp1*$^{+/-}$ mutant mice was described previously (Bebee et. al. 2015). *Fgf9* mutant mice were procured from Jackson Laboratories (0224362; B6N(Cg)-Fgf9$^{tm1b(KOMP)Wtsi/J}$; presented in text as *Fgf9*$^{+/-}$). For all experiments control littermates have at least one wild-type allele of *Esrp1*. Pregnant dames were euthanized by carbon dioxide, and embryos were isolated and euthanized by decapitation in 4ºC PBS. All animal procedures and experiments were approved by the Institutional Animal Care and Use Committee (IACUC) at the University of Pennsylvania.

Exome sequencing

Family members were enrolled under an IRB approved protocol of informed consent at the Children's Hospital of Philadelphia (CHOP). Blood was obtained from all eight family members and genomic DNA was extracted from whole blood using standard procedures. Exomes were captured using Agilent SureSelect V4 and sequenced at 100X coverage using Illumina HiSeq 2000. Only coding regions and splice site variants at >4x coverage were analyzed, and the results were further filtered using a population frequency <3% in the 1000 Genomes and Exome Sequencing Project servers. Mutations that did not segregate in an autosomal recessive inheritance pattern were then filtered out. All putative causative mutations were validated with Sanger sequencing.

ESRP1 mutation screening

An additional cohort of 144 pediatric probands with bilateral SNHL of unknown molecular etiology was screened for mutations in *ESRP1* and in the closely related gene *ESRP2*. These patients were all enrolled under an IRB approved protocol of informed consent at CHOP. PCR primers were designed for specific intronic sequences in *ESRP1* and

ESRP2 (Supplemental Table S2). DNA sequence analysis was performed using an ABI 3730XL automated DNA sequencer.

Generation of iPSCs

Peripheral blood mononuclear cells (PBMCs) were isolated from family members, transduced with EBV and transformed to lymphoblastoid cell lines (LCLs). The LCLs were maintained in RPMI media supplemented with 10% FBS, 1X Penn/Strep, 1X glutatmine in a 5% CO2 incubator. For iPSC generation, 2 million LCLs from the mother, father and 2 affected probands were transfected with nonintegrating, nontransmissible episomal plasmids expressing *OCT4*, *SOX2*, *KLF4*, *MYCL*, *LIN28A*, a p53 short hairpin (sh)RNA, and a green fluorescent protein (eGFP) via a single nucleofection (Hubbard et al., 2014). Transfected cells are then cultured in human embryonic stem cell (HES) media (DMEM/F12, 15% KOSR, 1X NEAA, 1X P/S, 1X glutamine, 2ME, 20ng/mL bFGF) in not adherent conditions for 6 days. Cells were then plated onto irradiated mouse embryonic fibroblasts (iMEFs) on day 6 in HES with the addition of 0.5mM sodium butyrate, and media was changed daily for a 14-17 days post-plating. iPSC-like colonies appeared between day 21-28 after nucleofection, colonies were isolated (~10/patient), and expanded on iMEFs using standard ES/IPSC culture conditions (Mills et al., 2013; Sullivan et al., 2014).

Repair of ESRP1 (c.665_683 del) allele in patient derived iPSCs

Patient derived iPSCs were maintained in feeder-free Geltrex (Life Technologies)-coated plastics and mTesr1 media (Stem Cell Technologies). For transfection, cells were dispersed with Accutase (Life Technologies) and re-suspended in P4 solution (Lonza) containing an *ESRP1* sgRNA-expressing pX330-mCherry plasmid and the cognate repair ssODN (see Key Resources table), and electroporated using a 4D Nucleofector

(Lonza). The repair template included a silent Cla I site which was used to test for integration (described below). Three days post-transfection, mCherry positive cells were recovered using a BD FACSJazz cell sorter and seeded onto a Geltrex-coated 10cm dish. One week post-seeding, colonies were manually picked for clonal expansion and genotyping. The site of potential repair was amplified and incubated with Cla I (see Key Resources table). Unmodified DNA was refractory to Cla I whilst repaired DNA was cleaved, yielding 235bp and 231bp fragments. Positive clones were expanded and Sanger sequenced to confirm repair of the paternal allele and absence of indel mutations on the maternal allele.

Viral expression of *ESRP1* mutation in human cell culture

Human *ESRP1* full-length cDNA was cloned from the ORFeome Collection (RBP clone #290) using GATEWAY into a pIBX-cFFB-Emerald vector. The c.775C>G mutation was introduced into the *ESRP1* cDNA by site directed mutagenesis. Wild type (WT) and mutant ESRP1 cDNAs were PCR amplified and cloned into pCRBlunt. The pMXs-cFF-B (IRESpuro) retroviral vector was cut with EcoRI, end-filled using Phusion, then cut with NotI. Wild type and mutant ESRP1 cDNAs were then subcloned from pCRBlunt using EcoRV and NotI. The resulting constructs include a Kozak, ESRP1 WT or c.775C>G mutant cDNA fused to a 2x FLAG tag at the carboxy terminus. Murine leukemia virus was generated using the viral packaging N16 cells were grown in DMEM, 10% FBS and transfected with the viral pMXs plasmids encoding WT or mutant ESRP1 in combination with VSV-G for pMXs EGFP, pMXs-cFF-B ESRP1 WT, and pMXs-cFF-B ESRP1 C>G (patient mutation). Virus was collected and applied in the indicated ratio with polybrene to triplicate wells of MDA-MB-231 cells grown in DMEM, 10% FBS, and Pennicillin/Streptomycin. Cells were collected into Trizol (Invitrogen) three days after

infection. Total RNA was extracted for RT-PCR evaluation of endogenous ESRP splicing targets. Expression levels of WT and mutant ESRP1 C>G were confirmed by Western blot.

RT-PCR

Total RNA was extracted from purified cochlear epithelium and cultured cells (iPSCs, MDA-MB-231, mESCs) using Trizol-LS (Invitrogen), precipitated in the presence of glycogen and resuspended in 10mM Tris pH 8.0. For CRISPR corrected iPSCs and control lines, total RNA was extracted using an RNeasy mini kit (Qiagen). For synthesis of cDNA, 100ng of total RNA from cochlear epithelium or 1ug of total RNA from cell culture was used for random hexamer primed M-MLV reverse transcriptase (Promega) or Oligo(dT) primed Omniscript reverse transcriptase (Qiagen). Analysis of gene expression was performed using SYBR green master mix (AppliedBiosystems) and primer sequences listed in Table S4. Real-time RT-PCR analysis was performed using a 7500 Fast Realtime machine (AppliedBiosystems).

Semi-quantitative radioactive RT-PCR products were separated on 5% PAGE gels, dried and exposed on phosphor screens, scanned on a Typhoon FLA 9500, and quantified using ImageQuant TL, version 7.0. Splicing ratios are represented as Percent Spliced In (PSI) of the alternative exon for cassette exons and were normalized to RT-PCR product sizes. Quantification of exon IIIb and IIIc for *Fgfr1*, *Fgfr2*, and *Fgfr3* required restriction enzyme digestion to discriminate the two isoforms. *Fgfr2* PCR products were digested with AvaI (IIIb) or HincII (IIIc). *Fgfr1* products were digested with BstXI (IIIb) and HincII (IIIc). *Fgfr3* products were digested with StuI (IIIb) and PstI (IIIc) (all restriction digestions were performed according to NEB guidelines at 5U/digestion). Primer sequences are listed (Table S4).

Inner ear paint fill

Paint fills were performed essentially as described (Martin and Swanson, 1993) with the use of White-Out Plus (Bic, Milford, CT,USA) as the contrast medium. Cochlear length and width measurements were made using ImageJ.

In situ hybridization

Embryos were collected from timed pregnant females (vaginal plug = E0.5). The inner ears were dissected from the head and fixed for 2 hours in 4% paraformaldehyde at 4°C, then washed in PBS. Inner ears were cryoprotected overnight in 30% sucrose/PBS then snap frozen in OCT embedding compound (Sakura Finetek Torrence, CA). Inner ears were serially sectioned along the transverse plane from anterior to posterior. The position of a given section through the cochlear duct was calculated based on its distance (μm) from the first and last section (#sections x thickness = position within cochlear duct along anterior-posterior axis). Mid-modiolar sections containing all three turns of the cochlear duct (base, mid-base, apex) were confirmed using the above calculation to ensure comparison of equivalent sections through control and mutant embryos. Sections were hybridized with digoxigenin-UTP-labeled riboprobes as previously described (Nissim et al., 2007).

Whole mount cochlear preparations

Inner ears were dissected and fixed in 4% paraformaldehyde for 2 hours at 4°C, then washed in PBS. Cochleae were microdissected in 0.1% PBST to expose the sensory epithelium, and incubated with a rabbit polyclonal anti-Myosin VIIa antibody (1:500; Proteus Biosciences Inc, 25-6790) and a Phalloidin conjugated Alexa488 probe (1:50; Molecular Probes, A12379), followed by a donkey anti-rabbit IgG secondary antibody

conjugated to Alexa594 (1:200). Hair cells were counted along the entire length of the cochlear duct, as well as per unit area (150μm) at base, mid and apical regions.

Immunohistochemistry

Inner ears were processed for immunohistochemistry in the same fashion as for in situ hybridization. Inner ear sections were stained with DAPI and antibodies found in Key Resources.

Western Blot

Total protein was extracted from patient derived and CRISPR corrected iPSCs in RIPA buffer. Lysate was separated on a Bis-Tris 4–12% gradient SDS-PAGE gel and transferred to nitrocellulose membrane. Membranes were blocked in 5% Non-fat Milk in 0.1% PBST then incubated overnight at 4°C in primary antibody and loading control (anti-Beta Actin M2; 1:10,000). Membranes were incubated in secondary Sheep anti-mIgG:HRP (1:2500; GE Healthcare) for one hour and protein detection was performed with ECL detection (Invitrogen) by chemiluminescence.

RNA-seq analysis

Cochlear epithelium from control and *Esrp1*$^{-/-}$ mouse embryos (n=3 pairs of biological replicates) were isolated at E16.5 exposed to collagenase P (0.1mg/ml) at 37^{o}C for 15 min to remove surrounding mesenchyme, and snap frozen in Trizol-LS (Invitrogen). RNA was extracted and precipitated in the presence of glycogen and resuspended in 10mM Tris pH 8.0. Total RNA (200ng) was used for poly A selected RNA-seq library preparation using the NEBNext® Ultra™ Directional RNA Library Prep Kit from Illumina® (mRNA) (New England Biolabs) (products: NEBNext® Poly(A) mRNA Magnetic Isolation Module (E7490S) and NEBNext® Ultra™ Directional RNA Library Prep Kit for Illumina® (E7420S). Biological replicates were individually barcoded, pooled, and sequenced on

two lanes of a HiSeq 2000 platform for 100x2 bp paired-end RNA-seq at the Penn Next Generation Sequencing Core (NGSC) Facility. Alignment and expression values were determined using RUM (Grant et al., 2011).

Characterization of alternative splicing switches

RNA-Seq reads were mapped to the reference mouse genome (mm10) using STAR with the option --alignSJoverhangMin 8 (Dobin et al., 2013). Alternative splicing events were analyzed using MAJIQ and VOILA with the default parameters (Vaquero-Garcia et al., 2016). Briefly, uniquely mapped, junction-spanning reads were used by MAJIQ to construct splice graphs for transcripts by using the Ensembl transcriptome annotation (release 82) supplemented with de-novo detected junctions. Here, de-novo refers to junctions that were not in the Ensembl transcriptome database, but had sufficient evidence in the RNA-Seq data (default: at least three reads mapping to at least two different start positions). The resulting gene splice graphs were analyzed for all identified local splice variations (LSVs), defined as splits in a splice graph to or from a given exon. Redundant LSVs were removed and each junction in the remaining LSVs was quantified for its expected percent spliced in (PSI) value in control and *Esrp1*$^{-/-}$ samples and expected change in PSI (ΔPSI) between WT and *Esrp1*$^{-/-}$ samples. PSI and ΔPSI correspond to the percent of isoforms and change in percent of isoforms, respectively, that use a specific junction compared to the other junctions in the given LSV. LSVs comprised of one or more junctions with an expected ΔPSI of at least 10% were then utilized by VOILA to produce gene and LSV splice graphs as well as violin plots representing PSI and ΔPSI quantifications (Table S1).

Quantification and Statistical Analysis

Statistical analysis of cell counts and splicing assays were performed using GraphPad Prism 7 software. Relevant information for each experiment including n-values, statistical tests and reported p-values are found in the legend corresponding to each figure. In all cases $P<0.05$ is considered statistically significant.

Cell counts were performed from equivalent sections through the cochlear duct using the cell counter feature in ImageJ. Cochlear length was measured from E14.5 paint fills and E18.5 and P0 cochlear epithelium preparations from the most basal to most apical turn of the cochlear duct using ImageJ.

RNA-seq results were processed using edgeR (Robinson et al., 2010) to detect differentially expressed transcripts with fold change >0.4 ($P<0.05$).

Data and Software Availability

RNA sequencing data is accessible at NCBI Gene Expression Omnibus under accession number: GSE90821

Interactive HTML output files for visualizing splicing variations between WT and *Esrp1*$^{-/-}$ samples are accessible at: http://majiq.biociphers.org/rohacek_2016/ and Table S1.

KEY RESOURCES TABLE

REAGENT or RESOURCE	SOURCE	IDENTIFIER
Antibodies (dilution)		
mouse anti-Atp1A1 (1:250)	Developmental Studies Hybridoma Bank	A5
mouse anti-β-Actin M2 (1:10000)	Sigma	AC-74
rabbit anti-Barttin (1:1000)	Thomas Jentsch (Leibniz-Institut für Molekulare Pharmakologie)	N/A
rat anti-CD44 (1:200)	BD Parmingen	550538
rabbit anti-Claudin-11 (1:100 +AR)	Novex	364500
mouse anti-Connexin-26/Gjb2 (1:200)	Thermo Scientific	71-0500

mouse anti-E-cadherin (1:200 +AR)	BD Transduction Laboratories	610181
mouse anti-Esrp1 (1:200)	Russ Carstens (UPenn)	N/A
rabbit anti-Esrrβ/Nr3b2 (1:500 +AR)	Jeremy Nathans (Johns Hopkins Univ.)	N/A
goat anti-Kcnq1 (1:300)	Santa Cruz	SC-10646
rabbit anti-MyosinVIIa (1:500)	Proteus Biosciences	25-6790
mouse anti-Neurofilament (1:200)	Developmental Studies Hybridoma Bank	2H3
rabbit anti-P27kip1 (1:400)	Thermo Scientific	PA5-27188
mouse anti-Pou4F3/Brn-3c (1:200 +AR)	Santa Cruz	sc-81980
rabbit anti-Prox1 (1:500)	Chemicon Billerica	AB5475
rabbit anti-Otx2 (1:1000)	Flora Vaccarino (Yale University)	N/A
Mouse anti-Sox2 (1:200 +AR)	R&D Systems	MAB2018
donkey anti-mouse IGG Alexa488 (1:200)	Molecular Probes	A-21202
donkey anti-rabbit IGG Alexa594 (1:200)	Molecular Probes	A-21207
rabbit anti-goat IGG Alexa488 (1:200)	Molecular Probes	A-11078
donkey anti-rat Alexa488 (1:200)	Molecular Probes	A-21208
*AR, antigen retrieval – boil for 6 minutes in 10mM citric acid buffer (pH 6.0)		
Chemicals, Peptides, and Recombinant Proteins		
Phalloidin conjugated Alexa488 (1:50)	Molecular Probes	A-12379
Critical Commercial Assays		
NEBNext® Poly(A) mRNA Magnetic Isolation Module	New England Biosystems	E7490S
Directional RNA Library Prep Kit for Illumina®	New England Biosystems	E7420S
Deposited Data		
RNA-seq raw and analyzed data	This paper	GSE90821
MAJIQ splicing analysis	This paper	http://majiq.biociphers.org/rohacek_2016/.
Experimental Models: Cell Lines		
Human: patient derived IPSCs	This paper	N/A
Human: MDA-MB-231 cells	ATCC	HTB-26

Mouse: *Esrp1*$^{-/-}$ embryonic stem cells	Cieply et al. 2016	N/A
Experimental Models: Organisms/Strains		
Mouse: *Esrp1*$^{+/-}$	Bebee et al. 2015	N/A
Mouse: *Fgf9*$^{+/-}$ - B6N(Cg)-Fgf9$^{tm1b(KOMP)Wtsi/J}$	The Jackson Laboratories	0224362
Human: Family members screened for *ESRP1* mutations were enrolled under an IRB approved protocol of informed consent at the Children's Hospital of Philadelphia (CHOP)	This paper	N/A
Human: A cohort of 144 pediatric probands with bilateral SNHL were enrolled under an IRB approved protocol of informed consent at CHOP	This paper	N/A
Recombinant DNA		
PMX-CFF-B	Modified from Toshio Kitamura	N/A
Sequence-Based Reagents		
PCR Primers for human ESRP1 and ESRP2 exons see Table S3	This paper	N/A
Primers used to detect gene specific alternative splicing switches by RT-PCR.see Table S4	This paper	N/A
sgRNA oligos for ESRP1 (c.665_683 del) CRISPR: F: caccGATGGAACTTATTGGGCACG R: aaacCGTGCCCAATAAGTTCCATC	This paper	N/A
ESRP1 (c.665_683 del) repair template: TATTGAGTCCTTTGAAGAATCTTGCAATATCTTGA TCTGAAGACTGCCATGGTAAACCTCGTGCCCTGA CTACGGTGTTATCATCGATAAGTTCCATCTTGCT GCTGTGGATGAAGCAAAACTTCAGGTTGCATGAT AAA	This paper	N/A
ESRP1 (c.665_683 del) repair PCR genotyping primers: F: CACAGGCAGCCATGTTTCTA R: TAGGCAGTTGTCTTGCAGGG	This paper	N/A
Software and Algorithms		
RUM	Grant et al. 2011	http://www.cbil.upenn.edu/RUM/

edgeR	Robinson et al. 2010	https://bioconductor.org/packages/release/bioc/html/edgeR.html
MAJIQ	Vaquero-Garcia et al., 2016	http://majiq.biociphers.org/
STAR	Dobin et al., 2013	https://github.com/alexdobin/STAR

Table 2.1. Esrp1 dependent alternative splicing events in the cochlear epithelium.

(see attached Excel file)

Table 2.2 Expression values of selected genes from RNA-seq on E16.5 control and *Esrp1*$^{-/-}$ cochlear epithelium.

Gene	Control FPKM	*Esrp1*$^{-/-}$ FPKM	Fold Change	P-Value
Atoh1	3.46 ± 0.59	2.43 ± 0.38	-0.596	0.040
Atp1a1	96.99 ± 19.03	81.56 ± 4.37	-0.334	0.089
Bsnd	0.53 ± 0.14	0.01 ± 0.01	-5.029	8.513E-16
Cd44	1.92 ± 0.18	1.37 ± 0.10	-0.570	0.014
Cldn11	13.24 ± 4.30	13.12 ± 2.44	-0.161	0.546
Esrrb	10.61 ± 2.38	0.72 ± 0.33	-4.012	3.959E-40
Etv4	6.32 ± 1.14	9.17 ± 1.78	0.403	0.047
Etv5	11.50 ± 1.01	11.81 ± 0.33	-0.048	0.758
Fgfr1	17.18 ± 0.52	18.69 ± 0.65	0.029	0.954
Fgfr2	15.10 ± 2.02	12.43 ± 1.30	-0.343	0.076
Fgfr3	6.55 ± 1.22	3.91 ± .054	-0.796	2.055E-04
Gjb2	55.99 ± 9.04	39.31 ± 7.70	-0.547	0.012
Gli1	1.92 ± 0.17	1.58 ± 0.24	-0.341	0.188
Hey1	15.66 ± 1.85	13.05 ± 1.59	-0.318	0.096
Hey2	7.27 ± 0.41	8.51 ± 1.14	0.176	0.501
Kcne1	1.52 ± 0.3	0.06 ± 0.03	-4.503	9.817E-24
Kcnq1	1.72 ± 0.3	0.97 ± 0.38	-0.989	0.004
Myo7a	2.29 ± 0.43	1.89 ± 0.76	-0.441	0.093
Otx2	8.75 ± 2.75	18.29 ± 1.12	0.995	9.071E-05
Pou4f3	5.89 ± 0.69	3.49 ± 1.11	-0.914	0.004
Prox1	3.67 ± 0.18	2.02 ± 0.57	-0.876	0.001
Ptch1	6.54 ± 0.68	6.18 ± 1.30	-0.128	0.492
Sox2	19.14 ± 0.28	18.54 ± 2.95	-0.110	0.501

Table 2.3. PCR primers used to amplify human *ESRP1* and *ESRP2* exons.

ESRP1 Primers			
Exon	**Forward primer (5'-3')**	**Reverse Primer (5'-3')**	**Size (bp)**
Exon 1	TAGCAGTAGCAAGGAAGGGG	GGGTCCAGACTCACAAGTGG	396
Exon 2	GAGAGCTTTGATTCTGCGTC	ATGAAGAGAAGCAGCGACC	445
Exon 3	AAGGGGAGCTACTTTGCAG	AGAACAGAGAAACTTGAATAAACC	279
Exon 4	TAGGTTCCTAATTGTGAGAGAAAC	ATTTTGGATAGGCCAATTTTATC	450
Exon 5-6	GTTGAATGACTGACTGATGGG	ATTAGCCAGGTATGGTAGCG	662
Exon 7-9	AACTAGGCAGTTGTCTTGCAG	AAAACCATTCATGACCCTATTC	686
Exon 10	CATTGGCAGGACTTTTATCAC	TGAGCAATGTAGGACTATTTTCAG	469
Exon 11	GTATCATGCTTTCCCTGCTG	CTTAGTGTGTAACTGAGGATTACG	675
Exon 12	TTGTCACTTTGCATGTTTTG	AGGGGCACAGAAAGTTACG	369
Exon 13	TGTGTAGATGGAACAGTGACTATG	GAGCTCTTGCACTGGCTATC	334
Exon 14	GCTCTGAGAAGTATAAGAAAGGTTG	ATCTGTTTCTTTCCTGGCTG	360
Exon 15	TCTAAATGTCCTATACTTTTGTTGG	TCTAAATGCCTTCAGAATCTTG	286
ESRP2 Primers			
Exon	**Forward primer (5'-3')**	**Reverse Primer (5'-3')**	**Size (bp)**
Exon 1-2	GTAACTCGCCTGGAGAGGG	ACAAGAGCCCAGTCCTGC	844
Exon 3-4	TTCCTCCTACCCTCACTTCC	ATACTCAGACACATGTACCCACAG	475
Exon 5	GGAGTAAACAGGATTAGTGCTTATG	GAGCAATAGGCATTTGTCATC	217
Exon 5	GTGTCTATGGAGGGGAGTTG	TAGAGAAGGTCACAGTGGGG	265
Exon 6-8	GCAGAACTTGGTGGGGAC	TATACACCTGTGGGTACAGAGAGC	599
Exon 6-8	TTTTGCAGAACTTGGTGG	CACCTGTGGGTACAGAGAGC	599
Exon 9-10	GGCCAATCTGAGTCAGGC	GTAGGGCAGGGACACAGAG	612
Exon 11	AGATGTACTGTTACTCCAGGGC	TACCCCTAACACACACCCC	353
Exon 12	GTGTGTGTTAGGGGTAAGGC	TAGAAGGTAGGGGCTTACAACAG	331
Exon 13	ATAGCGGGGACTCCTTTC	TTCCCCAGATTGGGACAG	323
Exon14-15	GGTCTCGGTCTAGGCCAC	GTTGAGGGTGCTGGTCTTC	469

Table 2.4. Primers used to quantify changes in alternative splicing and gene expression by RT-PCR.

Alternative Splicing Primers		
Gene	Forward-Primer	Reverse-primer
Mouse		
Arhgef11	TCAAGCTCAGAACCAGCAGGAAGT	TGCTCGATGGTGTGGAAGATCACA
Col11a2	GGACGGCCCTCAGACTCAGAAG	GCCAGGGGGTCCAGCTAATCCAG
Col11a2	GCCGCCCTGTCCGCTTTCTC	GGCCCTTGTCACCCCCACTACTG
Csnk1d	CTCACGGGCCGACAAGATACCT	GAGCTCCCGGCGTTAACATTTCAG
Ctnnd1	AACCTCGCTGGATTTGTCTTTC	TGATCCTGGGGTCCGTTGAGTTTC
Dgkd	CTAAACGCAGCCGTAGTGGTAAA	TTTGTTAGAGACAGGAAGCCCAAT
Enah	GCTGGGCGTGGGAATGGACCTCTT	TTGCCAGCTCTTTTCTCATCTCAT
Epb4.1	TTAACATCAACGGGCAAGTC	ATATCGGCATCTCCTGTGA
Eya4	GAGGTGCTTTCCCCATTG	ATTTCATCCGTTAAGACCATT
Eya4	TCCCCATTGAGAACATTTACAG	AGAGGTCCGAGTGGCTTGATA
Fgfr1	CCTGGGCAGCAATGTGGAGTT	AAGGCCCCGGTGCAGTAGATA
Fgfr2	CCCGGGTCTAGATTTATAGTGATGC CCAGCC	CCCGGGGAATTCACCACCATGCAGG CGATTAA
Fgfr3	TGCCGGCCAACCAGACAGC	GCGCAGGCGGCAGAGTATCACA
Flnb	GGCGAGGAGGTGGGCTTTGTAG	CCTGACGGCAAATGGAATCACCAA
Ganab	GCCCGGCTTTCTGTCTCTGGTC	CATCCCTGGGTGTTTCCTCA
Limch1	AGAGCCTGAAGCAACCCTGACG	TCGCCGGCGCTCCTCTTCT
Lsm14b	CCTCGGCGACACAGCTCAATGGT	ATCACAGCTGGGTCCTTCTCTTCC
Map3k7	TTCCTGCCACAAACGACAC	ATTCTGACACTAGGGCTGGATGAC
Nf2	TGACTTCAAGGATACGGACAT	CAAACAAGCCAGCCCTCTACT
Ocrl	TGAACTCCGGTGAAGATAAGATTG	GAAGGGGTCGCTCACTGGTA
Phactr4	TGGAAGCAGGGGACACAACAC	GGGCTAGAGGACCTGGCACTG
Ralgps2	ACCTGCTGGATGATAGTGTC	CTTCAGAGATTTGGCGGCATAGTA
Scrib	ATCCGCAAAGACACGCCCCACTAC	AGCCTTTTCCCCCTGCGATACTGA
Sec22c	CAGCCCTGGGTGTCCTCTC	CCAGCATCAGCAGCACCTTCA
Human		
ARHGEF11	GAAATTCTGGGATATGGGAGTC	GCCTGTTGAGCTTGAGAGTGA

ENAH	TGCTGGCCAGGAGGAGAAGA	ACTGGGCTGTGATAAGGGTGT
NF2	TGGCAGCAGCAAGCACA	CCCGGTAGCAGGAGAAGT
RALGPS	AGACCTCATGGCCTGCTTTTG	TGTAGGCTTTTTGCCTTCTTT
SYBR Green Primers		
hβACTIN	AGGCACCAGGGCGTGAT	GCCCACATAGGAATCCTTCTGAC
hESRP1	TGATCTTCGAAAAGAATTCAAGAAA	CGAGAGACTGAACTACTCTTCTCAAAA
hESRP2	CCCTACATGCTCTGCACTGA	GGAATTCTCTTCGGAGGTCA
mB2M	TCTCTCTTTCTGGCCTGGAG	AATGTCGGATGGATGAAACC
mAtoh1	ATGCACGGGCTGAACCA	TCGTTGTTGAAGGACGGGATA
mGli1	GGAAGTCCTATTCACGCCTTGA	CAACCTTCTTGCTCACACATGTAA
mHey1	CACTGCAGGAGGGAAAGGTTA	CCCCAAACTCCGATAGTCCAT
mHey2	AAGCGCCCTTGTGAGGAAA	TCGCTCCCCACGTCGAT
mPtch1	CTGGCTCTGATGACCGTTGA	GCACTCAGCTTGATCCCAATG

Chapter 3: *Gas2* is a Shh responsive gene required for hearing

Introduction

Hedgehog genes

Originally identified in a screen for developmental mutants in *drosophila* larvae, the Hedgehog (*Hh*) gene was named for the ectopic denticle phenotype seen in these animals which resemble the spikes on a hedgehog (Nüsslein-Volhard and Wieschaus, 1980). *Hh* mutant larvae also display a complete failure in anterior-posterior patterning and do not form a segmented body plan. This, and similar patterning phenotypes, are common amongst *Hh* mutants as these proteins are some of the most well described morphogens, molecules that diffuse across a tissue and pattern responding cells in a time and concentration gradient manner. Since their initial discovery, *Hh* genes have been found to play roles not only in developmental patterning, but also in cell proliferation, survival, and differentiation.

Orthologs to drosophila *Hh* are found in vertebrates (Echelard et al., 1993). Due to genome duplications in this clade, vertebrate *Hh* genes fall into three families: Desert Hedgehog (*Dhh*), Indian Hedgehog (*Ihh*), and Sonic Hedgehog (*Shh*). *Dhh* is expressed is a subset of gonadal cells and mutants for this gene present with infertility (Bitgood et al., 1996). I*hh* transcripts are found in the primitive endoderm and chondrocytes of the bone growth plates (Colnot et al., 2005; Dyer et al., 2001; St-Jacques et al., 1999). Mouse mutants for *Ihh* display variable phenotypes with half of the embryos dying from vasculature defects in the yolk-sac and the remaining having abnormal bone development. Humans with *Ihh* mutations develop acrocapitofemoral dysplasia, a disorder characterized by short stature and skeletal defects (Hellemans et al., 2003).

Shh is the most widely, and dynamically, expressed of the vertebrate *Hh* orthologs. Early in embryogenesis, *Shh* is expressed from the floorplate and notochord and is responsible for left-right and dorsal-ventral (DV) patterning (Echelard et al., 1993). This expression is maintained through mid to late gestation and functions to pattern the central nervous system and placodal derived structures such as the eye and inner ear (Chiang et al., 1996; Riccomagno et al., 2002). In the limb-bud, *Shh* is expressed in the zone of polarizing activity and is required for distal patterning of the limbs (Chiang et al., 1996; Echelard et al., 1993). As development progresses, *Shh* signaling is also active and plays roles in the organogenesis of nearly all epithelial tissues and organs. Mouse knockouts for *Shh* are profoundly dysmorphic and lack any defined anterior structures, such as the head, limbs and many internal organs (Chiang et al., 1996). Humans and other animals with defects in Hh signaling often present with holoprosencephaly and cyclopia, a failure to separate the eye fields and cerebral hemispheres, which results in late prenatal or early postnatal lethality (Belloni et al., 1996; Roessler et al., 1996).

Hedgehog signaling

While the core components of the Hedgehog signaling pathway are conserved between invertebrates and vertebrates, the latter contain additional factors that add to its complexity, thus the vertebrate system will be discussed here. Within the secreting cell, Hh protein is proteolytically cleaved into N- (N-Hh) and C-terminal (C-Hh) fragments (Bumcrot et al., 1995). The C-Hh acts as a posttranslational intermediary, transferring cholesterol to the N-Hh fragment which is thought to direct it to the secretory machinery (Kelley et al., 1996; Roessler et al., 1997). The N-Hh is secreted from the expressing cell and binds its cognate receptors on the receiving cells.

The Hh responsive cell expresses a host of specialized proteins required for signal transduction: the receptor, a 12-pass transmembrane receptor Patched (*Ptch*); co-receptors, Cell Adhesion Associated, Oncogene Regulated (*Cdo*), Brother of Cdo (*Boc*) and Growth arrest specific 1 (*Gas1*); the obligate transducer, a G-protein-coupled receptor-like seven-pass transmembrane protein Smoothened (*Smo*); and the Glioma-associated transcription factors (*Gli1*, *Gli2*, and *Gli3*) (Allen et al., 2007; Goodrich et al., 1997; van den Heuvel and Ingham, 1996; Hui et al., 1994; Kinzler et al., 1988; Lee et al., 1997; Marigo et al., 1996; Tenzen et al., 2006; Zhang and Jetten, 2001). Interestingly, in vertebrates the primary cilium (PC) is required for Hh signaling and many pathway components are localized there during signal response, though the exact reasons for this remain uncertain (Huangfu and Anderson, 2005; Huangfu et al., 2003; Liu et al., 2005).

In the absence of Hh ligand, Ptch is localized to the PC and prevents the accumulation of Smo therein, forcibly repressing the pathway (Rohatgi et al., 2007; Strutt et al., 2001; Taipale et al., 2002; Fig. 3.1A). Gli2 and 3 are bound by Suppressor of fused (*Sufu*) and sequestered into the cytoplasm where they are phosphorylated (Ding et al., 1999; Kogerman et al., 1999; Liu et al., 2005; Svärd et al., 2006). The phosphorylated Gli2/3 are then proteolytically cleaved (Haycraft et al., 2005; Pan et al., 2006; Wang et al., 2000). Gli2 is a transcriptional activator while Gli3 contains an N-terminal repressor domain and a C-terminal activator domain. Phosphorylation and cleavage marks the C-terminus for degradation, destroying Gli2 and allowing the N-terminus of Gli3 to translocate to the nucleus and act as a transcriptional repressor.

Binding of Ptch by Hh ligand internalizes much of the receptor-ligand complex, and allows Smo to translocate to the PC (Chen and Struhl, 1998; Corbit et al., 2005;

Martín et al., 2001; Murone et al., 1999; Fig. 3.1B). The exact mechanisms by which Smo localization are controlled are still under investigation, however, recent evidence has found that phosphorylation and cholesterol modifications accumulate on Smo during pathway activation and are prevented by Ptch localization within the cilia (Li et al., 2016; Martín et al., 2001; Xiao et al., 2017). Interestingly, this data corroborates findings that chemical Smo agonists cyclopamine, sonidegib, and vismodegib all bear structural similarity to cholesterol (Chen et al., 2002; Incardona et al., 1998). Activated Smo re-localizes the Sufu-Gli complex to the cilia, relieving the repression of Gli by Sufu (Ding et al., 1999; Kogerman et al., 1999; Liu et al., 2005; Svärd et al., 2006). Gli2/3 then remain in their full-length isoforms and translocate to the nucleus to act as transcriptional activators of Hh target genes, such as Gli1 (Haycraft et al., 2005; Lee et al., 1997; Pan et al., 2006; Wang et al., 2000). Interestingly, an additional Hh target gene is its receptor Ptch, which acts as a negative regulator of the pathway, likely to dampen and prevent overactive signaling (Chen and Struhl, 1996; Goodrich et al., 1997).

Growth Arrest Specific 2

The Growth Arrest Specific (*Gas*) genes were initially identified as transcripts with increased expression in mouse fibroblasts that had been serum starved into cell cycle arrest (Schneider et al., 1988). Growth arrest specific 2 (*Gas2*) was the second such identified transcript and is now known to encode for a cytoplasmic protein that interacts with the cytoskeleton (Brancolini and Schneider, 1994; Brancolini et al., 1992, 1992, 1995; Zhang et al., 2011). The N-terminus of the Gas2 protein contains an actin binding Calponin homology (CH) domain while the C-terminus encodes for a microtubule binding Gas2 domain (Brancolini et al., 1992b, 1995; Zhang et al., 2011a; Fig. 3.6A).

Gas2 itself is conserved only through vertebrates with orthologs found in zebrafish and lamprey, but is also part of a larger gene family known as the *Gas2*-like genes (Goriounov et al., 2003; Stroud et al., 2011, 2014; Zhang et al., 2011). Gas2-like proteins contain the same basic domain structure but also contain additional extensions of the C-terminal tail. Members of the Gas2-like family are conserved through flies and include the cytoskeletal linker Pickled Eggs (*Pigs*) (Girdler et al., 2016; Pines et al., 2010).

Gas2 and the Gas2-like proteins have been shown to interact with the cytoskeleton. In mouse and human cell lines, Gas2 colocalizes with actin and microtubules by immunofluorescence and in co-sedimentation and western blot assays (Brancolini et al., 1992; Girdler et al., 2016; Goriounov et al., 2003; Stroud et al., 2011). Structure function analyses have demonstrated that the CH and Gas2 domains interact with actin and microtubules respectively and that many Gas2-like proteins, including Pigs, have been shown to act as cross linkers between these two fibers. Interestingly, the Gas2-like proteins have also been shown to stabilize microtubules by interacting with end binding (EB) proteins that coat the tubule plus end (Goriounov et al., 2003; Stroud et al., 2014; Girdler et al., 2016). This interaction relies on the extended C-terminal domains found in Gas2-like proteins that is absent in Gas2 itself, leaving open the question of whether this function is conserved in the Gas2 protein. Gas2 has also been shown to be a target for caspase mediate cleavage, generating short CH containing and Gas2 domain containing fragments (Benetti et al., 2001; Brancolini et al., 1995; Lee et al., 1999; Sgorbissa et al., 1999; Zhang et al., 2011). The Gas2 domain fragment, as well as full length Gas2, has been shown to localize to microtubules during apoptosis and to prevent cell cycle progression in cell culture and *Xenopus* embryos.

The expression of *Gas2* has been described in only a few circumstances and its function in many of these tissues remains unclear. In culture, Gas2 is detected at the cell border and along actin based stress fibers and its expression is greatly increased under mitotic arrest conditions and during apoptosis (Benetti et al., 2001; Brancolini and Schneider, 1994; Brancolini et al., 1995; Lee et al., 1999). Overexpression of *Gas2* in cell culture induces membrane ruffling and can prevent mitosis, suggestive of a critical role for Gas2 in regulating cell cycle progression and cell death. In the mouse embryo, *Gas2* expression was found to be dynamic between E11.5 and E14.5 in the developing axial skeleton and myogenic regions of the limbs (Lee et al., 1999). *Gas2* is first expressed in and around sites of chondrocyte recruitment that will form the bone scaffolds, then becomes localized to regions of apoptotic cells in the interdigital tissues and surrounding mesenchyme. At E16.5, *Gas2* is also found in the somatic cells of the developing female gonad (York et al., 2016). This expression is maintained into adulthood and is restricted to the stromal tissue that surrounds the ovarian follicles. Few other studies have analyzed *Gas2* and so the full extent of expression remains to be determined.

Mouse knockouts for *Gas2* have recently been described, though with a narrow phenotypic focus (York et al., 2016). Broadly, *Gas2*-null mice are born in normal Mendelian ratios and exhibit no overt morphological or behavioral deficits. Female *Gas2* mutants were found to be infertile due to defects in oocyte cyst breakdown, follicle growth, and basal lamina organization. This phenotype correlated with an increase in *Notch1* expression and subsequent decreases in Notch signaling within the ovary. Interestingly, a similar phenomenon can be seen in *Pigs* deficient *Drosophila*, which demonstrate fusion of the egg chambers associated with alterations in Notch signaling

(Girdler et al., 2016; Pines et al., 2010). How *Gas2* regulates aspects of Notch signaling, as well as the potential for additional roles of *Gas2* in vertebrate development are areas in need of further investigation.

Rationale

While numerous genes have been implicated as playing key roles in the development of the cochlear duct and sense of hearing, many facets of this structure's origins, cell types, function and maturation still lack genetic and/or mechanistic components. Shh signaling has been shown to be crucial for the proper development of the cochlear duct (Bok et al., 2007; Brown and Epstein, 2011; Riccomagno et al., 2002). Mouse embryos with an inner ear specific deletion of smoothened (Smo^{ecko}) display a complete failure of cochlear outgrowth and morphogenesis as well as a loss of ventral otic identity (Brown and Epstein, 2011). We sought to utilize these embryos to discover new inner ear specific Hh targets as well as genes that might play novel roles in cochlear development and hearing.

In this study, we performed an RNA-seq experiment comparing control and Smo^{ecko} mutants at E11.5, a time point where the first outgrowth of the cochlear duct can be observed, and identified genes with the potential to be Hh targets and have novel functions in the inner ear. The expression of a number of these genes was examined by in situ hybridization and Shh signaling responsiveness validated on two different mutant backgrounds. Of the validated genes, *Gas2* was selected for further study based on its expression domain and potential to act as a regulator of cochlear morphogenesis. *Gas2* mutant mice were generated and examined for defects in cochlear development and function. While no defects were seen embryonically, adult *Gas2* mutants presented with severe hearing impairment in the absence of morphological defects of the cochlear duct.

Gas2 was found to be expressed in the supporting pillar and Deiter's cells of the organ of Corti and *Gas2*-null animals had progressive defects in microtubule organization within these cells that correlate with the onset of hearing. These findings implicate *Gas2* as a Shh responsive gene that is critical for the maintenance of the pillar cell cytoskeleton and sense of hearing.

Results

RNA-seq reveals novel Shh targets in the developing cochlea

To identify novel Shh targets, as well as discover genes with novel functions in cochlear development, we performed RNA-sequencing to compare the expression profiles of E11.5 control (*FoxG1Cre;Smo*$^{Loxp/+}$) and Smoothened ear conditional knockout (*FoxG1Cre;Smo*$^{\Delta/Loxp}$, referred to as *Smo*^{ecko}) otic vesicles. *Smo*^{ecko} mutants lack ventral otic tissues, including the cochlear duct, but retain the dorsal vestibular structures allowing us to enrich for genes expressed in the presumptive cochlear duct upon comparison with controls. We found 1,222 differentially expressed genes (FDR<0.05, RPKM>1) with 630 downregulated and 592 upregulated transcripts in *Smo*^{ecko} otic vesicles compared to controls (Fig. 3.2A). Genes found to be downregulated were enriched within gene ontology terms associated with inner ear morphogenesis, positive regulation of transcription, and sensory perception of sound as revealed by the DAVID 6.8 analysis tool (Fig. 3.2B). Genes that were upregulated did not fall into any inner ear specific categories (GO terms: positive regulation of epithelial to mesenchymal transition, positive regulation of cell migration, cell adhesion) and were not included for further analysis (Data not shown). Amongst the most differentially expressed downregulated genes several with known cochlear duct expression and roles in inner

ear development are found including *Otx2*, *Rspo2*, *Emx2*, *Pax2*, *Hey1* and *2*, *Eya1*, *Gata3*, *Sox2* and *FoxG1*. Further, *Gata3*, *Otx2*, and *Pax2* have previously been described as Shh responsive genes in the otocyst, providing evidence that our screen had identified cochlear enriched genes that may be Shh targets (Brown and Epstein, 2011; Fig. 3.2C).

To validate potential novel cochlear enriched genes we performed in situ hybridization and fluorescent antibody staining on E11.5 WT otic vesicles (Fig. 3.2D-AB; Fig. 3.5A,D). In addition to 4 previously described Shh responsive targets (*Gata3*, *Gli1*, *Otx2* and *Pax2*) the expression of 21 downregulated genes was examined. We found that all examined genes are expressed in the ventral otic epithelium, confirming that the RNA-seq experiment had enriched for cochlear transcripts. Interestingly, these genes were expressed in one of four discrete territories that overlapped the patterns of *Gata3*, *Gli1*, *Otx2* and *Pax2*. *Gli1* is broadly expressed throughout the ventral otic epithelium and marks the region responsive to Shh signaling (Fig. 3.2D). Six of the tested genes (*Dsp*, *Emx2*, *Eya1*, *Eya4*, *Mpzl2*, and *Pchdh11x*) showed a similar pattern of expression in the ventral otic vesicle (Fig. 3.2E-J). The ventral medial wall is marked by *Pax2* expression at this stage and additionally expresses 7 validated genes (*Brip1*, *Car13*, *Gas2*, *Fam107a*, *Fat3*, *Pls1* and *Six1*) (Fig. 3.2K-Q). The presumptive sensory epithelium at the ventral most tip of the otic vesicle expresses *Gata3* as well as 7 genes (*Ano1*, *Fst*, *Jag1, Lin28b*, *Slc39a8*, *Sox2*, and *Thrβ*) from our dataset (Fig. 3.2R-Y; Fig. 3.5A). Otx2 is expressed along the lateral wall of the otic vesicle along with two additional genes (*Capn6* and *Rspo2*) (Fig. 3.2Z-AB). In addition to these 21 downregulated genes, we also interrogated the expression of *Jag1* as a known regulator

of sensory cell fate that showed the potential to be a Shh target gene though it did not meet statistical significance in this experiment (FDR=0.156) (Fig. 3.2V; Fig. 3.5D).

We next sought to determine if the genes identified in our RNA-seq data set were regulated by Shh signaling. Given that the ventral otic tissue is absent in *Smo*^{ecko} mutants, transcripts could be identified as downregulated in this experiment because they require Shh signaling for their expression or because the tissue in which they are expressed is missing. To address this question, we examined expression of the identified genes by in situ hybridization or immunofluorescence on *Smo*^{ecko} otic vesicles at E10.5 (Fig. 3.3A-Q; Fig. 3.5G-J). At this stage the *Smo*^{ecko} mutant vesicle is morphologically similar to controls and thus any loss of expression would be presumed to originate directly from lack of Shh responsiveness. We were able to analyze the expression of 18 potential target genes in control and *Smo*^{ecko} mutants, 3 additional genes (*Fst*, *Pcdh11x*, and *Thrβ*) did not show expression in control tissue at this stage (data not shown). We found that expression of the majority of the analyzed genes (13/18) is completely abrogated in the *Smo*^{ecko} otic vesicle, suggesting that Shh signaling is required for their expression (Fig. 3.3A,B,E-J,L,N-Q).

The remaining 5 genes (*Eya1, Eya4*, *Jag1*, *Six1*, and *Sox2*) demonstrated a more complex response to loss of Shh signaling. *Eya1* and *Eya4* are expressed in a broad ventral pattern in controls of which the lateral domain is preserved in *Smo*^{ecko} mutants while the medial expression is lost (Fig. 3.3C,D). *Jag1*, *Six1*, and *Sox2* are restricted to a ventral medial domain in controls which is lost in the *Smo*^{ecko}. Interestingly, these genes also show a gain of ectopic expression on the lateral wall of the otic vesicle, which is maintained for Jag1 and Sox2 at E11.5 (Fig. 3.3K,M; Fig. 3.5C,F,G-J). These

data suggest that Shh signaling may be part of a more complex regulatory logic that governs the expression of this subset of genes.

Finally, we wanted to determine if Shh signaling was sufficient to drive the expression of genes identified by our experiment. To accomplish this, we performed in situ hybridization on E11.5 otic vesicles from a mouse line that ectopically expresses Shh ligand in the dorsal otocyst (*ShhP1*) (Fig. 3.4A). The majority (21/24) of the tested genes showed responsiveness to the ectopic Shh source and demonstrated altered expression domains (Fig. 3.4B-V). Many genes (*Ano1*, *Brip1*, *Exm2*, *Fam107a*, *Fst*, *Gas2*, *Gata3*, *Hey1*, *Jag1*, *Lin28b*, *Pax2, Pls1*, *Six1*, and *Sox2*) demonstrated induction of an ectopic, dorsal, expression domain that, at least partially, overlaps the region of *Shh* expression (Fig 3.4B,C,H,I,K-T; Fig. 3.5B,E). The expression domains of a subset of genes (*Car13*, *Slc39a8*, and *Thrβ*) were expanded laterally (Fig. 3.4J,U,V) while *Dsp*, *Eya1*, *E*ya4, *Mpzl2*, and *Pchd11x* became expressed throughout the entire otic vesicle (Fig. 3.4B,D-G). As the expression of these genes were also altered in the Smo^{ecko} mutants we conclude that Shh signaling is both necessary and sufficient for their expression. Interestingly, the genes expressed along the ventral-lateral wall of the otic vesicle (*Capn6*, *Otx2*, and *Rspo2*) did not show any alterations in their expression patterns in the *ShhP1* embryos (Fig. 3.4W-Y). We thus conclude that Shh signaling is required for the expression of these genes, however, it alone is not sufficient to induce it.

Gas2 is dynamically expressed in the developing and mature cochlear duct

From our list of Shh responsive genes we next set out to identify potential novel regulators of cochlear development. We chose to pursue *Growth Arrest Specific 2* (*Gas2*) based on its expression in the ventral otic vesicle at E11.5 and its previously described functions as a cytoskeletal binding protein which, we hypothesized, made it a

good candidate regulator of cochlear morphology and/or function (Fig. 3.6A,D). Previous studies have found that *Gas2* is expressed in the developing axial skeleton as early as E11.5, an observation we confirm by in situ hybridization, and maintained at least through E14.5 in the condensing mesenchyme and chondrocytes of the long bones (Fig. 3.6B). No previous data existed describing the expression of *Gas2* during inner ear development so we performed a time course of in situ hybridization to address when and where this gene is expressed in the cochlear duct. *Gas2* expression is detected in the ventral tip and medial wall of the otic vesicle starting around E10.5 and is maintained at E11.5 (Fig. 3.6C,D). At E14.5 *Gas2* transcript is detected in the presumptive sensory epithelium in the medial cochlear duct, although at a lower level than seen at E10.5 and 11.5, and low-level expression can be seen on the lateral wall (Fig. 3.6E). Through the remainder of prenatal development (E16.5-E18.5) expression is undetectable in the region of the developing organ of Corti but is maintained and upregulated on the lateral wall, particularly in the developing stria vascularis (Fig. 3.6F,G). Postnatally, *Gas2* is expressed in multiple cochlear regions including Reissner's membrane, the stria vascularis, the outer sulcus and the organ of Corti (Fig. 3.6H,I).

To better characterize the complex postnatal expression of *Gas2* we stained sectioned cochleae with a Gas2 specific antibody. At E11.5 the Gas2 antibody labels cells along the ventral medial wall of the otic vesicle in an identical pattern to *Gas2* transcript expression as detected by in situ hybridization, suggesting that the antibody is appropriately detecting endogenous Gas2 (Fig. 3.6J). Postnatal analysis at P14 confirms *Gas2* expression in the stria vascularis, spiral ligament, and the organ of Corti. Interestingly, within the organ of Corti, Gas2 is detected within the supporting pillar and Deiters' cells and is excluded from the sensory hair cells (Fig. 3.6K,L).

Generation of a *Gas2* knockout mouse line

To interrogate the function of *Gas2* in inner ear development, we generated a *Gas2* deficient mouse line utilizing ES-cells from the European Conditional Mouse Mutagenesis Program (EUCOMM) as part of the International Knockout Mouse Consortium (IKMC). ES-cells generated by the IKMC are a C57B/6N-Tac background and are heterozygous for a targeted Knockout first allele (tm1a) (Fig. 3.7A). This allele replaces an endogenous exon with one flanked by loxp sites and knocks-in a LacZ reporter and neomycin resistance cassette into the upstream intronic sequence. Exon 5 of the *Gas2* genomic sequence was targeted as it encodes for residues of both the actin and microtubule binding domains (Fig. 3.6A). The targeted allele is expected to produce a loss of function transcript due to a frameshift resulting in an early stop codon in exon 5 that would be a likely target for nonsense mediated decay.

ES-Cells containing the *Gas2* targeted allele (*Gas2*$^{tm1a/+}$) were injected into albino C57B/6N-tac blastocysts and chimeric mice obtained. High percentage chimeras (>90% black/agouti coat) were bred to albino C57B/6N-tac mice and the resulting pups were screened for the *Gas2-tm1a* allele by coat color and PCR genotyping (See methods and Table 3.1 for details). *Gas2*$^{tm1a/+}$ mice were intercrossed to generate homozygous animals. *Gas2*$^{tm1a/tm1a}$ mice are born at expected Mendelian ratios and display no defects in gross anatomy or behavior, similar to a previously described knockout line (York et al., 2016; Fig. 3.7C and data not shown). Loss of *Gas2* expression was confirmed by western blot on E14.5 limbs, as well as immunofluorescence and in situ hybridization on cochlear tissue at multiple stages (Fig. 3.7B,D-K). No Gas2 protein is detected in these samples and expression by in situ is profoundly reduced though not completely absent, a finding we attribute to the homology of the in situ probe to the 5' UTR of *Gas2*, thus

allowing it to detect newly transcribed mRNA that has yet to be degraded (Fig. 3.7D-K). An additional advantage of the EUCOMM Knockout first system is the ability to generate additional floxed and null alleles from the same construct. Experiments are underway to generate conditional (*Gas2-tm1c*) and null (*Gas2-tm1d*) alleles that can be utilized for additional experiments.

The development of the cochlea is unaffected by loss of *Gas2*

We examined *Gas2* mutants for defects in inner ear morphology at E14.5 using the paint fill technique (Fig. 3.8A,B). *Gas2* mutant inner ears did not present with any defects in gross morphology and all structures of the vestibular apparatus and cochlear duct appeared normal. We next stained sections through control and *Gas2* mutant ears at E11.5 and E18.5 with E-cadherin to look for any defects in early cochlear outgrowth or later maturation (Fig. 3.8C-F). At E11.5, the initiation of cochlear outgrowth is unperturbed by loss of *Gas2* and no detectable differences in morphology are seen at E18.5 between control and mutant samples. We further interrogated the development of the organ of Corti on control and mutant sections at E18.5 for hair (Myosin VIIa) and support (Sox2) cells as well as innervation (Neurofilament) and found that all were unaffected in *Gas2* mutants (Fig. 3.8.G-J). Examination of cochlear hair cells at E18.5 on whole mounted sensory epithelium revealed a normal compliment of these cells in the *Gas2* mutant embryos (Fig. 3.8K-M). We thus conclude that *Gas2* is not required for cochlear morphogenesis or for the development of the cell types within the cochlear duct during embryogenesis.

***Gas2* mutant mice have severe hearing impairment**

Given the lack of an embryonic inner ear phenotype and that the cell types of the cochlea appeared unaffected in *Gas2* mutants, we next sought to test these animals for

hearing deficits to potentially reveal a function for Gas2. Hearing was measured by auditory brainstem response (ABR) testing, utilizing both click and tone stimuli, in control and mutant animals at P42 and P70. Surprisingly, *Gas2* mutant animals displayed a failure to respond to click stimuli resulting in an abnormal ABR waveform, indicative of a defect in sensation at the level of the cochlea (Fig. 3.9A). When exposed to tone stimuli of varying frequencies, *Gas2* mutants showed an increased ABR threshold compared to controls (Fig. 3.9B). This defect was more pronounced at higher frequencies, with a ~50db upward shift between 20 and 56kHz, than lower frequencies which displayed a ~15db shift at 5kHz and a ~20db shift at 10kHz. These results were confirmed with an independent ABR cohort at P70 (data not shown).

We next sought a mechanism for the hearing loss detected in the *Gas2* mutant animals. Our previous observation that *Gas2* is expressed in the stria vascularis inspired us to ask if this tissue was functioning properly in these mutants. We stained control and *Gas2* mutant cochlea for markers of the multiple cell layers of the stria vascularis. The morphology of the stria vascularis appeared unchanged (Actin) and normal patterns of staining were observed for marginal (Kcnq1 and Atp1A1), intermediate (CD44), and basal (Claudin 11 and Connexin 26) cells in the *Gas2* mutants, indicating that these cells are both present and expressing the channel and junction proteins required for their function (Fig. 3.9C-N). To address the functionality of the stria vascularis we measured endocholear potential, a readout of ionic concentration within the cochlear duct, from control and *Gas2* mutant inner ears (Fig. 3.9O). No difference was found in the endocochlear potential of *Gas2* mutants when compared to controls suggesting that the stria vascularis is functioning as expected and that loss of *Gas2* in these cells in unlikely to be the cause of hearing loss in these animals.

To further interrogate hearing function in the *Gas2* mutants we measured distortion product otoacoustic emissions (DPOAEs). DPOAEs are reflective of outer hair cell amplifier function and basilar membrane mechanics. Interestingly, *Gas2* mutants displayed a lower DPOAE output than controls (Fig. 3.9P). Analysis of P42 sensory epithelium revealed a significant loss of outer hair cells, particularly in rows 2 and 3, in *Gas2* mutants compared to controls, however, inner hair cells and total hair cell numbers were unaffected (Fig. 3.9Q-T). In spite of these findings, the loss of a relatively small percentage of outer hair cells is unlikely to cause the altered DPOAEs or severe hearing deficit seen in *Gas2* mutants. While further analysis will be required to directly test outer hair cell functionality, our previous observations that *Gas2* is not expressed in these cells leads us to conclude that another mechanism is likely responsible for the altered DPOAE and ABR responses of *Gas2* mutants.

The pillar cell cytoskeleton is disrupted in *Gas2* mutant mice

In continuing to search for an explanation for the hearing deficits seen in *Gas2* mutant mice, we began to investigate a role for *Gas2* in support cells. Pillar cells have previously been described as containing dense networks of actin and modified microtubules to act as a structural support for the organ of Corti during hearing response (Arima et al., 1986; Chan and Hudspeth, 2005; Nam and Fettiplace, 2010, 2010; Slepecky et al., 1995; Tannenbaum and Slepecky, 1997; Tolomeo and Holley, 1997). Gas2 is a putative cytoskeletal interacting protein, binding microtubules and actin filaments, and is expressed in pillar cells. Based on this information, we examined the cytoskeletal networks of control and *Gas2* mutant pillar cells at P25. We confirm earlier reports that the pillar cells are enriched for post-translationally modified (acetylated and detyrosinated) microtubules as well as actin filaments (Fig. 3.10A,C,E,G). These

microtubule arrays are particularly evident in the pillar cell heads and phalangeal processes that extend between the rows of inner and outer hair cells. Surprisingly, we found that the pillar cells of *Gas2* mutants displayed severe defects in their microtubule network. The inner pillar cell head appears depleted of microtubules at the outer hair cell connection and only short, disordered, bundles remain at the inner hair cell connection (Fig. 3.10B,D,F). Staining for actin revealed a normal localization pattern and analysis of cellular morphology of the pillar cells showed no alterations in *Gas2* mutants compared to controls, suggesting that these cells are intact and that microtubules are uniquely affected by the loss of Gas2 (Fig. 3.10G-K).

We next set out to understand if the defects seen in *Gas2* mutant pillar cells was due to a failure to establish or to maintain the microtubule network. We analyzed control and *Gas2* mutants over a postnatal time course for detyrosinated tubulin, a marker of highly stable microtubules (Fig. 3.10L-W). Analysis of control and *Gas2* mutant pillar cells at P5, a time point when the cytoskeletal network is established, revealed strong staining for detyrosinated microtubules in both genotypes, suggesting that *Gas2* is dispensable for establishing the initial microtubule network in these cells (Fig. 3.10L-N). At P12 highly regular arrays of microtubule bundles are detected in control inner and outer pillar cell heads extending across the tunnel of Corti. *Gas2* mutants at this stage begin to display defects in microtubule organization with small gaps in the cytoskeletal network at the center of the inner pillar cell head, however, the total amount of microtubules is not affected (Fig. 3.10O-Q). At P16, shortly after the onset of hearing, *Gas2* mutant inner pillar cells display a marked reduction in tubulin, primarily at the center of the pillar cell head when compared to controls (Fig. 3.10R-T). These defects progress in the *Gas2* mutant such that by P25 nearly 75% of the microtubules have

been depleted from the inner pillar cell head compared to controls (Fig. 3.10O-Q). Interestingly, the outer pillar cell phalangeal process appears less affected in the *Gas2* mutants although occasional cells present with tubulin deficiencies or aberrant morphology (Fig. 3.10B,D,F,S,T,V,W).

To gain insight into the microtubule organization in the pillar cell body, we analyzed control and *Gas2* mutant sensory epithelia by transmission electron microscopy at P25. The body of control pillar cells display a dense meshwork of microtubules that occupy the majority of the cytoplasmic space (Fig. 3.11A,F). These microtubules are arrayed in regularly aligned rows and are tethered by crosslinking actin filaments (Fig. 3.11B,G). In *Gas2* mutants, we found that the microtubule network of the pillar cell body was disrupted when compared to controls (Fig. 3.11C,D,H,I). The bodies of *Gas2* mutant inner pillar cells show a trend for increased size and contained a more distributed network of microtubules when compared to controls (Fig. 3.11A-E). A small increase in cell size was found in *Gas2* mutant outer pillar cells along with alterations in microtubule distribution (Fig. 3.11F-J). The central region of *Gas2* mutant outer pillar cells contain irregularly spaced, single, microtubules with no apparent actin connections while small “islands” of interconnected microtubules remain at the periphery near the cell membrane. Close inspection of the disorganized microtubules of *Gas2* mutants revealed that these tubules appear to lack the actin crosslinks seen in controls that are required to maintain the cytoskeletal network (Fig. 3.11B,D,G,I). Combined with our immunofluorescence analysis, these data suggest that Gas2 is required for maintaining the microtubule cytoskeletal network in pillar cells.

Discussion

We utilized RNA sequencing to compare the transcriptomes of control and *Smo*^{ecko} otic vesicles and discovered a cohort of cochlear enriched transcripts. Our analysis of 21 of these genes by in situ hybridization on control inner ears at E11.5 revealed that they are expressed in four partially overlapping domains of the cochlear duct: broad ventral, medially restricted, ventral tip restricted, and lateral wall restricted. These domains are of particular note as they coincide with the expression patters of known Shh responsive transcription factors *Gli1*, *Pax2*, *Gata3*, and *Otx2* (Brown and Epstein, 2011). Based on these expression domains it is appealing to hypothesize that these transcription factors function downstream of, or in concert with, Shh signaling to regulate the activity of the examined genes. Analysis of the promoter regions and potential enhancers near genes in our dataset should be carried out to determine if binding sites for the transcription factors *Gli1*, *Pax2*, *Gata3*, and *Otx2* are enriched for in these regions and followed by ChIP studies to confirm these observations.

While our experiments do not address the regulatory logic of the analyzed genes, we are able to confirm that the majority of these show responsiveness to Shh signaling with in situ hybridization experiments on embryos with a loss of Shh signaling responsiveness (*Smo*^{ecko}) and with a gain of Shh in the dorsal otocyst (*ShhP1*). Further experiments will be required to test if these genes are direct targets of Shh signaling, however, two observations deserve attention. First, our results corroborate evidence for Shh responsiveness of a subset of analyzed genes. Previous experiments with an ear specific *Smo*^{m2} mouse line, which results in overactive Shh signaling response, and cochlear explants treated with Shh ligand found activation of *Hey1* and *2* (Benito-Gonzalez and Doetzlhofer, 2014; Tateya et al., 2013). We similarly find that *Hey1* shows

responsiveness to Shh signaling in our gain and loss of function studies, providing corroboration of these observations. *Fst* and *Bmp4* were described as being regulated by Shh signaling in an ear specific Smo^{m2} mouse line (Son et al., 2012, 2015). These genes were previously found to be expressed in an apical to basal gradient that correlates with auditory tonotopy, the ability of different regions of the cochlea to respond to different sound cues, and that an increase in *Fst* and decrease of *Bmp4* is observed in the Smo^{m2} inner ear. Here, we provide an additional example of *Fst* upregulation in response to ectopic Shh and that its expression is lost when Shh signaling is abrogated. While we did not examine *Bmp4* expression we note that it was identified as putatively upregulated in our RNA-seq dataset, suggesting a similar regulation by Shh. These data add support to the hypothesis that Shh signaling may be a factor in establishing, or maintaining, tonotopy in the cochlea.

Of interest, our expression analysis also contradicts a previous report that *Six1* is not regulated by Shh in the inner ear. In *Shh* null embryos *Six1* expression was found to be unaffected while we report alterations of *Six1* in the Smo^{ecko} and *ShhP1* lines (Ozaki et al., 2004). The discrepancies between these findings may be due, at least in part, to the alterations in Wnt signaling and gene expression patterns in the *Shh* null otocyst as well as a complex regulatory mechanism governing *Six1* expression. These findings are of particular interest as *Shh* and *Six1* null embryos share a similar inner ear phenotype, suggestive of cooperation between these factors. Further experiments will be required to address the responsiveness and cooperativity between Shh signaling and *Six1* expression and to reconcile these two reports.

An additional finding from our Shh signaling analysis is that the gene expression along the cochlear lateral wall is defined by a complex regulatory logic. Genes normally

restricted laterally at E11.5, *Otx2*, *Capn6*, and *Rspo2*, require Shh for their expression but are not activated in response to ectopic signaling. This suggests that additional regulators are required for their expression beyond Shh. Intriguingly, the loss of these factors coincides with the gain and/or maintenance of lateral expression for *Eya1*, *Eya4*, *Jag1*, *Six1*, and *Sox2* while their medial expression is lost. Previous reports of an inner ear specific deletion of *Otx2* found that the cochlear lateral wall of these mutants was re-specified into a sensory cell fate and ectopically expresses *Jag1* and *Sox2* (Vendrell et al., 2015). These data suggest that *Otx2* is downstream of Shh signaling and acts as a repressor of cell fate on the cochlear lateral wall. Further interrogation of the regulatory sequences of these genes along with other differentially expressed transcripts in the Smo^{ecko} mutant may reveal novel control mechanisms for sensory and lateral cell fates of the cochlear duct.

The goal of our RNA-seq experiment was to uncover novel regulators of cochlear development and function that are Shh responsive. We chose to pursue *Gas2* as a strong candidate gene given its previously described functions as a cytoskeletal binding protein. *Gas2* is expressed early in cochlear development at the ventral tip and along the medial wall and demonstrates responsiveness to alterations in Hh signaling in the ear. Later in development and postnatally, *Gas2* is enriched in the stria vascularis and support cells, particularly the pillar and Deiters' cells. We developed a *Gas2* knockout mouse line and found that cochlear morphogenesis and cell fate specification are unperturbed by the loss of this gene. In spite of these findings, *Gas2* mutant mice display profound hearing deficits. Another group has described that female *Gas2* deficient mice also present with ovarian dysfunction and low fertility (York et al., 2016). Interestingly, Perrault syndrome is a disorder characterized by hearing impairment and

female infertility due to ovarian failure caused by mutations in genes that function in the mitochondria: *CLPP*, *HARS2*, *HSD17B4*, *LARS2*, and *TWNK* (Gispert et al., 2013; Jenkinson et al., 2013; Lerat et al., 2016). The microtubule cytoskeleton is required for the proper localization of mitochondria and disruptions of this network, as seen in *Gas2* mutant mice, could lead to mislocalization and dysfunction of these organelles (Frederick and Shaw, 2007; Melkov and Abdu, 2018). This is particularly interesting as *Clpp* is also expressed in pillar and Deiters' cells at a similar timepoint as *Gas2* (Gispert et al., 2013). Experiments will need to be performed to address the localization and function of mitochondria within the Gas2 mutant pillar cells. Additionally, while Perrault syndrome has yet to be linked to disruptions in *GAS2*, we recommend that these and other cases where low fertility is comorbid with hearing loss be screened for mutations in *GAS2*.

Previous studies of *Gas2* mutant mice and *Pigs* deficient *drosophila* found an aberrant increase in Notch signaling that correlated with aspects of the ovarian phenotype in these models (Pines et al., 2010; York et al., 2016). Notch signaling is critically required in inner ear development for the specification of the proper numbers of hair and support cells (Brooker et al., 2006; Hao et al., 2012; Kiernan et al., 2006; Petrovic et al., 2014; Takebayashi et al., 2007; Tateya et al., 2011). Inner ear specific activation of Notch signaling, either embryonically or postnatally, leads to defects in sensory development with ectopic support cells, transformations of sensory cells, and dysmorphology of the cochlear duct (Campbell et al., 2016; Liu et al., 2012a, 2012b; Pan et al., 2013; Savoy-Burke et al., 2014; Tateya et al., 2015). As we did not observe any of these phenotypes in *Gas2* mutant cochlea we were not encouraged to investigate Notch signaling in these animals. While we do not anticipate observing an upregulation in

Notch signaling in *Gas2* cochlea it will be important for further studies to examine this pathway and rule out any potential contribution to the phenotypes seen in these mice.

Our findings that *Gas2* mutants exhibited hearing loss prompted us to examine the cell types in which this gene is expressed for signs of dysfunction. Mutations in genes affecting the function of the stria vascularis are known to cause hearing loss, thus, we examined the development and function of these cells (Chen and Nathans, 2007; Collin et al., 2008; Lee et al., 2000; Neyroud et al., 1997; Rickheit et al., 2008; Schlingmann et al., 2004). We found that the major cell types of the stria vascularis are intact in *Gas2* mutants and that endocochlear potential was generated normally. These data strongly suggest that the stria vascularis is not affected by the loss of *Gas2*. This leaves open the question of why *Gas2* is expressed in these cells and what its function therein may be. Little is understood about the cytoskeleton of the stria vascularis, however, it is known that adherens and tight junctions, protein structures often coupled to actin and microtubules, are required for its function (Chausovsky et al., 2000; Stehbens et al., 2006). A basal cell knockout of E-cadherin revealed that proper adherens junctions are required for generation of endocochlear potential, likely by preventing outward flow of ions from the endolymph (Trowe et al., 2011). In addition, mice deficient in Claudin-11, a critical component of tight junctions, display severe hearing loss coupled to decreased endocochlear potential in the absence of morphological defects (Kitajiri et al., 2004). While we found no evidence for a defect in the stria vascularis of *Gas2* mutants, it is intriguing to speculate on a potential link between Gas2 and E-cadherin or Claudin-11, or alternative roles for this gene in the stria vascularis that will need to be addressed in future studies.

The pillar cells of the organ of Corti possess a dense network of modified microtubules (Slepecky et al., 1995; Henderson et al., 1994; Tolomeo and Holley, 1997; Tannenbaum and Slepecky, 1997). Our observations of acetylated and detyrosinated microtubules in these cells are in agreement with previous findings and supports the idea that these cells contain a highly stable cytoskeletal network (Slepecky et al., 1995; Tannenbaum and Slepecky, 1997). We discovered that, in *Gas2* mutants the pillar cells microtubule network forms but is not maintained, such that around the onset of hearing these cells rapidly become depleted of tubulin. This suggests that *Gas2* is likely dispensable for building the cytoskeleton of the pillar cells but is required to maintain the microtubule network once hearing begins. Measurements of pillar cell stiffness by atomic force microscopy has found that this cellular property requires an intact microtubule network (Szarama et al., 2012a). Similar measurements on *Gas2* null pillar cells would corroborate these findings and lend additional insight into the defects seen in these mutants. Transmission electron micrographs of *Gas2* pillar cells revealed that the microtubules are disordered and lack many of the actin crosslinks required for their organization, indicative of a putative function for Gas2 as an actin/microtubule cross linker. Pillar cells that have been treated with Triton-X to disrupt actin-microtubule interactions also display a disorganization of the cytoskeleton, however, no in vivo experiment has yet tested the requirement for these crosslinks, or the pillar cell cytoskeleton in general, in hearing function (Tolomeo and Holley, 1997). These findings are particularly interesting as the morphology of the organ of Corti, including the pillar cells, appears largely unaffected by the loss of *Gas2*.

During the course of our experiments, we observed a dynamic loss of microtubules from the *Gas2* mutant pillar cell that appeared to begin near the central

region of these cells. This observation is of interest because it suggests that microtubules at the center of the cell are either more dynamic or more susceptible to catastrophe than those at the cell membrane. Adherens junctions, such as E-cadherin, are enriched at the cell-cell contacts of epithelial cells and recruit and stabilize the microtubule and actin cytoskeleton (Bellett et al., 2009; Chausovsky et al., 2000; Ligon et al., 2001; Stehbens et al., 2006; Waterman-Storer et al., 2000). It is likely that these interactions stabilize the microtubule networks in pillar cells and prevent catastrophe of these filaments longer than their more centrally localized counterparts. It is also possible that the central region of the pillar cell experiences quantitatively different forces during auditory evoked movements than the junctional regions which could increase strain on and destabilize microtubules (Chan and Hudspeth, 2005; Karavitaki and Mountain, 2007; Nam and Fettiplace, 2010). Further studies will be required to address the potentially stabilizing nature of adherens junctions in pillar cells and the stresses put on these cells during auditory responses.

The observed defects in the microtubule network of pillar cells coupled with the lack of phenotypes in other sites of *Gas2* expression lead us to conclude that pillar cell dysfunction is the root cause of the hearing deficits seen in these animals. While we found that *Gas2* mutant animals displayed loss of ~10% of outer hair cells this is unlikely to result in the level of hearing impairment or decrease in DPOAE response found in these mice. Additionally, *Gas2* is not found to be expressed in the sensory hair cells and their development and morphology appear unperturbed in these mutants. While additional work will be required to fully exclude any contribution of hair cell dysfunction to hearing loss in *Gas2* mutants, our findings suggest that these perturbation of these cells does not contribute to the phenotype. Our experiments have also determined that loss of

Gas2 expression from the stria vascularis is not contributing to hearing dysfunction. Previous work has described the requirement for pillar cells for the proper response to sound stimuli (Mansour et al., 2009, 2013; Mellado Lagarde et al., 2013; Shim et al., 2005). Furthermore, the microtubule cytoskeleton is likely required for the force bearing properties of these cells during hearing response (Chan and Hudspeth, 2005; Kraus and Aulbach-Kraus, 1981; Nam and Fettiplace, 2010; Slepecky et al., 1995; Szarama et al., 2012c; Tannenbaum and Slepecky, 1997; Tolomeo and Holley, 1997; Zetes et al., 2012). Of interest, we observed that the hearing loss in *Gas2* mutants was more severe at higher frequencies, corresponding to defects at the more basal regions of the cochlea. It has been observed that pillar cells at the cochlear base have a higher stiffness and greater numbers of microtubule than those at the apex, properties which are inversely correlated with basilar membrane stiffness (Dallos, 1996; Emadi and Richter, 2008; Kikuchi et al., 1991; Zetes et al., 2012). These intrinsic properties of the pillar cells and basilar membrane suggest that pillar cells at the base are reliant on their stiffness than those at the apex. This may explain the discrepancies in hearing impairment between high and low frequencies in the *Gas2* mutants. Based on these findings, we propose that the *Gas2* null mouse line may reveal, and provide an excellent model for testing, aspects of pillar cell functions that are required for hearing.

Author Contributions

Alex M. Rohacek[1], Tingfang Chen[1], Victor Muthu[1], Yao Yao[1], Staci M. Rakowiecki[1], Alexander S. Brown[1], Yingtao Zhao[1], Winnie Rao[2], Maria N. Geffen[2], Kevin K. Ohlemiller[3], Douglas J. Epstein[1]

[1]Department of Genetics, Perelman School of Medicine, University of Pennsylvania, Philadelphia, Pennsylvania, USA. [2]Department of Otorhinolaryngology, Perelman School of Medicine, University of Pennsylvania, Philadelphia, Pennsylvania, USA. [3]Department of Otolaryngology-Head and Neck Surgery, Washington University School of Medicine, St. Louis, Missouri, USA.

A.M.R, V.M, Y.Y, A.S.B, and D.J.E. conceived the study. A.M.R, V.M., Y.Y., A.S.B. and D.J.E designed mouse experiments. Y.Y., Y.Z. and A.S.B. contributed preliminary data not in the final study. A.M.R. and V.M. generated and analyzed RNA-seq data. A.M.R, Y.Y., S.M.R, and A.S.B. performed in situ hybridization experiments. A.M.R, T.C. and D.J.E. designed and performed all Gas2 experiments. A.M.R., S.M.R., W.R., M.N.G., and K.K.O. performed and analyzed ABR experiments. All authors analyzed the data, and discussed the results.

Acknowledgements

The authors would like to thank Klaus Kaestner, Jean Richa, and the Transgenic and Chimeric Mouse Facility at University of Pennsylvania for assistance with ES-Cell culture, blastocyst injections and generation of chimeric mice. We thank The Electron Microscopy Resource Laboratory of the University of Pennsylvania and the CBD Microscopy core for their assistance with imaging. We thank Benjamin Prosser and Eric

Joyce for their assistance with imaging and analyzing microtubule networks. This work was funded by grants from the National Institutes of Health, R01 DC006254 (DJE). AMR was supported by the Predoctoral Training Program in Genetics (T32 GM008216) and an NRSA fellowship F31DC014647.

Figures

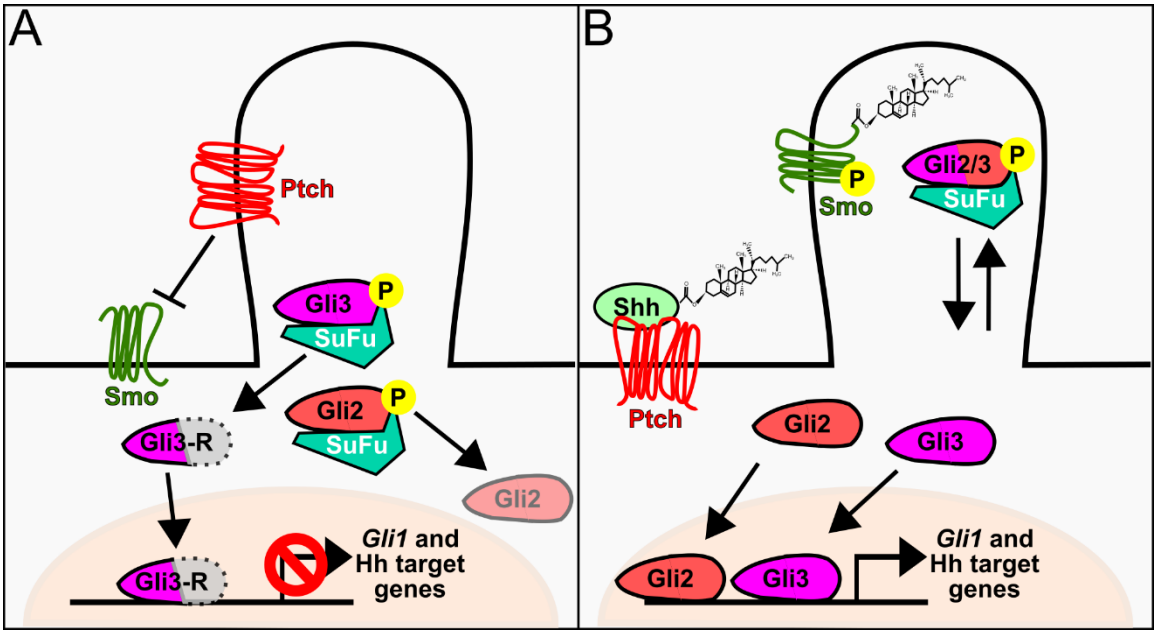

Figure 3.1. The Hedgehog signaling pathway. (A) In the absence of Hh ligand, Ptch is localized to the primary cilium and prevents the accumulation of Smo. Gli2 and 3 are bound by Suppressor of fused and sequestered into the cytoplasm where they are phosphorylated and proteolytically cleaved. Gli2 is degraded while N-terminal Gli3 can translocate to the nucleus and act as a transcriptional repressor. (B) Binding of Ptch by Hh ligand allows Smo to translocate to the primary cilium. Activated Smo re-localizes the Sufu-Gli complex to the cilia, relieving the repression of Gli by Sufu. Gli2/3 then remain in their full-length isoforms and translocate to the nucleus to act as transcriptional activators of Hh target genes such as the additional activator, Gli1.

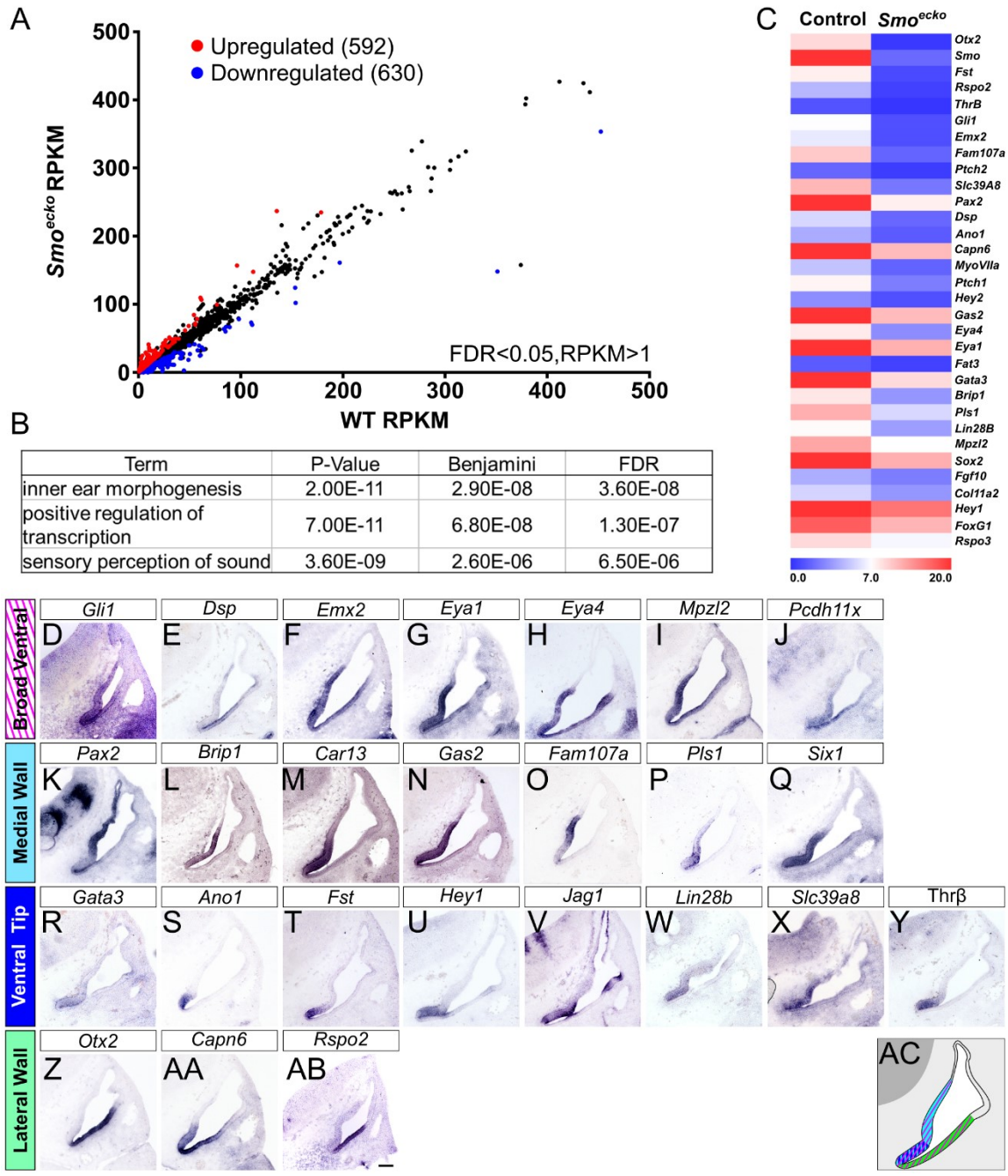

Term	P-Value	Benjamini	FDR
inner ear morphogenesis	2.00E-11	2.90E-08	3.60E-08
positive regulation of transcription	7.00E-11	6.80E-08	1.30E-07
sensory perception of sound	3.60E-09	2.60E-06	6.50E-06

Figure 3.2. RNA-seq on *Smo*^{ecko} mutants reveals cochlear enriched transcripts. (A) Plot of differentially expressed genes between wild type and *Smo*^{ecko} otic vesicles at E11.5 (n=4 replicates). (B) Gene Ontology term enrichment for differentially expressed

genes between wild type and *Smo*^{ecko} *otic vesicles*. (C) Heatmap of differentially expressed genes. (D-AB) Transverse sections through E11.5 wild type otic vesicles showing expression of genes identified by RNA-seq. (AC) Schematic displaying WT expression patterns at E11.5 for comparison. Scale bar = 100μm.

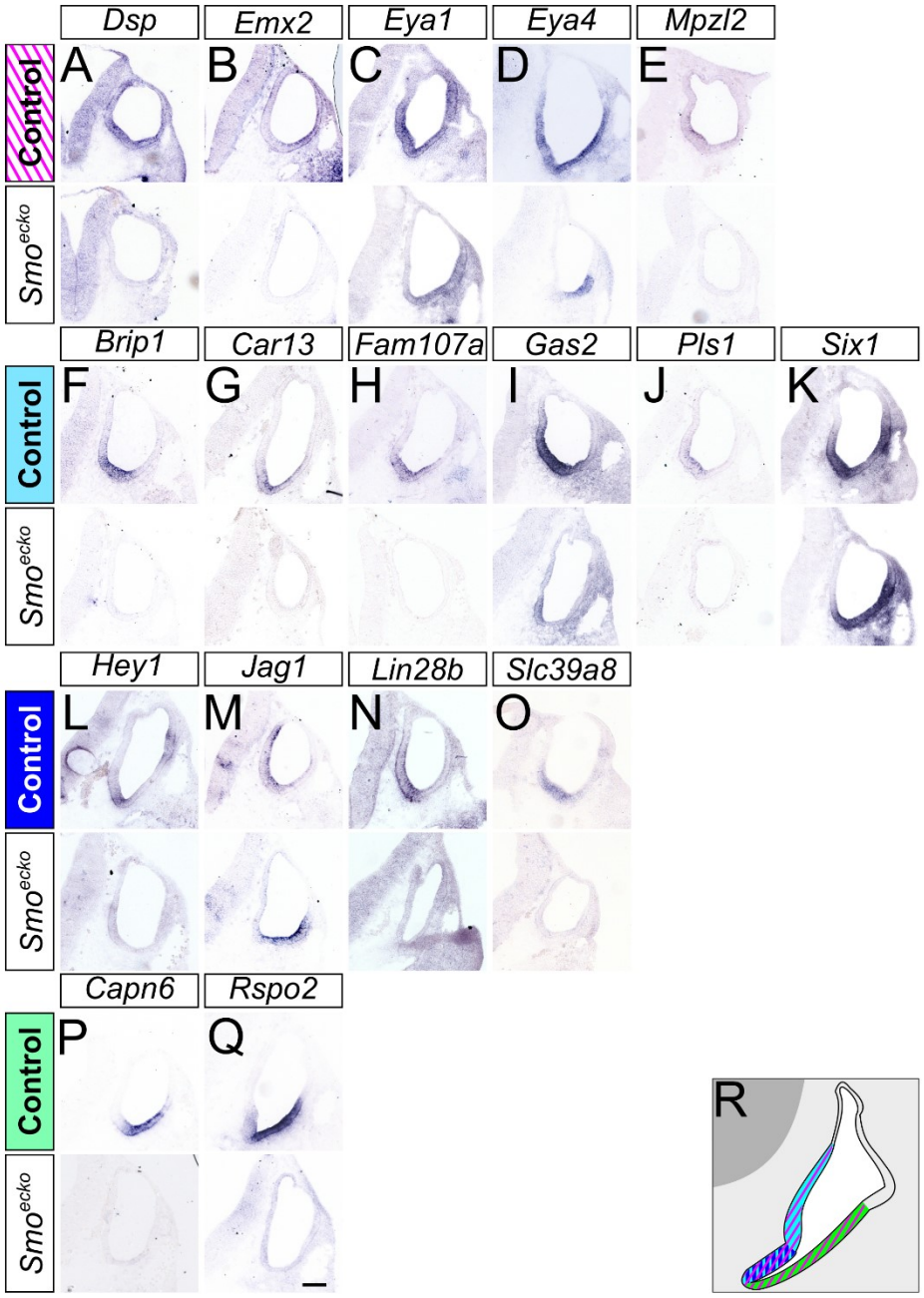

Figure 3.3. Loss of cochlear expressed genes in *Smo*^{ecko} mutants. (A-Q) Transverse sections through E10.5 Control and *Smo*^{ecko} otic vesicles showing differential expression of genes identified by RNA-seq (N≥3 for all panels). (R) Schematic displaying WT expression patterns at E11.5 for comparison. Scale bar = 100μm.

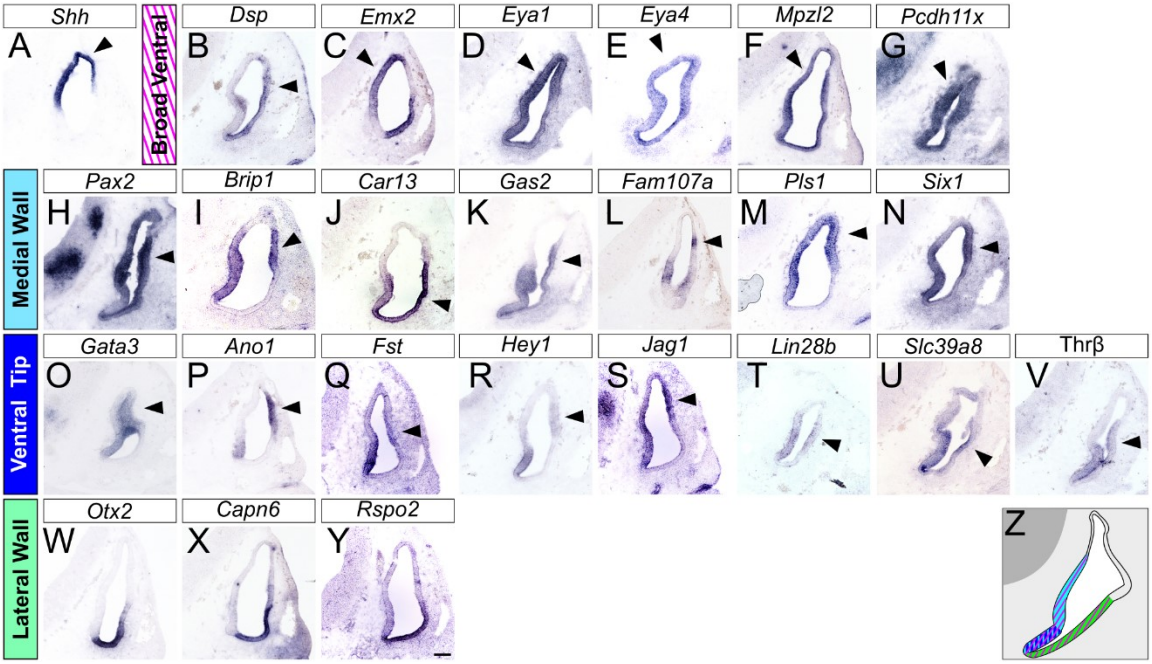

Figure 3.4. *ShhP1* mutants reveal Shh regulated genes. (A-Y) Transverse sections through E11.5 *ShhP1* otic vesicles showing differential expression of genes identified by RNA-seq (N≥3 for all panels). Black arrowheads indicate ectopic expression. (Z) Schematic displaying WT expression patterns at E11.5 for comparison. Scale bar = 100μm.

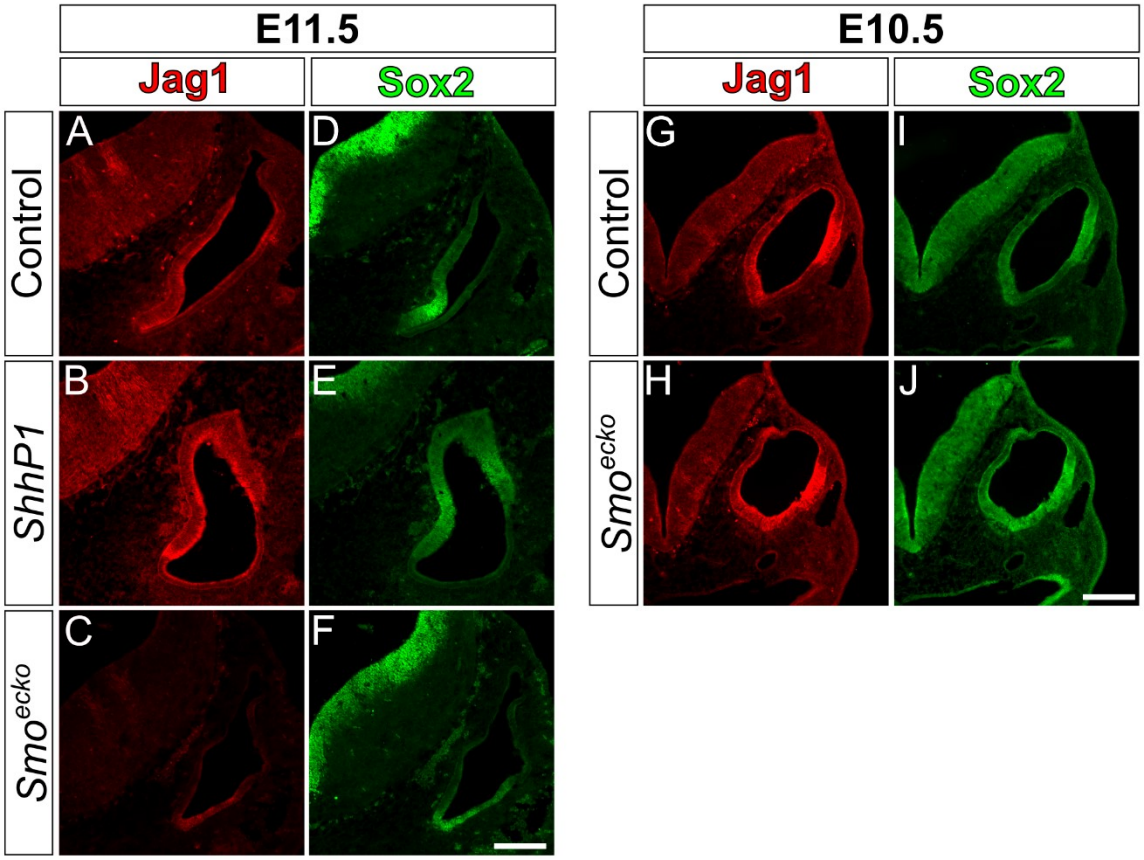

Figure 3.5 Sox2 and Jag1 respond to altered Shh signaling. (A-J) Transverse sections through E11.5 (A-F) Control, *ShhP1*, and *Smo*^{ecko} and E10.5 (G-J) Control and *Smo*^{ecko} otic vesicles showing ectopic localization of Sox2 and Jag1 (N=4 for all panels). Scale bar = 100μm.

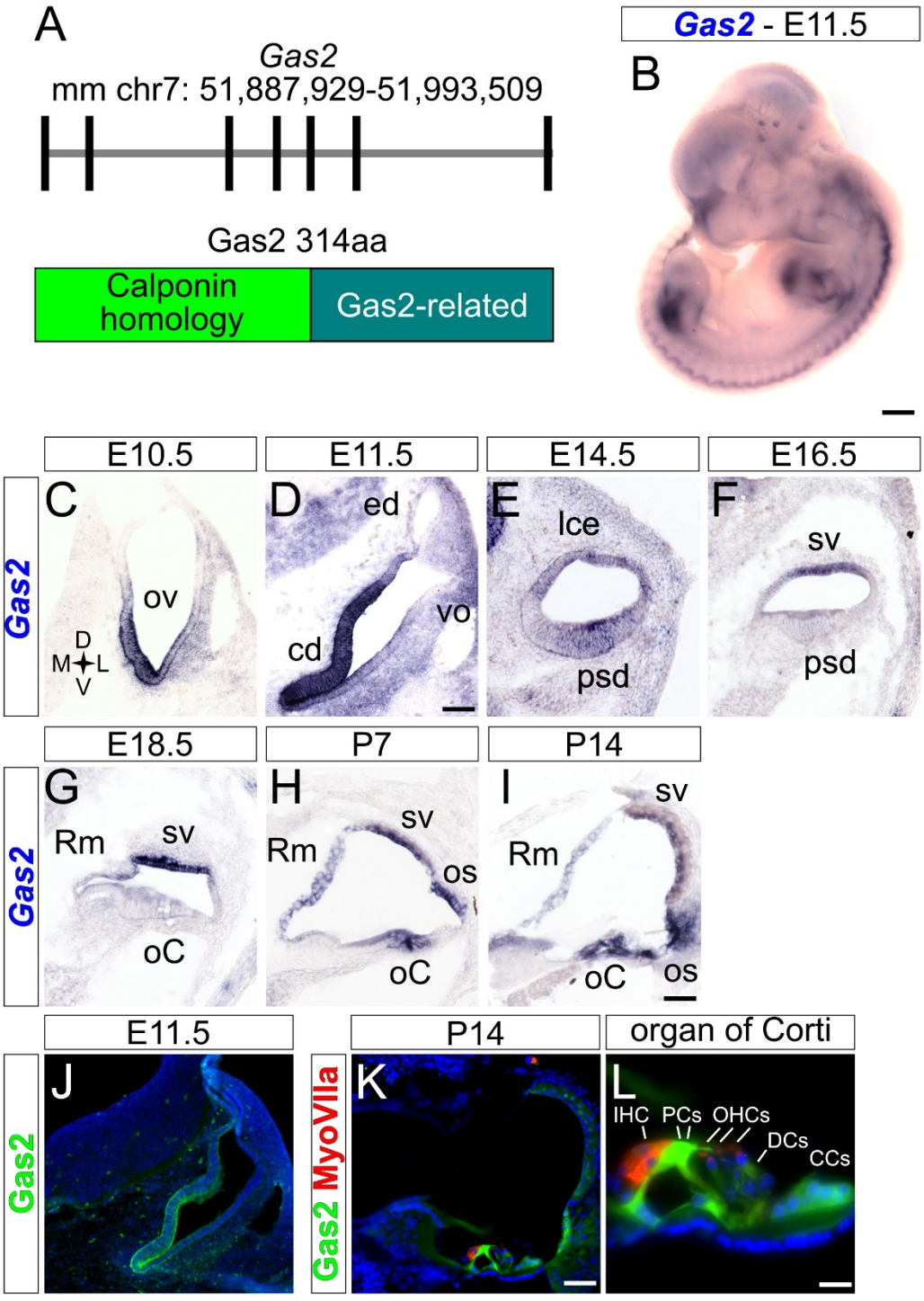

Figure 3.6. *Gas2* is expressed in the developing and postnatal cochlea. (A) Schematic of *Gas2* locus in the mouse genome and encoded protein. (B) E11.5 embryo

showing *Gas2* expression in limbs and somitic mesoderm. (C-I) Transverse sections through wild type otic vesicles (C,D) and cochlear ducts (E-I) over several developmental stages showing dynamic *Gas2* expression. (J-L) Transverse sections through wild type otic vesicle (J) and cochlear duct (K,L) showing Gas2 protein localization. Scale bar = 400μm (B), 100μm (C,D,J), 50μm (E-I, K) and 10μm (L). Abbreviations: Claudius Cells (CCs), cochlear duct (cd), Deiters' Cells (DCs), dorsal (D), endolymphatic duct (ed), Inner Hair Cell (IHC), lateral (L), lateral cochlear epithelium (lce), medial (M), prosensory domain (psd), organ of Corti (oC), otic vesicle (ov), Outer Hair Cells (OHCs), outer sulcus (os), Pillar Cells (PCs), Reissner's membrane (Rm), stria vascularis (sv), ventral (V), vestibular outpouch (vo).

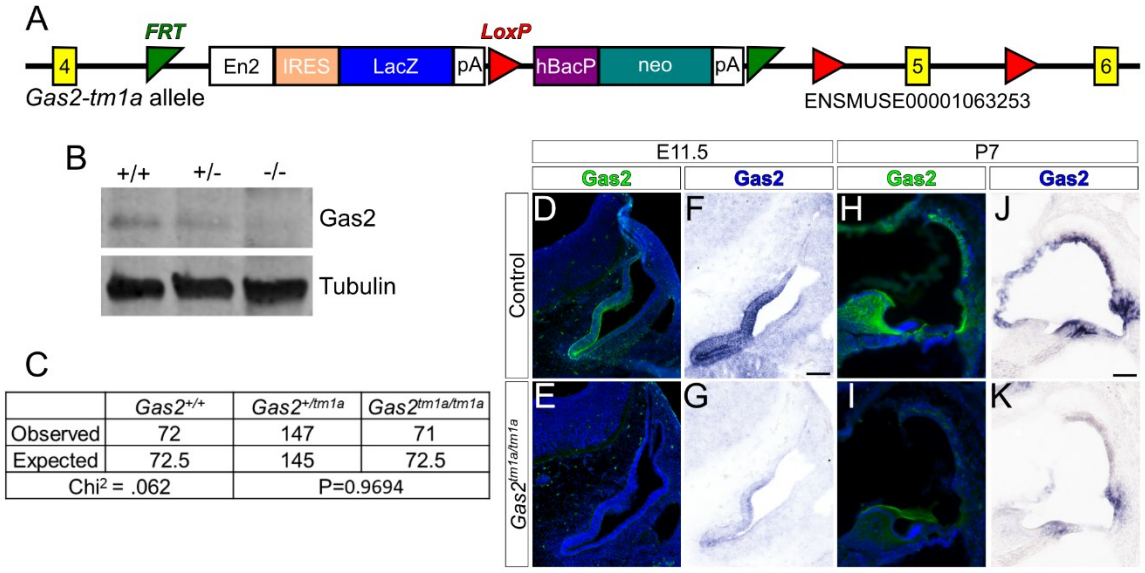

	$Gas2^{+/+}$	$Gas2^{+/tm1a}$	$Gas2^{tm1a/tm1a}$
Observed	72	147	71
Expected	72.5	145	72.5
Chi^2 = .062		P=0.9694	

Figure 3.7. Generation of a *Gas2* null mouse line. (A) Schematic of Knockout first (tm1a) targeted *Gas2* locus. (B) Western blot showing loss of Gas2 protein from E14.5 limb tissue in Control, heterozygous (+/-) and homozygous (-/-) tm1a embryos (N=3). (C) Table displaying statistically normal Mendelian ratios of *Gas2-tm1a* mice generated from heterozygous intercrosses. (D-K) Transverse sections through Control and *Gas2* mutant otic vesicles (D-G) and cochlear ducts (H-K) showing loss of Gas2 transcript and protein (N=3). Scale bar = 100μm (D-G) and 50μm (H-K).

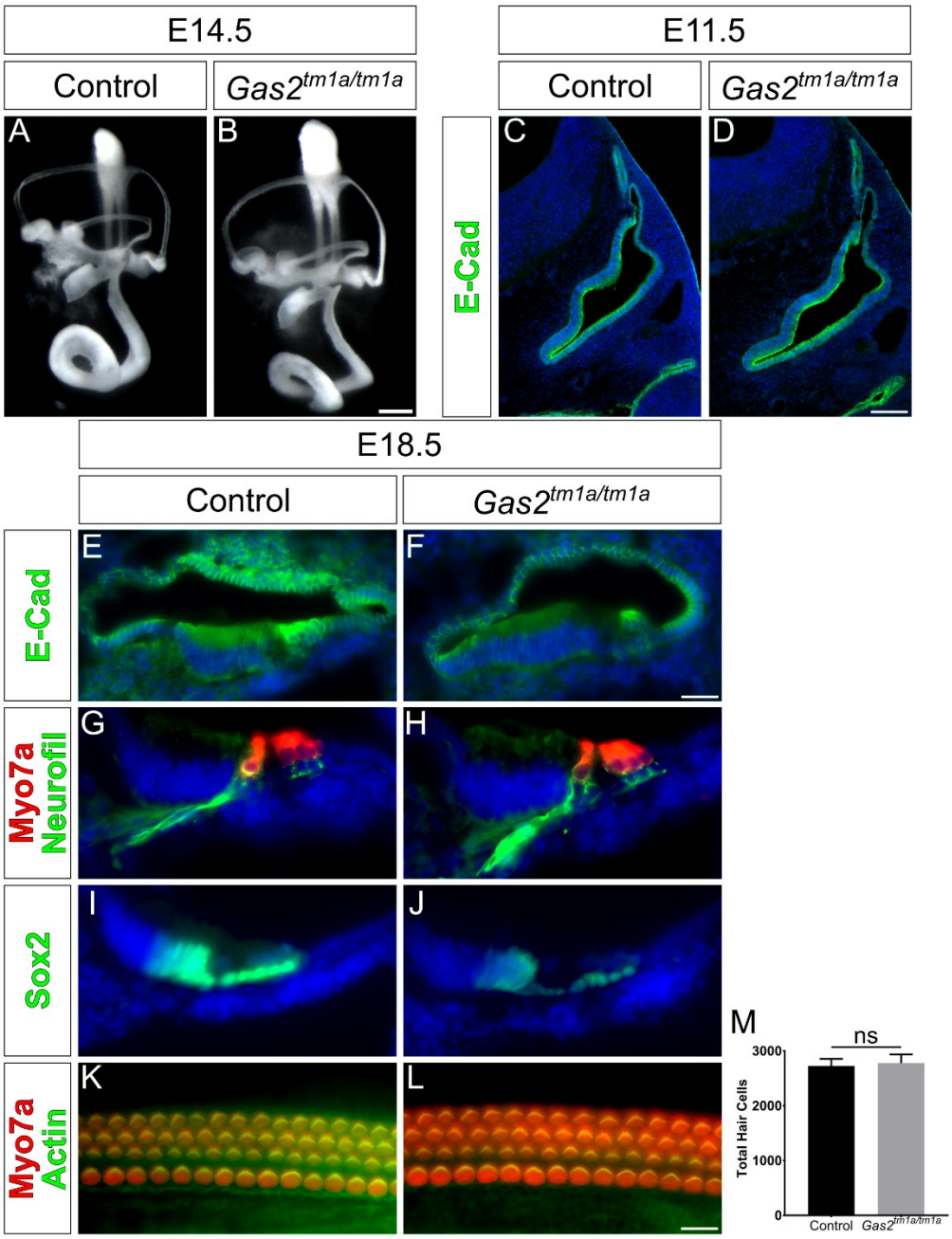

Figure 3.8. Inner ear development is unaffected by loss of *Gas2*. (A-B) Inner ear paint fills of control and *Gas2* mutant embryos at E14.5. (C-F) Transverse sections through control and *Gas2* mutant E11.5 otic vesicles (C,D) and E18.5 cochlear ducts (E,F) stained for E-cadherin to highlight morphology. (G-J) Transverse sections through

E18.5 control and mutant cochlea reveal normal (G,H) hair cell (Myo7a) morphology, innervation (Neurofil = neurofilament) and (I,J) support cell compliment (Sox2). (K,L) E18.5 whole mount preparations of control and *Gas2* mutant cochlear sensory epithelium stained with markers of hair cells (Myo7a) and actin/stereocilia (Phalloidin) with quantification (M) of total hair cells represented as mean ±SD (student's T-test, ns = not significant). N = 3 (A-J) and 5 (K-M). Scale bar = 100μm, (A,B), 50μm (C-F), and 10μm (G-L)

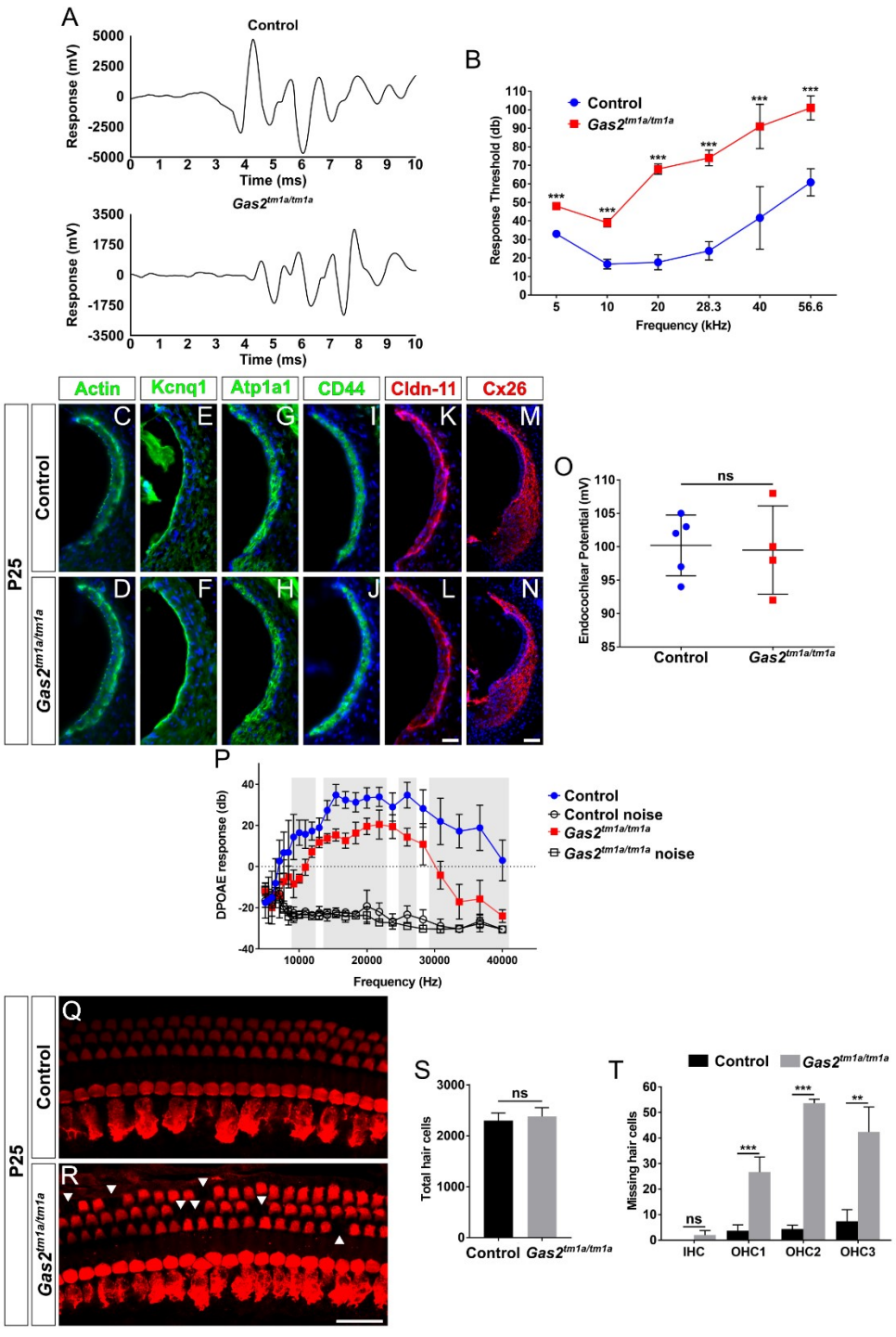

Figure 3.9. *Gas2* mutants exhibit severe hearing impairment. (A) Representative waveforms obtained from ABR click response from Control and *Gas2* mutants at P70

(N=8). (B) ABR thresholds from P56 Control (N=6) and *Gas2* mutants (N=5) (***P<0.001, multiple T-test with Holm-Sidak method). (C-N) Transverse sections through P25 Control and *Gas2* mutant cochlea stained for markers of the stria vascularis (N=3). (O) Graph of endocochlear potential readings from P56 Control (N=6) and *Gas2* mutant (N=5) animals (ns=not significant, T-test). (P) Graph of DPOAE recordings from P56 Control (N=6) and *Gas2* mutants (N=5), gray shading indicates significant difference (P<0.05, multiple T-test with Holm-Sidak method). (Q-R) Whole mount preparations of control and *Gas2* mutant cochlear sensory epithelium stained with markers of hair cells (Myosin VIIa) at P42, white arrowheads indicate missing hair cells. (S-T) Quantification of (S) total and (T) missing hair cells from control and *Gas2* mutants at P42 (N=3) presented as mean ±SD (ns=not significant, **P<0.01, ***P<0.001, T-test). Scale bar = (C-K, O-P) 25μm and (M-N) 50μm.

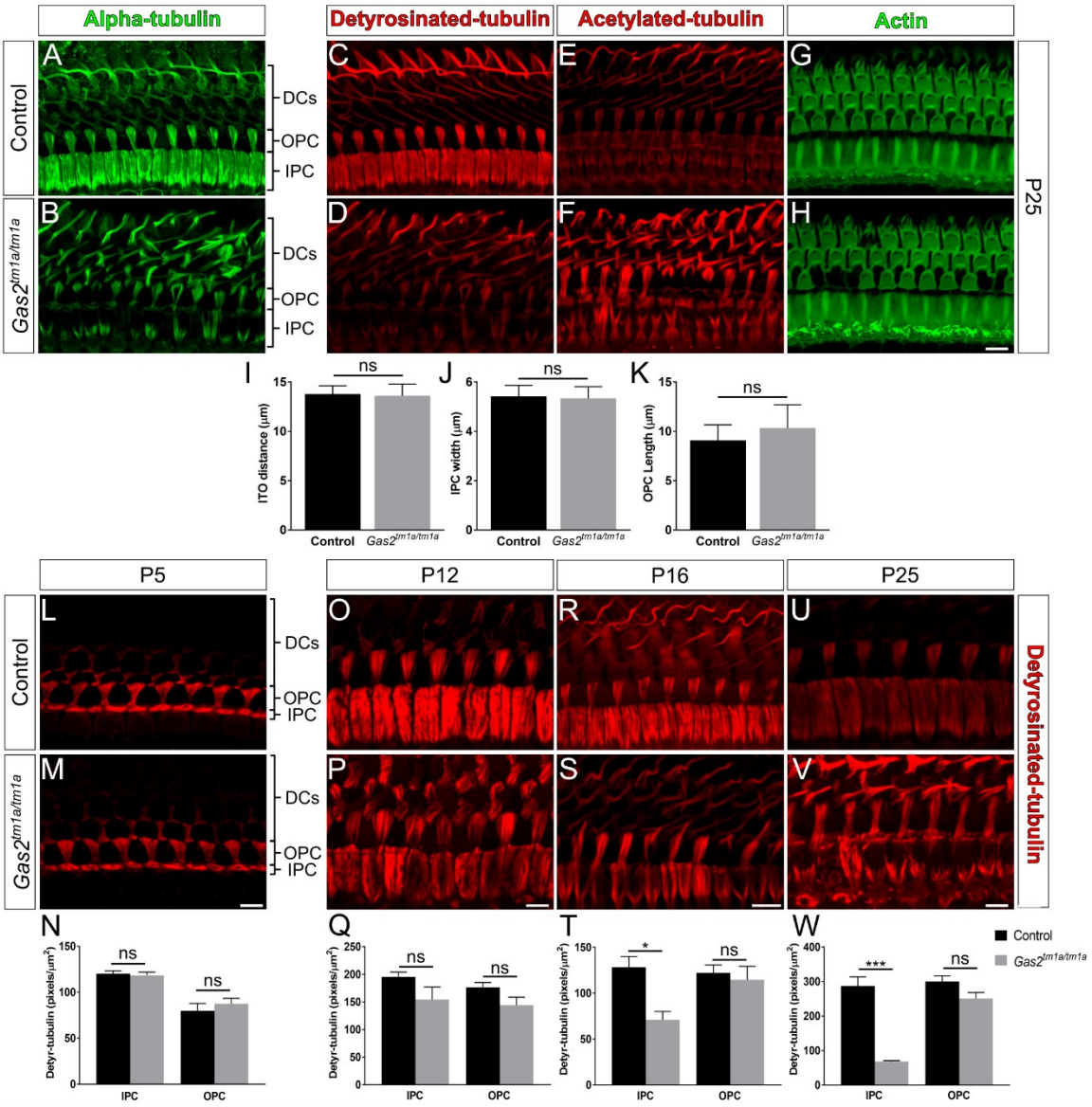

Figure 3.10. *Gas2* mutants display progressive loss of microtubules from the inner pillar cell head. (A-H) Whole mount preparations of P25 control and *Gas2* mutant cochlear sensory epithelium stained with markers of the microtubule (A-F) and actin (G,H) cytoskeleton (N=3). (I-K) Graphs of measurements from P25 control and mutant (I) inner to outer hair cell distance, (J) inner pillar cell head width, and (K) outer pillar cell head length presented as mean ±SE (N=5; ns=not significant, T-test). (L,M,O,P,R,S,U,V)

Whole mount preparations of control and *Gas2* mutant cochlear sensory epithelium at (L,M) P5 (N=4), (O,P) P12 (N=3), (R,S) P16 (N=3) and (U,V) P25 (N=5) stained for detyrosinated-tubulin showing progressive loss of microtubules in *Gas2* mutants. (N,Q,T,W) Quantification of detyrosinated-tubulin fluorescent pixels at (N) P5, (Q) P12, (T) P16, and (W) P25 presented as mean ±SE (ns=not significant, * P,0.05, ***P<0.001, T-test). Scale bar = (A-H,O,P,U,V) 5μm, (R,S) 8μm, and (L,M) 10μm. Abbreviations: Deiters' cells (DCs), Inner Pillar Cell (IPC), Inner hair cell To Outer hair cell distance (ITO), and Outer Pillar Cell (OPC).

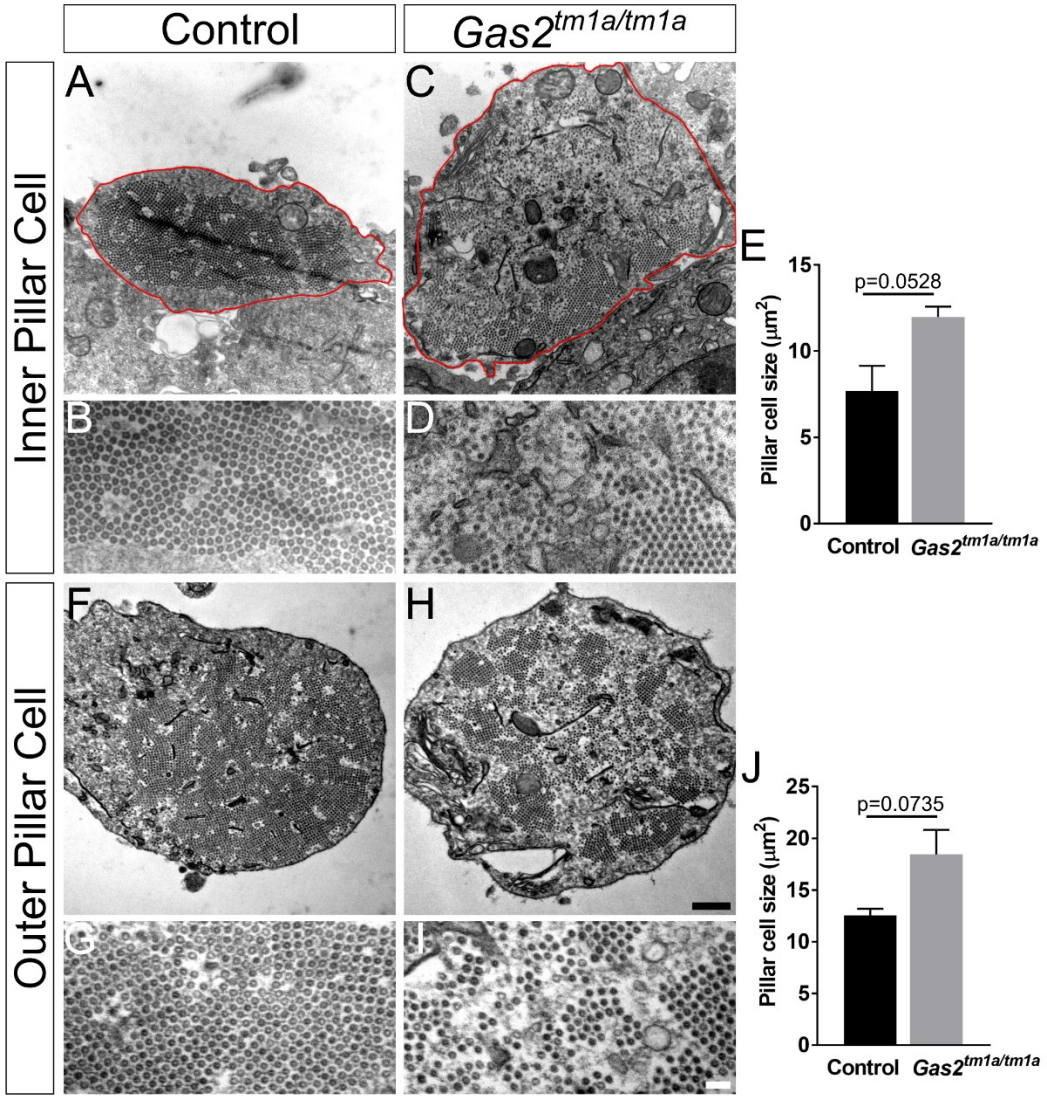

Figure 3.11. Electron microscopy reveals disorganization of the pillar cell microtubule network in Gas2 mutants. Transmission electron micrographs of P25 (A,B,F,G) control and (C,D,H,I) *Gas2* mutant (A-D) inner (red outline) and (F-I) outer pillar cells showing microtubule disorganization with (B,D,G,I) higher magnification of representative areas (N=3). (E,J) Graphs of (E) inner and (J) outer pillar cell size presented as mean ± SE (N=3, average of 3 cells per sample; T-test). Scale bar = (A,C,F,H) 500nm and (B,D,G,I) 100nm.

Materials and Methods

Mouse lines

Generation of *FoxG1*$^{Cre/+}$, *ShhP1*, *Smo*$^{+/-}$, and *Smo*$^{loxp/loxp}$ mouse lines are described elsewhere (Hébert and McConnell, 2000; Long et al., 2001; Riccomagno et al., 2002; Zhang et al., 2001).

The *Gas2*$^{tm1a/+}$ mouse line was generated from ES-cells obtained from the European Conditional Mouse Mutagenesis Program (EUCOMM) containing a targeted Knockout first allele in *Gas2* (Cone: HEPD0681_7_F03). Targeted ES-Cells were screened for proper targeting by PCR amplification of the 5' and 3' homology arms with one primer anchored in the genomic locus and the second within the targeting construct (5`F-GAAGTTCCTATTCCGAAGTTCCT, 5`R-CTGCCTGTGTTGAATGTTCTCAT, 7076bp amplicon; 3`F- CCTGCTTGCCGAATATCATGG, 3`R- ACTTCTGTGGAGTCTCAGCTC, 6493bp amplicon). ES-Cells containing the *Gas2* targeted allele (*Gas2*$^{tm1a/+}$) were injected into albino C57B/6N-tac blastocysts at the UPenn Transgenic and Chimeric Mouse Facility and chimeric mice obtained.

High percentage chimeras (>90% black/agouti coat) were bred to albino C57B/6N-tac mice and the resulting pups were screened for the Gas2-tm1a allele by coat color and PCR genotyping. Genotyping primers were designed to flank the floxed Gas2 exon 5 and generate bands of differing size for the targeted and WT allele (F-TTGGATCATATGGAGAGAGCCAT, R-GGGCATATCACAGGCCCATA, Products: 223bp – WT; 257bp – Loxp/Tm1a) using the following thermocycler program:
95ºC for 5 min, 95ºC for 30 sec, 58ºC for 30 sec, 72ºC for 18 sec, Repeat 2-4 for 31x, 72ºC for 10 min (*this program is utilized for all subsequently described primer sets).

Resulting *Gas2*$^{tm1a/+}$ mice were backcrossed to WT C57B/6N-tac for 10 generations and maintained by heterozygous intercrosses.

Conditional Gas2-tm1c mice were generated by crossing *Gas2*$^{tm1a/+}$ to a constitutively active Flp recombinase (B6.129S4-*Gt(ROSA) 26Sor*$^{tm2(FLP*)Sor}$/J [FLPo]) to remove the Lacz-Neomycin cassette. Recombination and loss of the cassette was confirmed by PCR genotyping (F-GGCGCATAACGATACCACGA, R-TATAAGCCGCCTACTGCGAC) which amplifies a 208bp fragment from the recombined region (*this will not detect a WT allele from the endogenous locus due to the placement of primers within the extended homology arms). Additional primer sets that amplify across the Lacz (F-AGAACAAGCAACATGCGCTC, R-GACCTTGGGACCACCTCATC, 611bp amplicon) and Neomycin (F-CTCCCCCTGAACCTGAAACATA, R-TTATATAAGCCGCCTACTGCGA, 360bp amplicon) inserts were also included as negative controls. Resulting *FLPo*;*Gas2*$^{tm1c/+}$ were backcrossed to WT C57B/6N-tac to remove the *FLPo* allele then intercrossed and maintained as homozygous *Gas2*$^{tm1c/tm1c}$.

The Gas2-tm1d allele was generated by crossing homozygous *Gas2*$^{tm1c/tm1c}$ to a germline expressed Cre recombinase (B6.FVB-Tg(EIIa-cre) C5379Lmgd/J [E2a-Cre]). Recombination and deletion of *Gas2* exon 5 was confirmed by PCR genotyping (F-GGCGCATAACGATACCACGA, R-GGGCATATCACAGGCCCATA, 225bp amplicon) as well as previously described primer sets as negative controls. Resulting *E2a-Cre*;*Gas2*$^{tm1d/+}$ animals were backcrossed to WT C57B/6N-tac to remove the *E2a-Cre* allele then intercrossed and maintained as *Gas2*$^{tm1d/+}$.

RNA sequencing

Otic vesicles from control (*FoxG1*$^{Cre/+}$; *Smo*$^{loxp/+}$) and *Smo*^{ecko} mouse embryos (n=4 pairs of biological replicates) were isolated at E11.5, exposed to collagenase P (1mg/ml) at

37ºC for 20 min to remove surrounding mesenchyme, and transferred into chilled RNA*later*™ Stabilization Solution (Invitrogen). RNA was extracted using an RNeasy Micro RNA extraction kit (Qiagen) according to standard protocols. Total RNA (200ng) was used for poly A selected RNA-seq library preparation using the NEBNext® Ultra™ Directional RNA Library Prep Kit from Illumina® (mRNA) (New England Biolabs) (products: NEBNext® Poly(A) mRNA Magnetic Isolation Module (E7490S) and NEBNext® Ultra™ Directional RNA Library Prep Kit for Illumina® (E7420S). Biological replicates were individually barcoded, pooled, and sequenced on one lane of a HiSeq 400 platform with a read depth of 45 million per library at the Penn Next Generation Sequencing Core (NGSC) Facility. Alignment and expression values were determined using RUM (Grant et al. 2011).

Inner ear paint fill

Paint fills were performed essentially as described (Martin and Swanson, 1993) with the use of White-Out Plus (Bic, Milford, CT, USA) as the contrast medium.

In situ hybridization

Embryos were collected from timed pregnant females (vaginal plug = E0.5). Postnatal mice were euthanized with CO_2 and the inner ears were dissected from the head and fixed for 2 hours in 4% paraformaldehyde at 4°C, then washed in PBS. Inner ears were cryoprotected overnight in 30% sucrose/PBS then snap frozen in OCT embedding compound (Sakura Finetek Torrence, CA). Inner ears were serially sectioned along the transverse plane from anterior to posterior. Sections were hybridized with digoxigenin-UTP-labeled riboprobes as previously described (Nissim et al., 2007).

Whole mount cochlear preparations

Inner ears were dissected and fixed in 4% paraformaldehyde for 2 hours at 4°C, then washed in PBS. Cochleae were microdissected in 0.1% PBST to expose the sensory epithelium, and incubated with antibodies found in Key Resources. Hair cells were counted along the entire length of the cochlear duct.

Immunohistochemistry

Inner ears were processed for immunohistochemistry in the same fashion as for in situ hybridization. Inner ear sections were stained with DAPI and antibodies found in Key Resources.

Western blots

E14.5 embryonic limbs were collected in RIPA buffer and protein extracted by manual homogenization. Total protein lysate was separated on 4-12% Mini-PROTEAN® TGX™ Precast Gels at 120V for 1 hour and transferred to PVDF membranes for 1 hour at 250mA. Membranes were blocked for 1 hour in Odyssey® Blocking Buffer (LI-COR) at RT and incubated overnight at 4ºC in primary antibodies found in Key Resources. Membranes were washed 4x 10 minutes with .1% Tween-PBS then incubated for 1 hour at RT with IRDye® 680LT Goat anti-Mouse IgG (1:20000) and IRDye® 800CW Goat anti-Rabbit IgG (1:20000) in Odyssey® Blocking Buffer. The membranes were washed 4x 10 minutes with .1% Tween-PBS then imaged on an Odyssey® CLx Imaging System (LI-COR).

Auditory Brainstem Response

All recordings were from the left ear. ABR recording was carried out using Tucker-Davis Technologies (TDT) System II hardware and software. Animals were anesthetized using ketamine and xylazine (80/15 mg/kg, intraperitoneal injection) and positioned dorsally in

a custom head holder. Subdermal platinum needle electrodes (Grass) were placed in the mid-back (ground), behind the right pinna (reference), and at the vertex (active). Body temperature was monitored throughout testing using a rectal probe, and maintained at 37.5 ± 1.0°C using a DC current-based isothermal pad (FHC). A TDT ES-1 speaker was placed 7 cm along the interaural axis. Stimuli were 5 ms tone bursts (1000 repetitions, 20/s, 1.0 ms rise/fall time) at frequencies of 5, 10, 20, 28.3, 40 and 56.6 kHz. Responses were amplified x100,000 and filtered at 100-10,000 Hz. Thresholds were taken to be the lowest sound level for which Wave I could be identified, using a 5dB minimum step size.

Mice were anesthetized with isoflurane (1–2.5%) and electrodes were inserted subdermally (recording electrode—posterior to the pinna of the exposed ear; reference electrode—anterior cranial midline; ground electrode—posterior cranial midline). Thresholds were obtained for tones at 8, 12, 16, 22, 28 kHz (5ms duration with 0.1ms ramp for 1200 repetitions) presented from 10–80 dB SPL in 10dB steps. ABR signals were amplified, filtered (band passed 300 Hz-2000 Hz), and averaged using Neuralynx (Cheetah software). Data was analyzed with MATLAB (The MathWorks, Inc.).

Distortion product otoacoustic emissions

DPOAE recordings were obtained in a separate session from ABR recordings, but the animals were prepared similarly as for ABRs. DPOAE iso-input (DP-gram) responses were obtained using EMAV (S. Neely, Z. Liu, BTNRH) in conjunction with TDT and custom hardware using f2 frequencies ranging from 5-40 kHz. F1 frequencies were given by f2/1.2. L1 and L2 levels were set at 75 and 65 dB SPL, respectively. Stimuli were delivered to the ear using a custom coupler inserted using an operating scope.

Each channel was output to a TDT EC-1 speaker. DPOAE responses were recorded using a Knowles FC-23652-P16 microphone calibrated to 40 kHz.

Endocochlear potential recording

After ABR and DPOAE recording, animals underwent a single terminal EP measurement from the cochlear lower basal turn of the left ear. Animals were anesthetized (60 mg/kg sodium pentobarbital, IP) and positioned ventrally in a custom head holder. Core temperature was maintained at 37.5 ± 1.0 ºC using a thermostatically-controlled heating pad in conjunction with a rectal probe (Yellow Springs Instruments Model 73A). An incision was made along the midline of the neck and soft tissues were blunt dissected and displaced laterally to expose the trachea and left bulla. A tracheostomy was then made and the musculature over the bulla was cut posteriorly to expose the bone overlying the round window. Using a fine drill, a hole was made in the left cochlear capsule directly over scala media of the lower basal turn. Glass capillary pipettes (40-80 MΩ) filled with 0.15 M KCl were mounted on a hydraulic microdrive (Frederick Haer) and advanced until a stable positive potential was observed that did not change with increased electrode depth. The signal from the recording electrode was led to an AM Systems Model 1600 intracellular amplifier. A silver/silver chloride ball inserted into the neck muscles served as ground.

Transmission electron microscopy

Inner ears were dissected from postnatal animals after euthanasia with CO_2. The apical turn was opened by cutting a hole in the otic capsule and the cochlea was perfused through the round window every 15 minutes with a mixture of 2% glutaraldehyde and 1% tannic acid in PBS for 90 minutes. The inner ear was then decalcified in 0.5M EDTA overnight at 4ºC. After decalcification the otic capsule, spiral ganglia and stria vascularis

were removed to expose the sensory epithelium. The sensory epithelium was then postfixed in 1% OsO_4 for 90 minutes, dehydrated in ethanol, permeated in propylene oxide, and embedded in Epon resin. Sections were taken on a diamond wafer blade, stained with uranyl acetate and lead citrate and imaged on Jeol-1010 Transmission electron microscope.

Quantification and Statistical Analysis

Statistical analysis was performed using GraphPad Prism 7 software. Relevant information for each experiment including n-values, statistical tests and reported p-values are found in the legend corresponding to each figure. In all cases $P<0.05$ is considered statistically significant.

Quantification of pillar cell size was performed on phalloidin and tubulin stained whole mount images using ImageJ. A total of 6 inner and 6 outer pillar cells were measured from each sample at approximately the mid-basal turn of the cochlea.

Quantification of detyrosinated tubulin fluorescence was performed on binary thresholded images and total white (positive) pixels per unit area was calculated using ImageJ. A total of 6 inner and 6 outer pillar cells were measured from each sample at approximately the mid-basal turn of the cochlea.

RNA-seq results were processed using edgeR (Robinson et al., 2010) to detect differentially expressed transcripts with $FDR<0.05$ and $RPKM>1$.

Data and Software Availability

RNA sequencing data will be made accessible at the NCBI Gene Expression Omnibus.

KEY RESOURCES TABLE

REAGENT or RESOURCE	SOURCE	IDENTIFIER
Antibodies (dilution)		
mouse anti-Acetylated-tubulin (1:200)	Sigma	T 6793
mouse anti-Alpha-tubulin (1:200)	Cell Signaling	3873
mouse anti-Atp1A1 (1:250)	Developmental Studies Hybridoma Bank	A5
rat anti-CD44 (1:200)	BD Parmingen	550538
rabbit anti-Claudin-11 (1:100 +AR)	Novex	364500
mouse anti-Connexin-26/Gjb2 (1:200)	Thermo Scientific	71-0500
rabbit anti Detyrosinated-tubulin (1:200)	abcam	ab48389
mouse anti-E-cadherin (1:200 +AR)	BD Transduction Laboratories	610181
mouse anti-Gas2 (IF-1:200; WB-1:2000)	Santa Cruz	SC-101241
rabbit anti-Gas2 (1:500)	Abcam	ab109762
rabbit anti-Jag1 (1:200 +AR)	Santa Cruz	SC-8303
goat anti-Kcnq1 (1:300)	Santa Cruz	SC-10646
rabbit anti-MyosinVIIa (1:500)	Proteus Biosciences	25-6790
mouse anti-Neurofilament (1:200)	Developmental Studies Hybridoma Bank	2H3
Mouse anti-Sox2 (1:200 +AR)	R&D Systems	MAB2018
donkey anti-mouse IGG Alexa488 (1:200)	Molecular Probes	A-21202
donkey anti-rabbit IGG Alexa594 (1:200)	Molecular Probes	A-21207
rabbit anti-goat IGG Alexa488 (1:200)	Molecular Probes	A-11078
donkey anti-rat Alexa488 (1:200)	Molecular Probes	A-21208
IRDye® 680LT Goat anti-Mouse IgG (1:20000)	LI-COR	925-68020
IRDye® 800CW Goat anti-Rabbit IgG (1:20000)	LI-COR	925-32211
*AR, antigen retrieval – boil for 6 minutes in 10mM citric acid buffer (pH 6.0)		
Chemicals, Peptides, and Recombinant Proteins		
Phalloidin conjugated Alexa488 (1:50)	Molecular Probes	A-12379
Odyssey® Blocking Buffer	LI-COR	927-40000
Critical Commercial Assays		
NEBNext® Poly(A) mRNA Magnetic Isolation Module	New England Biosystems	E7490S

Directional RNA Library Prep Kit for Illumina®	New England Biosystems	E7420S
Deposited Data		
RNA-seq raw and analyzed data	This paper	
Experimental Models: Cell Lines		
Mouse: *Gas2*$^{tm1a(EUCOMM)Hmgu}$	https://www.eummcr.org	HEPD0681_7_F03
Experimental Models: Organisms/Strains		
Mouse: *FoxG1*$^{Cre/+}$	Hebert and McConnell, 2000	N/A
Mouse: *ShhP1*	Riccomagno et al. 2002	NA
Mouse: *Smo*$^{+/-}$	Zhang et al. 2001	N/A
Mouse: *Smo*$^{loxp/loxp}$	Long et al. 2001	N/A
Mouse: *Gas2*$^{tm1a/+}$	This paper	N/A
Mouse: B6.129S4-*Gt(ROSA) 26Sor*$^{tm2(FLP*)Sor}$/J [FLPo (B6 ROSA26Flpo)]	The Jackson Labs	012930
Mouse: B6.FVB-Tg(EIIa-cre) C5379Lmgd/J (E2a-Cre)	The Jackson Labs	003724
Mouse: *Gas2*$^{tm1c/tm1c}$	This paper	N/A
Mouse: *Gas2*$^{tm1d/+}$	This paper	N/A
Sequence-Based Reagents		
Genotyping primers for *Gas2* alleles – see table 3.1		
Software and Algorithms		
RUM	Grant et al. 2011	http://www.cbil.upenn.edu/RUM/
edgeR	Robinson et al. 2010	https://bioconductor.org/packages/release/bioc/html/edgeR.html

Table 3.1 Primer sets for Gas2 allele genotyping.

Gas2 Genotyping Primers			
Target	**Forward primer (5'-3')**	**Reverse Primer (5'-3')**	**Size (bp)**
5' arm	GAAGTTCCTATTCCGAAGTTCCT	CTGCCTGTGTTGAATGTTCTCAT	7076
3' arm	CCTGCTTGCCGAATATCATGG	ACTTCTGTGGAGTCTCAGCTC	6493
Tm1a/Loxp	TTGGATCATATGGAGAGAGCCA T	GGGCATATCACAGGCCCATA	WT-223 Tm1a-257
Tm1c	GGCGCATAACGATACCACGA	TATAAGCCGCCTACTGCGAC	208
Gas2-LacZ	AGAACAAGCAACATGCGCTC	GACCTTGGGACCACCTCATC	611
Gas2-Neo	CTCCCCCTGAACCTGAAACATA	TTATATAAGCCGCCTACTGCGA	360
Tm1d	GGCGCATAACGATACCACGA	GGGCATATCACAGGCCCATA	225

Chapter 4: Conclusions and Future Directions

The development and function of the inner ear rely on a host of signaling pathways, post transcriptional processes, complex cell types, and mechanical interactions. Taken together, these properties of the inner ear provide us with an excellent model organ for understanding basic biology and for asking questions regarding the development of complex systems. Beyond that, the prevalence of hearing disorders amongst the human population lends medical relevance to the study of the development of the cochlear duct and its functional properties.

Hearing impairment and repair

As hearing loss and deafness represent the most common forms of sensory deficit in the developed world considerable effort has been spent attempting to repair all forms of hearing impairment. Current options for patients with hearing impairment are limited to imperfect mechanical devices, such as hearing aids and cochlear implants, that only partially relieve symptoms and are not available to cases with certain forms of hearing loss (Casazza and Meier, 2017; Cunningham and Tucci, 2017). In recent years, a number of cellular and gene therapy approaches have been undertaken to address these concerns including regenerating sensory hair cells and repairing of genetic lesions. Many groups have focused on the regeneration of sensory hair cells utilizing manipulations of the remaining cells within the cochlea. Manipulating Notch signaling and ectopically expressing *Atoh1* have proven able to convert supporting cells into hair cells, however, this comes at the expense of normal cochlear architecture and is unlikely to provide full hearing restoration (Mizutari et al., 2013; Richardson and Atkinson, 2015; White et al., 2006; Yang et al., 2012). It has been discovered that a small subset of

support cells express the factor *Lgr5*, a marker for stem cells, and that these Lgr5+ cells exhibit the capacity to replicate in culture and be differentiated into hair cells (Bramhall et al., 2014; Shi et al., 2012, 2013). If these cells could be reintroduced into the cochlea or endogenous cells programmed to replicate and differentiate to the same efficacy it could provide a potential therapy for age related hearing loss and some forms of congenital deafness.

In cases of congenital hearing impairment, however, additional factors must be considered apart from cell replacement therapy. The nature of many hearing loss mutations renders hair cell replacement problematic as these genes either affect other aspects of hearing, such as stria vascularis function, or affect the hair cells themselves, making it impossible to utilize cells from the patient that contain the mutation in question (Atik et al., 2015; Casazza and Meier, 2017; Kazmierczak and Müller, 2012; Raviv et al., 2010; Shearer et al., 1993; Venkatesh et al., 2015; Weil et al., 1995). Recent work with CRISPR-Cas9 and gene therapy approaches have shown that the ear is a potential target for genetic editing and replacement, however, much work is required before these methods are ready for the clinic (Akil et al., 2012; Gao et al., 2017; Gomes et al., 2016; György et al., 2017; Iizuka et al., 2015; Landegger et al., 2017; Tao et al., 2018). Of interest, we propose that the *Gas2* mutant mouse line developed in our work may provide an excellent platform for testing gene therapy approaches to hearing loss. An issue with many deafness phenotypes is that they result in the degeneration of cochlear cells or morphological defects that preclude postnatal repair. We have shown that *Gas2* mutants present with severe hearing impairment in the absence of gross morphological perturbation. Thus, the *Gas2* mutant may be an excellent model to test the efficacy and longevity of genetic repair strategies in a mammalian system

Alternative splicing

Our analysis of *Esrp1* mutant cochlea revealed a number of differentially spliced transcripts with unknown significance to inner ear development. We were able to establish that aberrant splicing of *Fgfr2* was responsible for defects in stria vascularis development of these embryos, however, that case was greatly abetted by the near 100% isoform switch of *Fgfr2*. Most other genes in this and in other studies do not exhibit such isoform exclusivity, making interrogation of these transcripts much more cumbersome. The ability to examine the contribution of shifts in 10-50% isoform usage has been a major hurdle in the field of alternative splicing research. The Tetracycline inducible rtTA-tetO system may provide a utility to begin interrogating isoform specific contributions to phenotypes (Gossen and Bujard, 1992; Gossen et al., 1995). By driving specific isoforms of a transcript under control of a tetO element it may be possible to generate dosage dependent expression. Experiments such as this will be required to move forward and understand how isoform dosage impacts cellular and developmental phenotypes.

Roles for *Esrps* in vestibular morphogenesis

We uncovered mutations in *ESRP1* by exome sequencing in patients with SNHL and dysgenesis of the lateral semicircular canal (SSC) of the vestibular apparatus. Analysis of *Esrp1* deficient mouse embryos revealed defects in cochlear duct development that are likely causative for hearing loss and a dysmorphia of the vestibular apparatus similar to those seen in the human patients. This vestibular phenotype presents as an apparent failure to resorb and refine the epithelial labyrinth of the common cruz and lateral SSC, leading to an expansion of these structures. Fascinatingly, a recent publication examining the loss of *esrp1* and *esrp2* in zebrafish

also described a horizonal SSC defect in double mutant fish (Burguera et al., 2017). These results demonstrate that *Esrps* play a critical and conserved role in SSC morphogenesis.

The mechanism by which this phenotype arises, however, remains to be explored. Our work and that of many others have demonstrated that many Esrp directed splicing events are cell-type specific, thus, a comparative analysis of the gene expression and alternative splicing events between control and Esrp mutant vestibular epithelia is required to gain insight into this phenotype. Several factors, however, stand out as potential contributors to the SSC phenotype in *Esrp* mutants. *Ntn1* instructs dorsal otic cells to undergo apoptosis and sculpt the SSCs (Nishitani et al., 2017; Salminen et al., 2000) and is regulated by *Lrig3* in the lateral SCC (Abraira et al., 2008). Additionally, regulation of canonical Wnt signaling has also been shown to impact SSC morphogenesis (Rakowiecki and Epstein, 2013). While these genes and pathways have yet to be shown to be targets of *Esrp1*, their contributions to SSC formation warrant investigation in these mutants. Of interest, mouse mutants for *Fgf9* also display a failure to resorb phenotype and Fgf receptors are known targets for *Esrp* directed splicing (Bebee et al., 2015; Burguera et al., 2017; Pirvola et al., 2004; Warzecha et al., 2009a). It has been shown, however, that *Fgf9* directs SSC morphogenesis through mesenchymal interactions, and thus any contribution of this factor to the phenotype seen in *Esrp* mutants must be indirect. While much work is needed to understand the mechanism behind the SSC dysgenesis seen in various *Esrp* mutants, the interrogation of these phenotypes may reveal novel regulators of vestibular development that are conserved across evolutionary time.

Establishing roles for early otic expression patterns

We performed a comparative expression experiment in control and Shh signaling deficient inner ears and discovered a cohort of cochlear enriched genes. Several of the identified transcripts encode for transcription factors and regulators of early cochlear patterning and development, such as *Gata3*, *Pax2*, and *Otx2.* Many genes have, as of yet, undescribed functions in cochlear development, and provide intriguing potential candidates for follow-up studies. Interestingly, several genes uncovered in our analysis (*Col11a2*, *Myo7a*, *Pls1*, *Rspo2*, and *Thrβ)* have been described in mouse knockouts to display hearing loss due to defects in hair cell development and sensory function (Krey et al., 2016; Mulvaney et al., 2013; Ng et al., 2015; Shpargel et al., 2004; Taylor et al., 2015; Vikkula et al., 1995; Weil et al., 1995). None have been described as having a function as early as E11.5 and most have not been described as expressed prior to hair cell development. Given the relative expression levels of these transcripts they cannot simply be ignored as statistical errors in our analysis and, thus, their expression at this stage deserves further interrogation. It is possible that these transcripts are the result of a pre-patterning mechanism, the establishment of a gene expression profile for sensory cells many days before the cells differentiate. Another possibility is that these genes do have a function at this early timepoint but it is masked in knockout animals by functional redundancy with additional factors. As little evidence exists to corroborate either of these hypotheses, further interrogation and experimentation will be required to draw conclusions about the expression of these genes.

Another interesting candidate from our screen, *Gas2*, also fits this category of its expression having unknown significance at E11.5. Our experiments in *Gas2* deficient mice revealed a hearing loss phenotype that is attributed to defects that arise postnatally

in the supporting pillar cells. As no abnormalities were observed embryonically we were unable to address any function that the early expression of *Gas2* has on cochlear development. It is possible that a morphogenetic function for *Gas2* is masked by the presence of potentially redundant cytoskeletal binding proteins, such as *Pls1* and *Dsp*, and that combinatorial knockouts would be required to drive a cochlear outgrowth phenotype.

Pillar cells and the sense of hearing

Perhaps the most fascinating finding from our investigation of *Gas2* null mice was the link between hearing loss and defects in the pillar cell cytoskeleton. It has been long appreciated that the pillar cells are defined by a highly stable, microtubule rich, cytoskeleton and that these cells are required for hearing function. The few syndromes that affect pillar cells and result in hearing loss are tied to fate specification of these cells, making a direct assay of their normal function impossible from these studies (Jacques et al., 2007b; Mansour et al., 2009; Mellado Lagarde et al., 2013; Mueller et al., 2002; Shim et al., 2005; Szarama et al., 2012b). Of interest, recent work has found that deletion of *Gjb2*, a gene encoding a gap junction protein that has previously been described as required for stria vascularis function, also affects the development of the pillar cell cytoskeleton (Chen et al., 2018). In *Gjb2* conditional knockouts the microtubule network of the pillar cells is disrupted and the tunnel of Corti fails to open, leading to hearing deficits. Microtubules have previously been shown to be important for proper membrane localization of gap junctions, suggesting there may be an intersection between the *Gjb2* and *Gas2* mutant phenotypes (Guo et al., 2003; Thomas et al., 2001). Future experiments will need to address the localization of connexin-26 (*Gjb2*) in *Gas2*

mutants and vice-versa as well the mechanism by which loss of *Gjb2* affects pillar cell development.

In *Gas2* mutants, the pillar cells are specified and appear to develop normally thus providing a unique model system in which to assay postnatal cellular dysfunction that is linked to hearing loss. Experiments are already planned and underway to generate a support cell specific deletion of *Gas2* utilizing the mouse lines we have derived and a *Sox2Cre*^{ERt2}, which is expressed in the pillar and Deiters' cells late in embryonic and throughout postnatal development (Gu et al., 2016). These mice would allow us to perform not only a cell type but also time specific deletion of *Gas2* utilizing tamoxifen administration. We can thus address the requirement for *Gas2* directly in pillar cells and at what times this gene is essential for hearing function.

We observed that the microtubule network of *Gas2* mutant pillar cells is disrupted and quickly lost shortly after the onset of hearing. That the microtubules appeared to form and extend initially, and that the morphology of mutant pillar cells was unaffected, we concluded that Gas2 is likely required for the maintenance of the microtubule network in these cells. Experiments are planned to test this hypothesis utilizing the *Sox2Cre*^{ERt2} mouse line to delete *Gas2* postnatally after hearing has begun. We would expect to observe a depletion of microtubules from *Gas2* mutant pillar cells after tamoxifen administration, similar to that seen in the *Gas2* null line at P16. This data would provide strong evidence that Gas2 is required for maintenance of the microtubule network of pillar cells. If we do not observe a loss of microtubules it will argue instead for a role of Gas2 in establishment of the microtubule network prior to hearing and that the timing of the phenotype in the *Gas2* null line is simply coincident due to the prolonged nature of pillar cell development.

An additional possibility is that the breakdown of microtubules in the absence of Gas2 is caused or exacerbated by hearing itself. This hypothesis relies on the current prevailing model that the pillar cells act as a “hinge”, the point of deflection during basilar membrane movements caused by sound waves traveling along the cochlear duct. We propose that this movement causes strain on the pillar cells, requiring them to be highly rigid and stable to provide structural support for the organ of Corti. This idea is supported by the presence of detyrosinated microtubules in the pillar cells, a modification that has been shown to increase cellular stiffness and increase compression-resistance in cardiomyocytes, as well as data collected from gerbil cochlear explants and finite element models (Chan and Hudspeth, 2005; Nam and Fettiplace, 2010; Ni et al., 2016; Robison et al., 2016; Slepecky et al., 1995). This model also posits that the observed decrease in DPOAEs and loss of outer hair cells in the *Gas2* mutants are a secondary consequences of altered pillar cell function and excessive movement of the organ of Corti. In essence, the loss of microtubules in the pillar cells results in decreased stiffness and increased movement of the organ of Corti during acoustic stimulation. This would cause the outer hair cells to contact the tectorial membrane with increased force, subsequently damaging these cells and altering the DPOAE response. This model could be tested by altering the noise exposure of *Gas2* deficient animals. Induction of conductive hearing loss by surgically removing the middle ear bones before the onset of hearing would be predicted to alleviate mechanical stress on the pillar cells and rescue the loss of microtubules and outer hair cells (Chhan et al., 2017; Qin et al., 2010). Alternatively, exposure to loud noise would have the opposite effect. The increased movement of the basilar membrane would put additional stress on the organ of Corti leading to a more rapid depletion of the microtubule network in pillar cells and greater

loss of outer hair cells. These experiments would provide some of the first in vivo evidence for the requirement of pillar cell rigidity for the sense of hearing.

Recent genetic mouse models have also been developed that could prove useful in testing the requirements of the microtubule network of pillar cells in hearing function. Spastin is a microtubule severing protein that, when overexpressed, severely disrupts cytoskeletal organization (Errico et al., 2002; Trotta et al., 2004). A mouse line in which a highly active form of Spastin was placed under control of a tetO response element has recently been described (Muroyama and Lechler, 2017). This allows for cell type specific activation of Spastin when combined with an rtTA driver and Doxycycline administration. Utilizing this system, it would be possible to disrupt the microtubule network of pillar cells, effectively mimicking the *Gas2* null phenotype, and test for hearing response in the resulting animals. In addition, it was recently discovered that vasohibin-1 (VASH1) in complex the small vasohibin binding protein (SVBP) act to detyrosinated microtubules (Aillaud et al., 2017; Nieuwenhuis et al., 2017). By knocking out this complex in pillar cells it is possible to inhibit the detyrosination of microtubules, potentially rendering them less stable and susceptible to mechanical perturbation during hearing. Data from these experiments could support or refute the hypothesis that a rigid microtubule cytoskeleton is required in pillar cells for the sense of hearing.

Conclusions

In conclusion, we have identified *Esrp1* and *Gas2* as novel hearing loss genes, adding to the list of previously established regulators of cochlear function. Our analysis of *Esrp1* mutants uncovered roles for an alternative splicing regulator in the development of the cochlear duct. Loss of *Esrp1* results in a shortened cochlear duct, delay in hair cell differentiation and maturation, and loss of the stria vascularis due to inappropriate Fgf

ligand usage in these cells. These findings provide strong evidence for *Esrp1* as a critical factor in inner ear development and opens the possibilities for studying additional alternative splicing events that may play a role in hearing and cochlear development. We utilized a genetic screen to identify hundreds of cochlear enriched transcripts that may be targets of Shh signaling in the inner ear. In validating these targets, we uncovered repeated use of similar expression domains that may be indicative of the regulatory logic governing cochlear duct patterning. Our analysis of *Gas2* as a putative Shh target gene in the cochlear duct revealed that it is required for auditory function. Loss of *Gas2* results in defects in the pillar cell cytoskeleton that may be linked to hearing dysfunction. These studies provide a unique model for studying pillar cell function and may be utilized as a test platform for genetic rescue of hearing loss.

BIBLIOGRAPHY

Abdolazimi, Y., Stojanova, Z., and Segil, N. (2016). Selection of cell fate in the organ of Corti involves the integration of Hes/Hey signaling at the Atoh1 promoter. Development *143*, 841–850.

Abraira, V.E., Del Rio, T., Tucker, A.F., Slonimsky, J., Keirnes, H.L., and Goodrich, L.V. (2008). Cross-repressive interactions between Lrig3 and netrin 1 shape the architecture of the inner ear. Dev. Camb. Engl. *135*, 4091–4099.

Acampora, D., Merlo, G.R., Paleari, L., Zerega, B., Postiglione, M.P., Mantero, S., Bober, E., Barbieri, O., Simeone, A., and Levi, G. (1999). Craniofacial, vestibular and bone defects in mice lacking the Distal-less-related gene Dlx5. Dev. Camb. Engl. *126*, 3795–3809.

Ahmed, M., Wong, E.Y.M., Sun, J., Xu, J., Wang, F., and Xu, P.-X. (2012). Eya1-Six1 interaction is sufficient to induce hair cell fate in the cochlea by activating Atoh1 expression in cooperation with Sox2. Dev. Cell *22*, 377–390.

Aillaud, C., Bosc, C., Peris, L., Bosson, A., Heemeryck, P., Van Dijk, J., Le Friec, J., Boulan, B., Vossier, F., Sanman, L.E., et al. (2017). Vasohibins/SVBP are tubulin carboxypeptidases (TCP) that regulate neuron differentiation. Science.

Akil, O., Seal, R.P., Burke, K., Wang, C., Alemi, A., During, M., Edwards, R.H., and Lustig, L.R. (2012). Restoration of hearing in the VGLUT3 knockout mouse using virally mediated gene therapy. Neuron *75*, 283–293.

Allen, B.L., Tenzen, T., and McMahon, A.P. (2007). The Hedgehog-binding proteins Gas1 and Cdo cooperate to positively regulate Shh signaling during mouse development. Genes Dev. *21*, 1244–1257.

Alvarez, Y., Alonso, M.T., Vendrell, V., Zelarayan, L.C., Chamero, P., Theil, T., Bösl, M.R., Kato, S., Maconochie, M., Riethmacher, D., et al. (2003). Requirements for FGF3 and FGF10 during inner ear formation. Dev. Camb. Engl. *130*, 6329–6338.

Arima, T., Uemura, T., and Yamamoto, T. (1986). Cytoskeletal organization in the supporting cell of the guinea pig organ of Corti. Hear. Res. *24*, 169–175.

Arnold, W.H., and Lang, T. (2001). Development of the membranous labyrinth of human embryos and fetuses using computer aided 3D-reconstruction. Ann. Anat. - Anat. Anz. *183*, 61–66.

Atik, T., Bademci, G., Diaz-Horta, O., Blanton, S.H., and Tekin, M. (2015). Whole-exome sequencing and its impact in hereditary hearing loss. Genet. Res. *97*, e4.

Avraham, K.B., Hasson, T., Steel, K.P., Kingsley, D.M., Russell, L.B., Mooseker, M.S., Copeland, N.G., and Jenkins, N.A. (1995). The mouse Snell's waltzer deafness gene

encodes an unconventional myosin required for structural integrity of inner ear hair cells. Nat. Genet. *11*, 369–375.

Avraham, K.B., Hasson, T., Sobe, T., Balsara, B., Testa, J.R., Skvorak, A.B., Morton, C.C., Copeland, N.G., and Jenkins, N.A. (1997). Characterization of unconventional MYO6, the human homologue of the gene responsible for deafness in Snell's waltzer mice. Hum. Mol. Genet. *6*, 1225–1231.

Barabino, S.M., Blencowe, B.J., Ryder, U., Sproat, B.S., and Lamond, A.I. (1990). Targeted snRNP depletion reveals an additional role for mammalian U1 snRNP in spliceosome assembly. Cell *63*, 293–302.

Bebee, T.W., Park, J.W., Sheridan, K.I., Warzecha, C.C., Cieply, B.W., Rohacek, A.M., Xing, Y., and Carstens, R.P. (2015). The splicing regulators Esrp1 and Esrp2 direct an epithelial splicing program essential for mammalian development. ELife *4*.

Bebee, T.W., Sims-Lucas, S., Park, J.W., Bushnell, D., Cieply, B., Xing, Y., Bates, C.M., and Carstens, R.P. (2016). Ablation of the epithelial-specific splicing factor Esrp1 results in ureteric branching defects and reduced nephron number. Dev. Dyn. Off. Publ. Am. Assoc. Anat. *245*, 991–1000.

Bellett, G., Carter, J.M., Keynton, J., Goldspink, D., James, C., Moss, D.K., and Mogensen, M.M. (2009). Microtubule plus-end and minus-end capture at adherens junctions is involved in the assembly of apico-basal arrays in polarised epithelial cells. Cell Motil. Cytoskeleton *66*, 893–908.

Belloni, E., Muenke, M., Roessler, E., Traverso, G., Siegel-Bartelt, J., Frumkin, A., Mitchell, H.F., Donis-Keller, H., Helms, C., Hing, A.V., et al. (1996). Identification of Sonic hedgehog as a candidate gene responsible for holoprosencephaly. Nat. Genet. *14*, 353–356.

Benetti, R., Del Sal, G., Monte, M., Paroni, G., Brancolini, C., and Schneider, C. (2001). The death substrate Gas2 binds m-calpain and increases susceptibility to p53-dependent apoptosis. EMBO J. *20*, 2702–2714.

Benito-Gonzalez, A., and Doetzlhofer, A. (2014). Hey1 and Hey2 control the spatial and temporal pattern of mammalian auditory hair cell differentiation downstream of Hedgehog signaling. J. Neurosci. Off. J. Soc. Neurosci. *34*, 12865–12876.

Berglund, J.A., Chua, K., Abovich, N., Reed, R., and Rosbash, M. (1997). The splicing factor BBP interacts specifically with the pre-mRNA branchpoint sequence UACUAAC. Cell *89*, 781–787.

Bermingham, N.A., Hassan, B.A., Price, S.D., Vollrath, M.A., Ben-Arie, N., Eatock, R.A., Bellen, H.J., Lysakowski, A., and Zoghbi, H.Y. (1999). Math1: an essential gene for the generation of inner ear hair cells. Science *284*, 1837–1841.

Bermingham-McDonogh, O., Oesterle, E.C., Stone, J.S., Hume, C.R., Huynh, H.M., and Hayashi, T. (2006). Expression of Prox1 during mouse cochlear development. J. Comp. Neurol. *496*, 172–186.

Bhonker, Y., Abu-Rayyan, A., Ushakov, K., Amir-Zilberstein, L., Shivatzki, S., Yizhar-Barnea, O., Elkan-Miller, T., Tayeb-Fligelman, E., Kim, S.M., Landau, M., et al. (2016). The GPSM2/LGN GoLoco motifs are essential for hearing. Mamm. Genome Off. J. Int. Mamm. Genome Soc. *27*, 29–46.

Bindereif, A., and Green, M.R. (1987). An ordered pathway of snRNP binding during mammalian pre-mRNA splicing complex assembly. EMBO J. *6*, 2415–2424.

Birkenhäger, R., Otto, E., Schürmann, M.J., Vollmer, M., Ruf, E.M., Maier-Lutz, I., Beekmann, F., Fekete, A., Omran, H., Feldmann, D., et al. (2001). Mutation of BSND causes Bartter syndrome with sensorineural deafness and kidney failure. Nat. Genet. *29*, 310–314.

Bitgood, M.J., Shen, L., and McMahon, A.P. (1996). Sertoli cell signaling by Desert hedgehog regulates the male germline. Curr. Biol. CB *6*, 298–304.

Black, D.L. (2003). Mechanisms of alternative pre-messenger RNA splicing. Annu. Rev. Biochem. *72*, 291–336.

Bok, J., Bronner-Fraser, M., and Wu, D.K. (2005). Role of the hindbrain in dorsoventral but not anteroposterior axial specification of the inner ear. Dev. Camb. Engl. *132*, 2115–2124.

Bok, J., Dolson, D.K., Hill, P., Rüther, U., Epstein, D.J., and Wu, D.K. (2007). Opposing gradients of Gli repressor and activators mediate Shh signaling along the dorsoventral axis of the inner ear. Dev. Camb. Engl. *134*, 1713–1722.

Bok, J., Zenczak, C., Hwang, C.H., and Wu, D.K. (2013). Auditory ganglion source of Sonic hedgehog regulates timing of cell cycle exit and differentiation of mammalian cochlear hair cells. Proc. Natl. Acad. Sci. U. S. A.

Bourgeois, C.F., Popielarz, M., Hildwein, G., and Stevenin, J. (1999). Identification of a bidirectional splicing enhancer: differential involvement of SR proteins in 5’ or 3’ splice site activation. Mol. Cell. Biol. *19*, 7347–7356.

Bramhall, N.F., Shi, F., Arnold, K., Hochedlinger, K., and Edge, A.S.B. (2014). Lgr5-positive supporting cells generate new hair cells in the postnatal cochlea. Stem Cell Rep. *2*, 311–322.

Brancolini, C., and Schneider, C. (1994). Phosphorylation of the growth arrest-specific protein Gas2 is coupled to actin rearrangements during Go-->G1 transition in NIH 3T3 cells. J. Cell Biol. *124*, 743–756.

Brancolini, C., Bottega, S., and Schneider, C. (1992). Gas2, a growth arrest-specific protein, is a component of the microfilament network system. J. Cell Biol. *117*, 1251–1261.

Brancolini, C., Benedetti, M., and Schneider, C. (1995). Microfilament reorganization during apoptosis: the role of Gas2, a possible substrate for ICE-like proteases. EMBO J. *14*, 5179–5190.

Brooker, R., Hozumi, K., and Lewis, J. (2006). Notch ligands with contrasting functions: Jagged1 and Delta1 in the mouse inner ear. Dev. Camb. Engl. *133*, 1277–1286.

Brown, A.S., and Epstein, D.J. (2011). Otic ablation of smoothened reveals direct and indirect requirements for Hedgehog signaling in inner ear development. Dev. Camb. Engl. *138*, 3967–3976.

Bumcrot, D.A., Takada, R., and McMahon, A.P. (1995). Proteolytic processing yields two secreted forms of sonic hedgehog. Mol. Cell. Biol. *15*, 2294–2303.

Burguera, D., Marquez, Y., Racioppi, C., Permanyer, J., Torres-Méndez, A., Esposito, R., Albuixech-Crespo, B., Fanlo, L., D'Agostino, Y., Gohr, A., et al. (2017). Evolutionary recruitment of flexible Esrp -dependent splicing programs into diverse embryonic morphogenetic processes. Nat. Commun. *8*, 1799.

Burton, Q., Cole, L.K., Mulheisen, M., Chang, W., and Wu, D.K. (2004). The role of Pax2 in mouse inner ear development. Dev. Biol. *272*, 161–175.

Cable, J., Barkway, C., and Steel, K.P. (1992). Characteristics of stria vascularis melanocytes of viable dominant spotting (Wv/Wv) mouse mutants. Hear. Res. *64*, 6–20.

Cai, T., and Groves, A.K. (2015). The Role of Atonal Factors in Mechanosensory Cell Specification and Function. Mol. Neurobiol. *52*, 1315–1329.

Campbell, D.P., Chrysostomou, E., and Doetzlhofer, A. (2016). Canonical Notch signaling plays an instructive role in auditory supporting cell development. Sci. Rep. *6*, 19484.

Cantos, R., Cole, L.K., Acampora, D., Simeone, A., and Wu, D.K. (2000). Patterning of the mammalian cochlea. Proc. Natl. Acad. Sci. U. S. A. *97*, 11707–11713.

Casazza, G., and Meier, J.D. (2017). Evaluation and management of syndromic congenital hearing loss. Curr. Opin. Otolaryngol. Head Neck Surg. *25*, 378–384.

Chacon-Heszele, M.F., Ren, D., Reynolds, A.B., Chi, F., and Chen, P. (2012). Regulation of cochlear convergent extension by the vertebrate planar cell polarity pathway is dependent on p120-catenin. Dev. Camb. Engl. *139*, 968–978.

Chan, D.K., and Hudspeth, A.J. (2005). Mechanical responses of the organ of corti to acoustic and electrical stimulation in vitro. Biophys. J. *89*, 4382–4395.

Chang, W., Brigande, J.V., Fekete, D.M., and Wu, D.K. (2004a). The development of semicircular canals in the inner ear: role of FGFs in sensory cristae. Dev. Camb. Engl. *131*, 4201–4211.

Chang, W., Brigande, J.V., Fekete, D.M., and Wu, D.K. (2004b). The development of semicircular canals in the inner ear: role of FGFs in sensory cristae. Dev. Camb. Engl. *131*, 4201–4211.

Chang, W., Lin, Z., Kulessa, H., Hebert, J., Hogan, B.L.M., and Wu, D.K. (2008). Bmp4 is essential for the formation of the vestibular apparatus that detects angular head movements. PLoS Genet. *4*, e1000050.

Chausovsky, A., Bershadsky, A.D., and Borisy, G.G. (2000). Cadherin-mediated regulation of microtubule dynamics. Nat. Cell Biol. *2*, 797–804.

Chen, J., and Nathans, J. (2007). Estrogen-related receptor beta/NR3B2 controls epithelial cell fate and endolymph production by the stria vascularis. Dev. Cell *13*, 325–337.

Chen, M., and Manley, J.L. (2009). Mechanisms of alternative splicing regulation: insights from molecular and genomics approaches. Nat. Rev. Mol. Cell Biol. *10*, 741–754.

Chen, P., and Segil, N. (1999). p27(Kip1) links cell proliferation to morphogenesis in the developing organ of Corti. Dev. Camb. Engl. *126*, 1581–1590.

Chen, Y., and Struhl, G. (1996). Dual roles for patched in sequestering and transducing Hedgehog. Cell *87*, 553–563.

Chen, Y., and Struhl, G. (1998). In vivo evidence that Patched and Smoothened constitute distinct binding and transducing components of a Hedgehog receptor complex. Dev. Camb. Engl. *125*, 4943–4948.

Chen, J.K., Taipale, J., Cooper, M.K., and Beachy, P.A. (2002). Inhibition of Hedgehog signaling by direct binding of cyclopamine to Smoothened. Genes Dev. *16*, 2743–2748.

Chen, S., Xie, L., Xu, K., Cao, H.-Y., Wu, X., Xu, X.-X., Sun, Y., and Kong, W.-J. (2018). Developmental abnormalities in supporting cell phalangeal processes and cytoskeleton in the GJB2 knockdown mouse model. Dis. Model. Mech.

Chhan, D., McKinnon, M.L., and Rosowski, J.J. (2017). Identification of induced and naturally occurring conductive hearing loss in mice using bone conduction. Hear. Res. *346*, 45–54.

Chiang, C., Litingtung, Y., Lee, E., Young, K.E., Corden, J.L., Westphal, H., and Beachy, P.A. (1996). Cyclopia and defective axial patterning in mice lacking Sonic hedgehog gene function. Nature *383*, 407–413.

Cieply, B., and Carstens, R.P. (2015). Functional roles of alternative splicing factors in human disease. Wiley Interdiscip. Rev. RNA *6*, 311–326.

Cieply, B., Park, J.W., Nakauka-Ddamba, A., Bebee, T.W., Guo, Y., Shang, X., Lengner, C.J., Xing, Y., and Carstens, R.P. (2016). Multiphasic and Dynamic Changes in Alternative Splicing during Induction of Pluripotency Are Coordinated by Numerous RNA-Binding Proteins. Cell Rep. *15*, 247–255.

Collin, R.W.J., Kalay, E., Tariq, M., Peters, T., van der Zwaag, B., Venselaar, H., Oostrik, J., Lee, K., Ahmed, Z.M., Caylan, R., et al. (2008). Mutations of ESRRB encoding estrogen-related receptor beta cause autosomal-recessive nonsyndromic hearing impairment DFNB35. Am. J. Hum. Genet. *82*, 125–138.

Colnot, C., de la Fuente, L., Huang, S., Hu, D., Lu, C., St-Jacques, B., and Helms, J.A. (2005). Indian hedgehog synchronizes skeletal angiogenesis and perichondrial maturation with cartilage development. Dev. Camb. Engl. *132*, 1057–1067.

Corbit, K.C., Aanstad, P., Singla, V., Norman, A.R., Stainier, D.Y.R., and Reiter, J.F. (2005). Vertebrate Smoothened functions at the primary cilium. Nature *437*, 1018–1021.

Cunningham, L.L., and Tucci, D.L. (2017). Hearing Loss in Adults. N. Engl. J. Med. *377*, 2465–2473.

Dabdoub, A., Puligilla, C., Jones, J.M., Fritzsch, B., Cheah, K.S.E., Pevny, L.H., and Kelley, M.W. (2008). Sox2 signaling in prosensory domain specification and subsequent hair cell differentiation in the developing cochlea. Proc. Natl. Acad. Sci. U. S. A. *105*, 18396–18401.

Dallos, P. (1996). Overview: Cochlear Neurobiology. In The Cochlea, (Springer, New York, NY), pp. 1–43.

De Moerlooze, L., Spencer-Dene, B., Revest, J.M., Hajihosseini, M., Rosewell, I., and Dickson, C. (2000). An important role for the IIIb isoform of fibroblast growth factor receptor 2 (FGFR2) in mesenchymal-epithelial signalling during mouse organogenesis. Dev. Camb. Engl. *127*, 483–492.

Deloria, A.J., Höflmayer, D., Kienzl, P., Łopatecka, J., Sampl, S., Klimpfinger, M., Braunschmid, T., Bastian, F., Lu, L., Marian, B., et al. (2016). Epithelial splicing regulatory protein 1 and 2 paralogues correlate with splice signatures and favorable outcome in human colorectal cancer. Oncotarget *7*, 73800–73816.

Ding, Q., Fukami, S. i, Meng, X., Nishizaki, Y., Zhang, X., Sasaki, H., Dlugosz, A., Nakafuku, M., and Hui, C. c (1999). Mouse suppressor of fused is a negative regulator of

sonic hedgehog signaling and alters the subcellular distribution of Gli1. Curr. Biol. CB *9*, 1119–1122.

Dittmar, K.A., Jiang, P., Park, J.W., Amirikian, K., Wan, J., Shen, S., Xing, Y., and Carstens, R.P. (2012). Genome-wide determination of a broad ESRP-regulated posttranscriptional network by high-throughput sequencing. Mol. Cell. Biol. *32*, 1468–1482.

Dobin, A., Davis, C.A., Schlesinger, F., Drenkow, J., Zaleski, C., Jha, S., Batut, P., Chaisson, M., and Gingeras, T.R. (2013). STAR: ultrafast universal RNA-seq aligner. Bioinforma. Oxf. Engl. *29*, 15–21.

Driver, E.C., Pryor, S.P., Hill, P., Turner, J., Rüther, U., Biesecker, L.G., Griffith, A.J., and Kelley, M.W. (2008). Hedgehog Signaling Regulates Sensory Cell Formation and Auditory Function in Mice and Humans. J. Neurosci. *28*, 7350–7358.

Driver, E.C., Northrop, A., and Kelley, M.W. (2017). Cell migration, intercalation and growth regulate mammalian cochlear extension. Dev. Camb. Engl. *144*, 3766–3776.

Dyer, M.A., Farrington, S.M., Mohn, D., Munday, J.R., and Baron, M.H. (2001). Indian hedgehog activates hematopoiesis and vasculogenesis and can respecify prospective neurectodermal cell fate in the mouse embryo. Dev. Camb. Engl. *128*, 1717–1730.

Echelard, Y., Epstein, D.J., St-Jacques, B., Shen, L., Mohler, J., McMahon, J.A., and McMahon, A.P. (1993). Sonic hedgehog, a member of a family of putative signaling molecules, is implicated in the regulation of CNS polarity. Cell *75*, 1417–1430.

Emadi, G., and Richter, C.-P. (2008). Developmental changes of mechanics measured in the gerbil cochlea. J. Assoc. Res. Otolaryngol. JARO *9*, 22–32.

Erkman, L., McEvilly, R.J., Luo, L., Ryan, A.K., Hooshmand, F., O'Connell, S.M., Keithley, E.M., Rapaport, D.H., Ryan, A.F., and Rosenfeld, M.G. (1996). Role of transcription factors Brn-3.1 and Brn-3.2 in auditory and visual system development. Nature *381*, 603–606.

Errico, A., Ballabio, A., and Rugarli, E.I. (2002). Spastin, the protein mutated in autosomal dominant hereditary spastic paraplegia, is involved in microtubule dynamics. Hum. Mol. Genet. *11*, 153–163.

Etheridge, S.L., Ray, S., Li, S., Hamblet, N.S., Lijam, N., Tsang, M., Greer, J., Kardos, N., Wang, J., Sussman, D.J., et al. (2008). Murine dishevelled 3 functions in redundant pathways with dishevelled 1 and 2 in normal cardiac outflow tract, cochlea, and neural tube development. PLoS Genet. *4*, e1000259.

Fagoonee, S., Bearzi, C., Di Cunto, F., Clohessy, J.G., Rizzi, R., Reschke, M., Tolosano, E., Provero, P., Pandolfi, P.P., Silengo, L., et al. (2013). The RNA binding protein

ESRP1 fine-tunes the expression of pluripotency-related factors in mouse embryonic stem cells. PloS One *8*, e72300.

Fekete, D.M., Homburger, S.A., Waring, M.T., Riedl, A.E., and Garcia, L.F. (1997). Involvement of programmed cell death in morphogenesis of the vertebrate inner ear. Dev. Camb. Engl. *124*, 2451–2461.

Flagella, M., Clarke, L.L., Miller, M.L., Erway, L.C., Giannella, R.A., Andringa, A., Gawenis, L.R., Kramer, J., Duffy, J.J., Doetschman, T., et al. (1999). Mice lacking the basolateral Na-K-2Cl cotransporter have impaired epithelial chloride secretion and are profoundly deaf. J. Biol. Chem. *274*, 26946–26955.

Frederick, R.L., and Shaw, J.M. (2007). Moving mitochondria: establishing distribution of an essential organelle. Traffic Cph. Den. *8*, 1668–1675.

Freyer, L., Aggarwal, V., and Morrow, B.E. (2011). Dual embryonic origin of the mammalian otic vesicle forming the inner ear. Dev. Camb. Engl. *138*, 5403–5414.

Fritzsch, B., Dillard, M., Lavado, A., Harvey, N.L., and Jahan, I. (2010). Canal cristae growth and fiber extension to the outer hair cells of the mouse ear require Prox1 activity. PloS One *5*, e9377.

Fu, X.-D., and Ares, M. (2014). Context-dependent control of alternative splicing by RNA-binding proteins. Nat. Rev. Genet. *15*, 689–701.

Furness, D.N. (2015). Molecular basis of hair cell loss. Cell Tissue Res. *361*, 387–399.

Gao, X., Tao, Y., Lamas, V., Huang, M., Yeh, W.-H., Pan, B., Hu, Y.-J., Hu, J.H., Thompson, D.B., Shu, Y., et al. (2017). Treatment of autosomal dominant hearing loss by *in vivo* delivery of genome editing agents. Nature.

Girdler, G.C., Applewhite, D.A., Perry, W.M.G., Rogers, S.L., and Röper, K. (2016). The Gas2 family protein Pigs is a microtubule +TIP that affects cytoskeleton organisation. J. Cell Sci. *129*, 121–134.

Gispert, S., Parganlija, D., Klinkenberg, M., Dröse, S., Wittig, I., Mittelbronn, M., Grzmil, P., Koob, S., Hamann, A., Walter, M., et al. (2013). Loss of mitochondrial peptidase Clpp leads to infertility, hearing loss plus growth retardation via accumulation of CLPX, mtDNA and inflammatory factors. Hum. Mol. Genet. *22*, 4871–4887.

Golden, E.J., Benito-Gonzalez, A., and Doetzlhofer, A. (2015). The RNA-binding protein LIN28B regulates developmental timing in the mammalian cochlea. Proc. Natl. Acad. Sci. U. S. A. *112*, E3864-3873.

Gomes, M.M., Wang, L., Jiang, H., Kahl, C.A., and Brigande, J.V. (2016). A Rapid, Cost-Effective Method to Prepare Recombinant Adeno-Associated Virus for Efficient Gene Transfer to the Developing Mouse Inner Ear. Methods Mol. Biol. Clifton NJ *1427*, 43–57.

Goodrich, L.V., Milenković, L., Higgins, K.M., and Scott, M.P. (1997). Altered neural cell fates and medulloblastoma in mouse patched mutants. Science *277*, 1109–1113.

Goriounov, D., Leung, C.L., and Liem, R.K.H. (2003). Protein products of human Gas2-related genes on chromosomes 17 and 22 (hGAR17 and hGAR22) associate with both microfilaments and microtubules. J. Cell Sci. *116*, 1045–1058.

Gossen, M., and Bujard, H. (1992). Tight control of gene expression in mammalian cells by tetracycline-responsive promoters. Proc. Natl. Acad. Sci. U. S. A. *89*, 5547–5551.

Gossen, M., Freundlieb, S., Bender, G., Müller, G., Hillen, W., and Bujard, H. (1995). Transcriptional activation by tetracyclines in mammalian cells. Science *268*, 1766–1769.

Göttgens, E.-L., Span, P.N., and Zegers, M.M. (2016). Roles and Regulation of Epithelial Splicing Regulatory Proteins 1 and 2 in Epithelial-Mesenchymal Transition. Int. Rev. Cell Mol. Biol. *327*, 163–194.

Grant, G.R., Farkas, M.H., Pizarro, A.D., Lahens, N.F., Schug, J., Brunk, B.P., Stoeckert, C.J., Hogenesch, J.B., and Pierce, E.A. (2011). Comparative analysis of RNA-Seq alignment algorithms and the RNA-Seq unified mapper (RUM). Bioinforma. Oxf. Engl. *27*, 2518–2528.

Graveley, B.R., Hertel, K.J., and Maniatis, T. (2001). The role of U2AF35 and U2AF65 in enhancer-dependent splicing. RNA N. Y. N *7*, 806–818.

Gu, R., Brown, R.M., Hsu, C.-W., Cai, T., Crowder, A.L., Piazza, V.G., Vadakkan, T.J., Dickinson, M.E., and Groves, A.K. (2016). Lineage tracing of Sox2-expressing progenitor cells in the mouse inner ear reveals a broad contribution to non-sensory tissues and insights into the origin of the organ of Corti. Dev. Biol. *414*, 72–84.

Guo, Y., Martinez-Williams, C., and Rannels, D.E. (2003). Gap junction-microtubule associations in rat alveolar epithelial cells. Am. J. Physiol. Lung Cell. Mol. Physiol. *285*, L1213-1221.

György, B., Sage, C., Indzhykulian, A.A., Scheffer, D.I., Brisson, A.R., Tan, S., Wu, X., Volak, A., Mu, D., Tamvakologos, P.I., et al. (2017). Rescue of Hearing by Gene Delivery to Inner-Ear Hair Cells Using Exosome-Associated AAV. Mol. Ther. J. Am. Soc. Gene Ther. *25*, 379–391.

Haddon, C.M., and Lewis, J.H. (1991). Hyaluronan as a propellant for epithelial movement: the development of semicircular canals in the inner ear of Xenopus. Dev. Camb. Engl. *112*, 541–550.

Hao, J., Koesters, R., Bouchard, M., Gridley, T., Pfannenstiel, S., Plinkert, P.K., Zhang, L., and Praetorius, M. (2012). Jagged1-mediated Notch signaling regulates mammalian inner ear development independent of lateral inhibition. Acta Otolaryngol. (Stockh.) *132*, 1028–1035.

Hasson, T., Heintzelman, M.B., Santos-Sacchi, J., Corey, D.P., and Mooseker, M.S. (1995). Expression in cochlea and retina of myosin VIIa, the gene product defective in Usher syndrome type 1B. Proc. Natl. Acad. Sci. U. S. A. *92*, 9815–9819.

Hayakawa, A., Saitoh, M., and Miyazawa, K. (2017). Dual Roles for Epithelial Splicing Regulatory Proteins 1 (ESRP1) and 2 (ESRP2) in Cancer Progression. Adv. Exp. Med. Biol. *925*, 33–40.

Hayashi, T., Cunningham, D., and Bermingham-McDonogh, O. (2007). Loss of Fgfr3 leads to excess hair cell development in the mouse organ of Corti. Dev. Dyn. Off. Publ. Am. Assoc. Anat. *236*, 525–533.

Haycraft, C.J., Banizs, B., Aydin-Son, Y., Zhang, Q., Michaud, E.J., and Yoder, B.K. (2005). Gli2 and Gli3 localize to cilia and require the intraflagellar transport protein polaris for processing and function. PLoS Genet. *1*, e53.

Hébert, J.M., and McConnell, S.K. (2000). Targeting of cre to the Foxg1 (BF-1) Locus Mediates loxP Recombination in the Telencephalon and Other Developing Head Structures. Dev. Biol. *222*, 296–306.

Hellemans, J., Coucke, P.J., Giedion, A., De Paepe, A., Kramer, P., Beemer, F., and Mortier, G.R. (2003). Homozygous mutations in IHH cause acrocapitofemoral dysplasia, an autosomal recessive disorder with cone-shaped epiphyses in hands and hips. Am. J. Hum. Genet. *72*, 1040–1046.

Helms, A.W., Abney, A.L., Ben-Arie, N., Zoghbi, H.Y., and Johnson, J.E. (2000). Autoregulation and multiple enhancers control Math1 expression in the developing nervous system. Dev. Camb. Engl. *127*, 1185–1196.

Henderson, C.G., Tucker, J.B., Chaplin, M.A., Mackie, J.B., Maidment, S.N., Mogensen, M.M., and Paton, C.C. (1994). Reorganization of the centrosome and associated microtubules during the morphogenesis of a mouse cochlear epithelial cell. J. Cell Sci. *107 (Pt 2)*, 589–600.

Henderson, C.G., Tucker, J.B., Mogensen, M.M., Mackie, J.B., Chaplin, M.A., Slepecky, N.B., and Leckie, L.M. (1995). Three microtubule-organizing centres collaborate in a mouse cochlear epithelial cell during supracellularly coordinated control of microtubule positioning. J. Cell Sci. *108 (Pt 1)*, 37–50.

van den Heuvel, M., and Ingham, P.W. (1996). smoothened encodes a receptor-like serpentine protein required for hedgehog signalling. Nature *382*, 547–551.

Hibino, H., Horio, Y., Inanobe, A., Doi, K., Ito, M., Yamada, M., Gotow, T., Uchiyama, Y., Kawamura, M., Kubo, T., et al. (1997). An ATP-dependent inwardly rectifying potassium channel, KAB-2 (Kir4. 1), in cochlear stria vascularis of inner ear: its specific subcellular localization and correlation with the formation of endocochlear potential. J. Neurosci. Off. J. Soc. Neurosci. *17*, 4711–4721.

Hilding, D.A., and Ginzberg, R.D. (1977). Pigmentation of the stria vascularis. The contribution of neural crest melanocytes. Acta Otolaryngol. (Stockh.) *84*, 24–37.

Huangfu, D., and Anderson, K.V. (2005). Cilia and Hedgehog responsiveness in the mouse. Proc. Natl. Acad. Sci. U. S. A. *102*, 11325–11330.

Huangfu, D., Liu, A., Rakeman, A.S., Murcia, N.S., Niswander, L., and Anderson, K.V. (2003). Hedgehog signalling in the mouse requires intraflagellar transport proteins. Nature *426*, 83–87.

Hui, C.C., Slusarski, D., Platt, K.A., Holmgren, R., and Joyner, A.L. (1994). Expression of three mouse homologs of the Drosophila segment polarity gene cubitus interruptus, Gli, Gli-2, and Gli-3, in ectoderm- and mesoderm-derived tissues suggests multiple roles during postimplantation development. Dev. Biol. *162*, 402–413.

Iizuka, T., Kamiya, K., Gotoh, S., Sugitani, Y., Suzuki, M., Noda, T., Minowa, O., and Ikeda, K. (2015). Perinatal Gjb2 gene transfer rescues hearing in a mouse model of hereditary deafness. Hum. Mol. Genet. *24*, 3651–3661.

Incardona, J.P., Gaffield, W., Kapur, R.P., and Roelink, H. (1998). The teratogenic Veratrum alkaloid cyclopamine inhibits sonic hedgehog signal transduction. Dev. Camb. Engl. *125*, 3553–3562.

Ishii, H., Saitoh, M., Sakamoto, K., Kondo, T., Katoh, R., Tanaka, S., Motizuki, M., Masuyama, K., and Miyazawa, K. (2014). Epithelial splicing regulatory proteins 1 (ESRP1) and 2 (ESRP2) suppress cancer cell motility via different mechanisms. J. Biol. Chem. *289*, 27386–27399.

Ito, M., Spicer, S.S., and Schulte, B.A. (1995). Cytological changes related to maturation of the organ of Corti and opening of Corti's tunnel. Hear. Res. *88*, 107–123.

Jacques, B.E., Montcouquiol, M.E., Layman, E.M., Lewandoski, M., and Kelley, M.W. (2007a). Fgf8 induces pillar cell fate and regulates cellular patterning in the mammalian cochlea. Dev. Camb. Engl. *134*, 3021–3029.

Jacques, B.E., Montcouquiol, M.E., Layman, E.M., Lewandoski, M., and Kelley, M.W. (2007b). Fgf8 induces pillar cell fate and regulates cellular patterning in the mammalian cochlea. Dev. Camb. Engl. *134*, 3021–3029.

Jenkinson, E.M., Rehman, A.U., Walsh, T., Clayton-Smith, J., Lee, K., Morell, R.J., Drummond, M.C., Khan, S.N., Naeem, M.A., Rauf, B., et al. (2013). Perrault syndrome is caused by recessive mutations in CLPP, encoding a mitochondrial ATP-dependent chambered protease. Am. J. Hum. Genet. *92*, 605–613.

Jeong, H.M., Han, J., Lee, S.H., Park, H.-J., Lee, H.J., Choi, J.-S., Lee, Y.M., Choi, Y.-L., Shin, Y.K., and Kwon, M.J. (2017). ESRP1 is overexpressed in ovarian cancer and

promotes switching from mesenchymal to epithelial phenotype in ovarian cancer cells. Oncogenesis *6*, e389.

Kachar, B., Parakkal, M., Kurc, M., Zhao, Y., and Gillespie, P.G. (2000). High-resolution structure of hair-cell tip links. Proc. Natl. Acad. Sci. U. S. A. *97*, 13336–13341.

Kanzaki, S., Beyer, L.A., Swiderski, D.L., Izumikawa, M., Stöver, T., Kawamoto, K., and Raphael, Y. (2006). p27(Kip1) deficiency causes organ of Corti pathology and hearing loss. Hear. Res. *214*, 28–36.

Karavitaki, K.D., and Mountain, D.C. (2007). Imaging electrically evoked micromechanical motion within the organ of corti of the excised gerbil cochlea. Biophys. J. *92*, 3294–3316.

Kawamoto, K., Ishimoto, S.-I., Minoda, R., Brough, D.E., and Raphael, Y. (2003). Math1 gene transfer generates new cochlear hair cells in mature guinea pigs in vivo. J. Neurosci. Off. J. Soc. Neurosci. *23*, 4395–4400.

Kazmierczak, P., and Müller, U. (2012). Sensing sound: molecules that orchestrate mechanotransduction by hair cells. Trends Neurosci. *35*, 220–229.

Kazmierczak, P., Sakaguchi, H., Tokita, J., Wilson-Kubalek, E.M., Milligan, R.A., Müller, U., and Kachar, B. (2007). Cadherin 23 and protocadherin 15 interact to form tip-link filaments in sensory hair cells. Nature *449*, 87–91.

Kelley, R.L., Roessler, E., Hennekam, R.C., Feldman, G.L., Kosaki, K., Jones, M.C., Palumbos, J.C., and Muenke, M. (1996). Holoprosencephaly in RSH/Smith-Lemli-Opitz syndrome: does abnormal cholesterol metabolism affect the function of Sonic Hedgehog? Am. J. Med. Genet. *66*, 478–484.

Kempfle, J.S., Turban, J.L., and Edge, A.S.B. (2016). Sox2 in the differentiation of cochlear progenitor cells. Sci. Rep. *6*, 23293.

Kiernan, A.E., Pelling, A.L., Leung, K.K.H., Tang, A.S.P., Bell, D.M., Tease, C., Lovell-Badge, R., Steel, K.P., and Cheah, K.S.E. (2005). Sox2 is required for sensory organ development in the mammalian inner ear. Nature *434*, 1031–1035.

Kiernan, A.E., Xu, J., and Gridley, T. (2006). The Notch ligand JAG1 is required for sensory progenitor development in the mammalian inner ear. PLoS Genet. *2*, e4.

Kikuchi, K., and Hilding, D. (1965). The development of the organ of Corti in the mouse. Acta Otolaryngol. (Stockh.) *60*, 207–221.

Kikuchi, T., Takasaka, T., Tonosaki, A., Katori, Y., and Shinkawa, H. (1991). Microtubules of guinea pig cochlear epithelial cells. Acta Otolaryngol. (Stockh.) *111*, 286–290.

Kim, H., Ankamreddy, H., Lee, D.J., Kong, K.-A., Ko, H.W., Kim, M.H., and Bok, J. (2014). Pax3 function is required specifically for inner ear structures with melanogenic fates. Biochem. Biophys. Res. Commun. *445*, 608–614.

Kinzler, K.W., Ruppert, J.M., Bigner, S.H., and Vogelstein, B. (1988). The GLI gene is a member of the Kruppel family of zinc finger proteins. Nature *332*, 371–374.

Kirjavainen, A., Sulg, M., Heyd, F., Alitalo, K., Ylä-Herttuala, S., Möröy, T., Petrova, T.V., and Pirvola, U. (2008). Prox1 interacts with Atoh1 and Gfi1, and regulates cellular differentiation in the inner ear sensory epithelia. Dev. Biol. *322*, 33–45.

Kitajiri, S., Miyamoto, T., Mineharu, A., Sonoda, N., Furuse, K., Hata, M., Sasaki, H., Mori, Y., Kubota, T., Ito, J., et al. (2004). Compartmentalization established by claudin-11-based tight junctions in stria vascularis is required for hearing through generation of endocochlear potential. J. Cell Sci. *117*, 5087–5096.

Kogerman, P., Grimm, T., Kogerman, L., Krause, D., Undén, A.B., Sandstedt, B., Toftgård, R., and Zaphiropoulos, P.G. (1999). Mammalian suppressor-of-fused modulates nuclear-cytoplasmic shuttling of Gli-1. Nat. Cell Biol. *1*, 312–319.

Kopecky, B., Johnson, S., Schmitz, H., Santi, P., and Fritzsch, B. (2012). Scanning thin-sheet laser imaging microscopy elucidates details on mouse ear development. Dev. Dyn. Off. Publ. Am. Assoc. Anat. *241*, 465–480.

Kraus, H.J., and Aulbach-Kraus, K. (1981). Morphological changes in the cochlea of the mouse after the onset of hearing. Hear. Res. *4*, 89–102.

Krey, J.F., Krystofiak, E.S., Dumont, R.A., Vijayakumar, S., Choi, D., Rivero, F., Kachar, B., Jones, S.M., and Barr-Gillespie, P.G. (2016). Plastin 1 widens stereocilia by transforming actin filament packing from hexagonal to liquid. J. Cell Biol. *215*, 467–482.

Ladher, R.K., Wright, T.J., Moon, A.M., Mansour, S.L., and Schoenwolf, G.C. (2005). FGF8 initiates inner ear induction in chick and mouse. Genes Dev. *19*, 603–613.

Landegger, L.D., Pan, B., Askew, C., Wassmer, S.J., Gluck, S.D., Galvin, A., Taylor, R., Forge, A., Stankovic, K.M., Holt, J.R., et al. (2017). A synthetic AAV vector enables safe and efficient gene transfer to the mammalian inner ear. Nat. Biotechnol. *35*, 280–284.

Lanford, P.J., Lan, Y., Jiang, R., Lindsell, C., Weinmaster, G., Gridley, T., and Kelley, M.W. (1999). Notch signalling pathway mediates hair cell development in mammalian cochlea. Nat. Genet. *21*, 289–292.

Lawoko-Kerali, G., Rivolta, M.N., and Holley, M. (2002). Expression of the transcription factors GATA3 and Pax2 during development of the mammalian inner ear. J. Comp. Neurol. *442*, 378–391.

Lee, J., Platt, K.A., Censullo, P., and Ruiz i Altaba, A. (1997). Gli1 is a target of Sonic hedgehog that induces ventral neural tube development. Dev. Camb. Engl. *124*, 2537–2552.

Lee, K.K., Tang, M.K., Yew, D.T., Chow, P.H., Yee, S.P., Schneider, C., and Brancolini, C. (1999). gas2 is a multifunctional gene involved in the regulation of apoptosis and chondrogenesis in the developing mouse limb. Dev. Biol. *207*, 14–25.

Lee, M.P., Ravenel, J.D., Hu, R.J., Lustig, L.R., Tomaselli, G., Berger, R.D., Brandenburg, S.A., Litzi, T.J., Bunton, T.E., Limb, C., et al. (2000). Targeted disruption of the Kvlqt1 gene causes deafness and gastric hyperplasia in mice. J. Clin. Invest. *106*, 1447–1455.

Lee, Y.-S., Liu, F., and Segil, N. (2006). A morphogenetic wave of p27Kip1 transcription directs cell cycle exit during organ of Corti development. Dev. Camb. Engl. *133*, 2817–2826.

Lerat, J., Jonard, L., Loundon, N., Christin-Maitre, S., Lacombe, D., Goizet, C., Rouzier, C., Van Maldergem, L., Gherbi, S., Garabedian, E.-N., et al. (2016). An Application of NGS for Molecular Investigations in Perrault Syndrome: Study of 14 Families and Review of the Literature. Hum. Mutat. *37*, 1354–1362.

Li, S., Li, S., Han, Y., Tong, C., Wang, B., Chen, Y., and Jiang, J. (2016). Regulation of Smoothened Phosphorylation and High-Level Hedgehog Signaling Activity by a Plasma Membrane Associated Kinase. PLoS Biol. *14*, e1002481.

Ligon, L.A., Karki, S., Tokito, M., and Holzbaur, E.L. (2001). Dynein binds to beta-catenin and may tether microtubules at adherens junctions. Nat. Cell Biol. *3*, 913–917.

Lin, Z., Cantos, R., Patente, M., and Wu, D.K. (2005). Gbx2 is required for the morphogenesis of the mouse inner ear: a downstream candidate of hindbrain signaling. Dev. Camb. Engl. *132*, 2309–2318.

Liu, A., Wang, B., and Niswander, L.A. (2005). Mouse intraflagellar transport proteins regulate both the activator and repressor functions of Gli transcription factors. Dev. Camb. Engl. *132*, 3103–3111.

Liu, Z., Owen, T., Fang, J., Srinivasan, R.S., and Zuo, J. (2012a). In vivo Notch reactivation in differentiating cochlear hair cells induces Sox2 and Prox1 expression but does not disrupt hair cell maturation. Dev. Dyn. Off. Publ. Am. Assoc. Anat. *241*, 684–696.

Liu, Z., Owen, T., Fang, J., and Zuo, J. (2012b). Overactivation of Notch1 signaling induces ectopic hair cells in the mouse inner ear in an age-dependent manner. PloS One *7*, e34123.

Locher, H., de Groot, J.C.M.J., van Iperen, L., Huisman, M.A., Frijns, J.H.M., and Chuva de Sousa Lopes, S.M. (2015). Development of the stria vascularis and potassium regulation in the human fetal cochlea: Insights into hereditary sensorineural hearing loss. Dev. Neurobiol. *75*, 1219–1240.

Long, F., Zhang, X.M., Karp, S., Yang, Y., and McMahon, A.P. (2001). Genetic manipulation of hedgehog signaling in the endochondral skeleton reveals a direct role in the regulation of chondrocyte proliferation. Dev. Camb. Engl. *128*, 5099–5108.

Mager, L.F., Koelzer, V., Stuber, R., Thoo, L., Keller, I., Koeck, I., Langenegger, M., Simillion, C., Pfister, S., Faderl, M., et al. (2017). The ESRP1-GPR137 axis contributes to intestinal pathogenesis. ELife *6*, e28366.

Mansour, S.L., Twigg, S.R.F., Freeland, R.M., Wall, S.A., Li, C., and Wilkie, A.O.M. (2009). Hearing loss in a mouse model of Muenke syndrome. Hum. Mol. Genet. *18*, 43–50.

Mansour, S.L., Li, C., and Urness, L.D. (2013). Genetic rescue of Muenke syndrome model hearing loss reveals prolonged FGF-dependent plasticity in cochlear supporting cell fates. Genes Dev. *27*, 2320–2331.

Marigo, V., Davey, R.A., Zuo, Y., Cunningham, J.M., and Tabin, C.J. (1996). Biochemical evidence that patched is the Hedgehog receptor. Nature *384*, 176–179.

Martin, P., and Swanson, G.J. (1993). Descriptive and experimental analysis of the epithelial remodellings that control semicircular canal formation in the developing mouse inner ear. Dev. Biol. *159*, 549–558.

Martín, V., Carrillo, G., Torroja, C., and Guerrero, I. (2001). The sterol-sensing domain of Patched protein seems to control Smoothened activity through Patched vesicular trafficking. Curr. Biol. CB *11*, 601–607.

Matlin, A.J., and Moore, M.J. (2007). Spliceosome assembly and composition. Adv. Exp. Med. Biol. *623*, 14–35.

May-Simera, H.L., Petralia, R.S., Montcouquiol, M., Wang, Y.-X., Szarama, K.B., Liu, Y., Lin, W., Deans, M.R., Pazour, G.J., and Kelley, M.W. (2015). Ciliary proteins Bbs8 and Ift20 promote planar cell polarity in the cochlea. Dev. Camb. Engl. *142*, 555–566.

Mehta, D., Noon, S.E., Schwartz, E., Wilkens, A., Bedoukian, E.C., Scarano, I., Crenshaw, E.B., and Krantz, I.D. (2016). Outcomes of evaluation and testing of 660 individuals with hearing loss in a pediatric genetics of hearing loss clinic. Am. J. Med. Genet. A. *170*, 2523–2530.

Melkov, A., and Abdu, U. (2018). Regulation of long-distance transport of mitochondria along microtubules. Cell. Mol. Life Sci. CMLS *75*, 163–176.

Mellado Lagarde, M.M., Cox, B.C., Fang, J., Taylor, R., Forge, A., and Zuo, J. (2013). Selective ablation of pillar and deiters' cells severely affects cochlear postnatal development and hearing in mice. J. Neurosci. Off. J. Soc. Neurosci. *33*, 1564–1576.

Merlo, G.R., Paleari, L., Mantero, S., Zerega, B., Adamska, M., Rinkwitz, S., Bober, E., and Levi, G. (2002). The Dlx5 homeobox gene is essential for vestibular morphogenesis in the mouse embryo through a BMP4-mediated pathway. Dev. Biol. *248*, 157–169.

Mills, J.A., Wang, K., Paluru, P., Ying, L., Lu, L., Galvão, A.M., Xu, D., Yao, Y., Sullivan, S.K., Sullivan, L.M., et al. (2013). Clonal genetic and hematopoietic heterogeneity among human-induced pluripotent stem cell lines. Blood *122*, 2047–2051.

Mizutari, K., Fujioka, M., Hosoya, M., Bramhall, N., Okano, H.J., Okano, H., and Edge, A.S.B. (2013). Notch inhibition induces cochlear hair cell regeneration and recovery of hearing after acoustic trauma. Neuron *77*, 58–69.

Moayedi, Y., Basch, M.L., Pacheco, N.L., Gao, S.S., Wang, R., Harrison, W., Xiao, N., Oghalai, J.S., Overbeek, P.A., Mardon, G., et al. (2014). The candidate splicing factor Sfswap regulates growth and patterning of inner ear sensory organs. PLoS Genet. *10*, e1004055.

Mogensen, M.M., Mackie, J.B., Doxsey, S.J., Stearns, T., and Tucker, J.B. (1997). Centrosomal deployment of gamma-tubulin and pericentrin: evidence for a microtubule-nucleating domain and a minus-end docking domain in certain mouse epithelial cells. Cell Motil. Cytoskeleton *36*, 276–290.

Montcouquiol, M., Rachel, R.A., Lanford, P.J., Copeland, N.G., Jenkins, N.A., and Kelley, M.W. (2003). Identification of Vangl2 and Scrb1 as planar polarity genes in mammals. Nature *423*, 173–177.

Montcouquiol, M., Sans, N., Huss, D., Kach, J., Dickman, J.D., Forge, A., Rachel, R.A., Copeland, N.G., Jenkins, N.A., Bogani, D., et al. (2006). Asymmetric localization of Vangl2 and Fz3 indicate novel mechanisms for planar cell polarity in mammals. J. Neurosci. Off. J. Soc. Neurosci. *26*, 5265–5275.

Morsli, H., Choo, D., Ryan, A., Johnson, R., and Wu, D.K. (1998). Development of the Mouse Inner Ear and Origin of Its Sensory Organs. J. Neurosci. *18*, 3327–3335.

Mueller, K.L., Jacques, B.E., and Kelley, M.W. (2002). Fibroblast growth factor signaling regulates pillar cell development in the organ of corti. J. Neurosci. Off. J. Soc. Neurosci. *22*, 9368–9377.

Mulvaney, J.F., Yatteau, A., Sun, W.W., Jacques, B., Takubo, K., Suda, T., Yamada, W., and Dabdoub, A. (2013). Secreted factor R-Spondin 2 is involved in refinement of patterning of the mammalian cochlea. Dev. Dyn. Off. Publ. Am. Assoc. Anat. *242*, 179–188.

Murone, M., Rosenthal, A., and de Sauvage, F.J. (1999). Sonic hedgehog signaling by the patched-smoothened receptor complex. Curr. Biol. CB *9*, 76–84.

Muroyama, A., and Lechler, T. (2017). A transgenic toolkit for visualizing and perturbing microtubules reveals unexpected functions in the epidermis. ELife *6*.

Nakano, Y., Jahan, I., Bonde, G., Sun, X., Hildebrand, M.S., Engelhardt, J.F., Smith, R.J.H., Cornell, R.A., Fritzsch, B., and Bánfi, B. (2012). A mutation in the Srrm4 gene causes alternative splicing defects and deafness in the Bronx waltzer mouse. PLoS Genet. *8*, e1002966.

Nam, J.-H., and Fettiplace, R. (2010). Force transmission in the organ of Corti micromachine. Biophys. J. *98*, 2813–2821.

Neves, J., Uchikawa, M., Bigas, A., and Giraldez, F. (2012). The prosensory function of Sox2 in the chicken inner ear relies on the direct regulation of Atoh1. PloS One *7*, e30871.

Neves, J., Vachkov, I., and Giraldez, F. (2013). Sox2 regulation of hair cell development: incoherence makes sense. Hear. Res. *297*, 20–29.

Neyroud, N., Tesson, F., Denjoy, I., Leibovici, M., Donger, C., Barhanin, J., Fauré, S., Gary, F., Coumel, P., Petit, C., et al. (1997). A novel mutation in the potassium channel gene KVLQT1 causes the Jervell and Lange-Nielsen cardioauditory syndrome. Nat. Genet. *15*, 186–189.

Ng, L., Cordas, E., Wu, X., Vella, K.R., Hollenberg, A.N., and Forrest, D. (2015). Age-Related Hearing Loss and Degeneration of Cochlear Hair Cells in Mice Lacking Thyroid Hormone Receptor β1. Endocrinology *156*, 3853–3865.

Ni, G., Elliott, S.J., and Baumgart, J. (2016). Finite-element model of the active organ of Corti. J. R. Soc. Interface *13*, 20150913.

Nieuwenhuis, J., Adamopoulos, A., Bleijerveld, O.B., Mazouzi, A., Stickel, E., Celie, P., Altelaar, M., Knipscheer, P., Perrakis, A., Blomen, V.A., et al. (2017). Vasohibins encode tubulin detyrosinating activity. Science.

Nishitani, A.M., Ohta, S., Yung, A.R., Del Rio, T., Gordon, M.I., Abraira, V.E., Avilés, E.C., Schoenwolf, G.C., Fekete, D.M., and Goodrich, L.V. (2017). Distinct functions for netrin 1 in chicken and murine semicircular canal morphogenesis. Dev. Camb. Engl. *144*, 3349–3360.

Nissim, S., Allard, P., Bandyopadhyay, A., Harfe, B.D., and Tabin, C.J. (2007). Characterization of a novel ectodermal signaling center regulating Tbx2 and Shh in the vertebrate limb. Dev. Biol. *304*, 9–21.

Noramly, S., and Grainger, R.M. (2002). Determination of the embryonic inner ear. J. Neurobiol. *53*, 100–128.

Nüsslein-Volhard, C., and Wieschaus, E. (1980). Mutations affecting segment number and polarity in Drosophila. Nature *287*, 795–801.

Oh, S.H., Johnson, R., and Wu, D.K. (1996). Differential expression of bone morphogenetic proteins in the developing vestibular and auditory sensory organs. J. Neurosci. Off. J. Soc. Neurosci. *16*, 6463–6475.

Ohlemiller, K.K., Jones, S.M., and Johnson, K.R. (2016). Application of Mouse Models to Research in Hearing and Balance. J. Assoc. Res. Otolaryngol. JARO *17*, 493–523.

Ohta, S., Wang, B., Mansour, S.L., and Schoenwolf, G.C. (2016). SHH ventralizes the otocyst by maintaining basal PKA activity and regulating GLI3 signaling. Dev. Biol. *420*, 100–109.

Okano, T., Xuan, S., and Kelley, M.W. (2011). Insulin-like growth factor signaling regulates the timing of sensory cell differentiation in the mouse cochlea. J. Neurosci. Off. J. Soc. Neurosci. *31*, 18104–18118.

Ozaki, H., Nakamura, K., Funahashi, J., Ikeda, K., Yamada, G., Tokano, H., Okamura, H., Kitamura, K., Muto, S., Kotaki, H., et al. (2004). Six1 controls patterning of the mouse otic vesicle. Dev. Camb. Engl. *131*, 551–562.

Pan, N., Jahan, I., Kersigo, J., Kopecky, B., Santi, P., Johnson, S., Schmitz, H., and Fritzsch, B. (2011). Conditional deletion of Atoh1 using Pax2-Cre results in viable mice without differentiated cochlear hair cells that have lost most of the organ of Corti. Hear. Res. *275*, 66–80.

Pan, Q., Shai, O., Lee, L.J., Frey, B.J., and Blencowe, B.J. (2008). Deep surveying of alternative splicing complexity in the human transcriptome by high-throughput sequencing. Nat. Genet. *40*, 1413–1415.

Pan, W., Jin, Y., Stanger, B., and Kiernan, A.E. (2010). Notch signaling is required for the generation of hair cells and supporting cells in the mammalian inner ear. Proc. Natl. Acad. Sci. U. S. A. *107*, 15798–15803.

Pan, W., Jin, Y., Chen, J., Rottier, R.J., Steel, K.P., and Kiernan, A.E. (2013). Ectopic expression of activated notch or SOX2 reveals similar and unique roles in the development of the sensory cell progenitors in the mammalian inner ear. J. Neurosci. Off. J. Soc. Neurosci. *33*, 16146–16157.

Pan, Y., Bai, C.B., Joyner, A.L., and Wang, B. (2006). Sonic hedgehog signaling regulates Gli2 transcriptional activity by suppressing its processing and degradation. Mol. Cell. Biol. *26*, 3365–3377.

Patuzzi, R. (2011). Ion flow in stria vascularis and the production and regulation of cochlear endolymph and the endolymphatic potential. Hear. Res. *277*, 4–19.

Petrovic, J., Formosa-Jordan, P., Luna-Escalante, J.C., Abelló, G., Ibañes, M., Neves, J., and Giraldez, F. (2014). Ligand-dependent Notch signaling strength orchestrates lateral induction and lateral inhibition in the developing inner ear. Dev. Camb. Engl. *141*, 2313–2324.

Pines, M.K., Housden, B.E., Bernard, F., Bray, S.J., and Röper, K. (2010). The cytolinker Pigs is a direct target and a negative regulator of Notch signalling. Dev. Camb. Engl. *137*, 913–922.

Pirvola, U., Spencer-Dene, B., Xing-Qun, L., Kettunen, P., Thesleff, I., Fritzsch, B., Dickson, C., and Ylikoski, J. (2000). FGF/FGFR-2(IIIb) signaling is essential for inner ear morphogenesis. J. Neurosci. Off. J. Soc. Neurosci. *20*, 6125–6134.

Pirvola, U., Zhang, X., Mantela, J., Ornitz, D.M., and Ylikoski, J. (2004). Fgf9 signaling regulates inner ear morphogenesis through epithelial-mesenchymal interactions. Dev. Biol. *273*, 350–360.

Pritchard, U. (1878). The development of the organ of Corti. J. Anat. Physiol. *13*, 99.

Puligilla, C., and Kelley, M.W. (2016). Dual role for Sox2 in specification of sensory competence and regulation of Atoh1 function. Dev. Neurobiol.

Qin, Z., Wood, M., and Rosowski, J.J. (2010). Measurement of conductive hearing loss in mice. Hear. Res. *263*, 93–103.

Raj, B., and Blencowe, B.J. (2015). Alternative Splicing in the Mammalian Nervous System: Recent Insights into Mechanisms and Functional Roles. Neuron *87*, 14–27.

Rakowiecki, S., and Epstein, D.J. (2013). Divergent roles for Wnt/β-catenin signaling in epithelial maintenance and breakdown during semicircular canal formation. Development *140*, 1730–1739.

Raviv, D., Dror, A.A., and Avraham, K.B. (2010). Hearing loss: a common disorder caused by many rare alleles. Ann. N. Y. Acad. Sci. *1214*, 168–179.

Riccomagno, M.M., Martinu, L., Mulheisen, M., Wu, D.K., and Epstein, D.J. (2002). Specification of the mammalian cochlea is dependent on Sonic hedgehog. Genes Dev. *16*, 2365–2378.

Riccomagno, M.M., Takada, S., and Epstein, D.J. (2005). Wnt-dependent regulation of inner ear morphogenesis is balanced by the opposing and supporting roles of Shh. Genes Dev. *19*, 1612–1623.

Richardson, R.T., and Atkinson, P.J. (2015). Atoh1 gene therapy in the cochlea for hair cell regeneration. Expert Opin. Biol. Ther. *15*, 417–430.

Rickheit, G., Maier, H., Strenzke, N., Andreescu, C.E., De Zeeuw, C.I., Muenscher, A., Zdebik, A.A., and Jentsch, T.J. (2008). Endocochlear potential depends on Cl- channels: mechanism underlying deafness in Bartter syndrome IV. EMBO J. *27*, 2907–2917.

Robinson, M.D., McCarthy, D.J., and Smyth, G.K. (2010). edgeR: a Bioconductor package for differential expression analysis of digital gene expression data. Bioinforma. Oxf. Engl. *26*, 139–140.

Robison, P., Caporizzo, M.A., Ahmadzadeh, H., Bogush, A.I., Chen, C.Y., Margulies, K.B., Shenoy, V.B., and Prosser, B.L. (2016). Detyrosinated microtubules buckle and bear load in contracting cardiomyocytes. Science *352*, aaf0659.

Robledo, R.F., and Lufkin, T. (2006). Dlx5 and Dlx6 homeobox genes are required for specification of the mammalian vestibular apparatus. Genes. N. Y. N 2000 *44*, 425–437.

Roessler, E., Belloni, E., Gaudenz, K., Jay, P., Berta, P., Scherer, S.W., Tsui, L.C., and Muenke, M. (1996). Mutations in the human Sonic Hedgehog gene cause holoprosencephaly. Nat. Genet. *14*, 357–360.

Roessler, E., Belloni, E., Gaudenz, K., Vargas, F., Scherer, S.W., Tsui, L.C., and Muenke, M. (1997). Mutations in the C-terminal domain of Sonic Hedgehog cause holoprosencephaly. Hum. Mol. Genet. *6*, 1847–1853.

Rohatgi, R., Milenkovic, L., and Scott, M.P. (2007). Patched1 regulates hedgehog signaling at the primary cilium. Science *317*, 372–376.

Salminen, M., Meyer, B.I., Bober, E., and Gruss, P. (2000). Netrin 1 is required for semicircular canal formation in the mouse inner ear. Dev. Camb. Engl. *127*, 13–22.

Salt, A.N., Melichar, I., and Thalmann, R. (1987). Mechanisms of endocochlear potential generation by stria vascularis. The Laryngoscope *97*, 984–991.

Savoy-Burke, G., Gilels, F.A., Pan, W., Pratt, D., Que, J., Gan, L., White, P.M., and Kiernan, A.E. (2014). Activated notch causes deafness by promoting a supporting cell phenotype in developing auditory hair cells. PloS One *9*, e108160.

Schlingmann, K.P., Konrad, M., Jeck, N., Waldegger, P., Reinalter, S.C., Holder, M., Seyberth, H.W., and Waldegger, S. (2004). Salt wasting and deafness resulting from mutations in two chloride channels. N. Engl. J. Med. *350*, 1314–1319.

Schneider, C., King, R.M., and Philipson, L. (1988). Genes specifically expressed at growth arrest of mammalian cells. Cell *54*, 787–793.

Sgorbissa, A., Benetti, R., Marzinotto, S., Schneider, C., and Brancolini, C. (1999). Caspase-3 and caspase-7 but not caspase-6 cleave Gas2 in vitro: implications for microfilament reorganization during apoptosis. J. Cell Sci. *112 (Pt 23)*, 4475–4482.

Shapiro, I.M., Cheng, A.W., Flytzanis, N.C., Balsamo, M., Condeelis, J.S., Oktay, M.H., Burge, C.B., and Gertler, F.B. (2011). An EMT-driven alternative splicing program occurs in human breast cancer and modulates cellular phenotype. PLoS Genet. *7*, e1002218.

Shearer, A.E., Hildebrand, M.S., and Smith, R.J. (1993). Hereditary Hearing Loss and Deafness Overview. In GeneReviews(®), M.P. Adam, H.H. Ardinger, R.A. Pagon, S.E. Wallace, L.J. Bean, H.C. Mefford, K. Stephens, A. Amemiya, and N. Ledbetter, eds. (Seattle (WA): University of Washington, Seattle), p.

Shi, F., Kempfle, J.S., and Edge, A.S.B. (2012). Wnt-responsive Lgr5-expressing stem cells are hair cell progenitors in the cochlea. J. Neurosci. Off. J. Soc. Neurosci. *32*, 9639–9648.

Shi, F., Hu, L., and Edge, A.S.B. (2013). Generation of hair cells in neonatal mice by β-catenin overexpression in Lgr5-positive cochlear progenitors. Proc. Natl. Acad. Sci. U. S. A. *110*, 13851–13856.

Shibata, S., Miwa, T., Wu, H.-H., Levitt, P., and Ohyama, T. (2016). Hepatocyte Growth Factor-c-MET Signaling Mediates the Development of Nonsensory Structures of the Mammalian Cochlea and Hearing. J. Neurosci. Off. J. Soc. Neurosci. *36*, 8200–8209.

Shim, K., Minowada, G., Coling, D.E., and Martin, G.R. (2005). Sprouty2, a mouse deafness gene, regulates cell fate decisions in the auditory sensory epithelium by antagonizing FGF signaling. Dev. Cell *8*, 553–564.

Shpargel, K.B., Makishima, T., and Griffith, A.J. (2004). Col11a1 and Col11a2 mRNA expression in the developing mouse cochlea: implications for the correlation of hearing loss phenotype with mutant type XI collagen genotype. Acta Otolaryngol. (Stockh.) *124*, 242–248.

Siemens, J., Lillo, C., Dumont, R.A., Reynolds, A., Williams, D.S., Gillespie, P.G., and Müller, U. (2004). Cadherin 23 is a component of the tip link in hair-cell stereocilia. Nature *428*, 950–955.

Siletti, K., Tarchini, B., and Hudspeth, A.J. (2017). Daple coordinates organ-wide and cell-intrinsic polarity to pattern inner-ear hair bundles. Proc. Natl. Acad. Sci. U. S. A. *114*, E11170–E11179.

Slepecky, N.B., Henderson, C.G., and Saha, S. (1995). Post-translational modifications of tubulin suggest that dynamic microtubules are present in sensory cells and stable microtubules are present in supporting cells of the mammalian cochlea. Hear. Res. *91*, 136–147.

Sloan-Heggen, C.M., and Smith, R.J.H. (2016). Navigating genetic diagnostics in patients with hearing loss. Curr. Opin. Pediatr. *28*, 705–712.

Smith, C.A. (1957). Structure of the stria vascularis and the spiral prominence. Ann. Otol. Rhinol. Laryngol. *66*, 521–536.

Solomon, K.S., and Fritz, A. (2002). Concerted action of two dlx paralogs in sensory placode formation. Dev. Camb. Engl. *129*, 3127–3136.

Son, E.J., Wu, L., Yoon, H., Kim, S., Choi, J.Y., and Bok, J. (2012). Developmental gene expression profiling along the tonotopic axis of the mouse cochlea. PloS One *7*, e40735.

Son, E.J., Ma, J.-H., Ankamreddy, H., Shin, J.-O., Choi, J.Y., Wu, D.K., and Bok, J. (2015). Conserved role of Sonic Hedgehog in tonotopic organization of the avian basilar papilla and mammalian cochlea. Proc. Natl. Acad. Sci. U. S. A. *112*, 3746–3751.

Steel, K.P., and Barkway, C. (1989). Another role for melanocytes: their importance for normal stria vascularis development in the mammalian inner ear. Dev. Camb. Engl. *107*, 453–463.

Stehbens, S.J., Paterson, A.D., Crampton, M.S., Shewan, A.M., Ferguson, C., Akhmanova, A., Parton, R.G., and Yap, A.S. (2006). Dynamic microtubules regulate the local concentration of E-cadherin at cell-cell contacts. J. Cell Sci. *119*, 1801–1811.

St-Jacques, B., Hammerschmidt, M., and McMahon, A.P. (1999). Indian hedgehog signaling regulates proliferation and differentiation of chondrocytes and is essential for bone formation. Genes Dev. *13*, 2072–2086.

Stroud, M.J., Kammerer, R.A., and Ballestrem, C. (2011). Characterization of G2L3 (GAS2-like 3), a new microtubule- and actin-binding protein related to spectraplakins. J. Biol. Chem. *286*, 24987–24995.

Stroud, M.J., Nazgiewicz, A., McKenzie, E.A., Wang, Y., Kammerer, R.A., and Ballestrem, C. (2014). GAS2-like proteins mediate communication between microtubules and actin through interactions with end-binding proteins. J. Cell Sci. *127*, 2672–2682.

Strutt, H., Thomas, C., Nakano, Y., Stark, D., Neave, B., Taylor, A.M., and Ingham, P.W. (2001). Mutations in the sterol-sensing domain of Patched suggest a role for vesicular trafficking in Smoothened regulation. Curr. Biol. CB *11*, 608–613.

Sullivan, S.K., Mills, J.A., Koukouritaki, S.B., Vo, K.K., Lyde, R.B., Paluru, P., Zhao, G., Zhai, L., Sullivan, L.M., Wang, Y., et al. (2014). High-level transgene expression in induced pluripotent stem cell-derived megakaryocytes: correction of Glanzmann thrombasthenia. Blood *123*, 753–757.

Svärd, J., Heby-Henricson, K., Henricson, K.H., Persson-Lek, M., Rozell, B., Lauth, M., Bergström, A., Ericson, J., Toftgård, R., and Teglund, S. (2006). Genetic elimination of

Suppressor of fused reveals an essential repressor function in the mammalian Hedgehog signaling pathway. Dev. Cell *10*, 187–197.

Szarama, K.B., Gavara, N., Petralia, R.S., Kelley, M.W., and Chadwick, R.S. (2012a). Cytoskeletal changes in actin and microtubules underlie the developing surface mechanical properties of sensory and supporting cells in the mouse cochlea. Dev. Camb. Engl. *139*, 2187–2197.

Szarama, K.B., Stepanyan, R., Petralia, R.S., Gavara, N., Frolenkov, G.I., Kelley, M.W., and Chadwick, R.S. (2012b). Fibroblast growth factor receptor 3 regulates microtubule formation and cell surface mechanical properties in the developing organ of Corti. Bioarchitecture *2*, 214–219.

Tachibana, M. (2001). Cochlear melanocytes and MITF signaling. J. Investig. Dermatol. Symp. Proc. *6*, 95–98.

Tachibana, M., Hara, Y., Vyas, D., Hodgkinson, C., Fex, J., Grundfast, K., and Arnheiter, H. (1992). Cochlear disorder associated with melanocyte anomaly in mice with a transgenic insertional mutation. Mol. Cell. Neurosci. *3*, 433–445.

Taipale, J., Cooper, M.K., Maiti, T., and Beachy, P.A. (2002). Patched acts catalytically to suppress the activity of Smoothened. Nature *418*, 892–897.

Takebayashi, S., Yamamoto, N., Yabe, D., Fukuda, H., Kojima, K., Ito, J., and Honjo, T. (2007). Multiple roles of Notch signaling in cochlear development. Dev. Biol. *307*, 165–178.

Tange, T.O., Damgaard, C.K., Guth, S., Valcárcel, J., and Kjems, J. (2001). The hnRNP A1 protein regulates HIV-1 tat splicing via a novel intron silencer element. EMBO J. *20*, 5748–5758.

Tannenbaum, J., and Slepecky, N.B. (1997). Localization of microtubules containing posttranslationally modified tubulin in cochlear epithelial cells during development. Cell Motil. Cytoskeleton *38*, 146–162.

Tao, Y., Huang, M., Shu, Y., Ruprecht, A., Wang, H., Tang, Y., Vandenberghe, L.H., Wang, Q., Gao, G., Kong, W.-J., et al. (2018). Delivery of Adeno-Associated Virus Vectors in Adult Mammalian Inner-Ear Cell Subtypes Without Auditory Dysfunction. Hum. Gene Ther.

Tasaki, I., and Spyropoulos, C.S. (1959). Stria vascularis as source of endocochlear potential. J. Neurophysiol. *22*, 149–155.

Tateya, T., Imayoshi, I., Tateya, I., Ito, J., and Kageyama, R. (2011). Cooperative functions of Hes/Hey genes in auditory hair cell and supporting cell development. Dev. Biol. *352*, 329–340.

Tateya, T., Imayoshi, I., Tateya, I., Hamaguchi, K., Torii, H., Ito, J., and Kageyama, R. (2013). Hedgehog signaling regulates prosensory cell properties during the basal-to-apical wave of hair cell differentiation in the mammalian cochlea. Development *140*, 3848–3857.

Tateya, T., Sakamoto, S., Imayoshi, I., and Kageyama, R. (2015). In vivo overactivation of the Notch signaling pathway in the developing cochlear epithelium. Hear. Res. *327*, 209–217.

Taylor, R., Bullen, A., Johnson, S.L., Grimm-Günter, E.-M., Rivero, F., Marcotti, W., Forge, A., and Daudet, N. (2015). Absence of plastin 1 causes abnormal maintenance of hair cell stereocilia and a moderate form of hearing loss in mice. Hum. Mol. Genet. *24*, 37–49.

Tenzen, T., Allen, B.L., Cole, F., Kang, J.-S., Krauss, R.S., and McMahon, A.P. (2006). The cell surface membrane proteins Cdo and Boc are components and targets of the Hedgehog signaling pathway and feedback network in mice. Dev. Cell *10*, 647–656.

Thomas, T., Jordan, K., and Laird, D.W. (2001). Role of cytoskeletal elements in the recruitment of Cx43-GFP and Cx26-YFP into gap junctions. Cell Commun. Adhes. *8*, 231–236.

Tolomeo, J.A., and Holley, M.C. (1997). Mechanics of microtubule bundles in pillar cells from the inner ear. Biophys. J. *73*, 2241–2247.

Torban, E., Patenaude, A.-M., Leclerc, S., Rakowiecki, S., Gauthier, S., Andelfinger, G., Epstein, D.J., and Gros, P. (2008). Genetic interaction between members of the Vangl family causes neural tube defects in mice. Proc. Natl. Acad. Sci. U. S. A. *105*, 3449–3454.

Toyoda, S., Shiraki, N., Yamada, S., Uwabe, C., Imai, H., Matsuda, T., Yoneyama, A., Takeda, T., and Takakuwa, T. (2015). Morphogenesis of the Inner Ear at Different Stages of Normal Human Development. Anat. Rec. *298*, 2081–2090.

Traunmüller, L., Gomez, A.M., Nguyen, T.-M., and Scheiffele, P. (2016). Control of neuronal synapse specification by a highly dedicated alternative splicing program. Science *352*, 982–986.

Trotta, N., Orso, G., Rossetto, M.G., Daga, A., and Broadie, K. (2004). The hereditary spastic paraplegia gene, spastin, regulates microtubule stability to modulate synaptic structure and function. Curr. Biol. CB *14*, 1135–1147.

Trowe, M.-O., Maier, H., Petry, M., Schweizer, M., Schuster-Gossler, K., and Kispert, A. (2011). Impaired stria vascularis integrity upon loss of E-cadherin in basal cells. Dev. Biol. *359*, 95–107.

Tucker, J.B., Paton, C.C., Richardson, G.P., Mogensen, M.M., and Russell, I.J. (1992). A cell surface-associated centrosomal layer of microtubule-organizing material in the inner pillar cell of the mouse cochlea. J. Cell Sci. *102 (Pt 2)*, 215–226.

Tucker, J.B., Mogensen, M.M., Paton, C.C., Mackie, J.B., Henderson, C.G., and Leckie, L.M. (1995). Formation of two microtubule-nucleating sites which perform differently during centrosomal reorganization in a mouse cochlear epithelial cell. J. Cell Sci. *108 (Pt 4)*, 1333–1345.

Ule, J., Ule, A., Spencer, J., Williams, A., Hu, J.-S., Cline, M., Wang, H., Clark, T., Fraser, C., Ruggiu, M., et al. (2005). Nova regulates brain-specific splicing to shape the synapse. Nat. Genet. *37*, 844–852.

Urness, L.D., Paxton, C.N., Wang, X., Schoenwolf, G.C., and Mansour, S.L. (2010). FGF signaling regulates otic placode induction and refinement by controlling both ectodermal target genes and hindbrain Wnt8a. Dev. Biol. *340*, 595–604.

Urness, L.D., Wang, X., Shibata, S., Ohyama, T., and Mansour, S.L. (2015). Fgf10 is required for specification of non-sensory regions of the cochlear epithelium. Dev. Biol. *400*, 59–71.

Vaquero-Garcia, J., Barrera, A., Gazzara, M.R., González-Vallinas, J., Lahens, N.F., Hogenesch, J.B., Lynch, K.W., and Barash, Y. (2016). A new view of transcriptome complexity and regulation through the lens of local splicing variations. ELife *5*, e11752.

Vendrell, V., López-Hernández, I., Durán Alonso, M.B., Feijoo-Redondo, A., Abello, G., Gálvez, H., Giráldez, F., Lamonerie, T., and Schimmang, T. (2015). Otx2 is a target of N-myc and acts as a suppressor of sensory development in the mammalian cochlea. Dev. Camb. Engl. *142*, 2792–2800.

Venkatesh, M.D., Moorchung, N., and Puri, B. (2015). Genetics of non syndromic hearing loss. Med. J. Armed Forces India *71*, 363–368.

Vikkula, M., Mariman, E.C., Lui, V.C., Zhidkova, N.I., Tiller, G.E., Goldring, M.B., van Beersum, S.E., de Waal Malefijt, M.C., van den Hoogen, F.H., and Ropers, H.H. (1995). Autosomal dominant and recessive osteochondrodysplasias associated with the COL11A2 locus. Cell *80*, 431–437.

Vuong, C.K., Black, D.L., and Zheng, S. (2016). The neurogenetics of alternative splicing. Nat. Rev. Neurosci. *17*, 265–281.

Wallis, D., Hamblen, M., Zhou, Y., Venken, K.J.T., Schumacher, A., Grimes, H.L., Zoghbi, H.Y., Orkin, S.H., and Bellen, H.J. (2003). The zinc finger transcription factor Gfi1, implicated in lymphomagenesis, is required for inner ear hair cell differentiation and survival. Dev. Camb. Engl. *130*, 221–232.

Wang, B., Fallon, J.F., and Beachy, P.A. (2000). Hedgehog-regulated processing of Gli3 produces an anterior/posterior repressor gradient in the developing vertebrate limb. Cell *100*, 423–434.

Wang, E.T., Sandberg, R., Luo, S., Khrebtukova, I., Zhang, L., Mayr, C., Kingsmore, S.F., Schroth, G.P., and Burge, C.B. (2008). Alternative isoform regulation in human tissue transcriptomes. Nature *456*, 470–476.

Wang, J., Mark, S., Zhang, X., Qian, D., Yoo, S.-J., Radde-Gallwitz, K., Zhang, Y., Lin, X., Collazo, A., Wynshaw-Boris, A., et al. (2005). Regulation of polarized extension and planar cell polarity in the cochlea by the vertebrate PCP pathway. Nat. Genet. *37*, 980–985.

Wang, Y., Guo, N., and Nathans, J. (2006). The role of Frizzled3 and Frizzled6 in neural tube closure and in the planar polarity of inner-ear sensory hair cells. J. Neurosci. Off. J. Soc. Neurosci. *26*, 2147–2156.

Wang, Y., Ma, M., Xiao, X., and Wang, Z. (2012). Intronic splicing enhancers, cognate splicing factors and context-dependent regulation rules. Nat. Struct. Mol. Biol. *19*, 1044–1052.

Warzecha, C.C., and Carstens, R.P. (2012). Complex changes in alternative pre-mRNA splicing play a central role in the epithelial-to-mesenchymal transition (EMT). Semin. Cancer Biol. *22*, 417–427.

Warzecha, C.C., Sato, T.K., Nabet, B., Hogenesch, J.B., and Carstens, R.P. (2009a). ESRP1 and ESRP2 are epithelial cell-type-specific regulators of FGFR2 splicing. Mol. Cell *33*, 591–601.

Warzecha, C.C., Shen, S., Xing, Y., and Carstens, R.P. (2009b). The epithelial splicing factors ESRP1 and ESRP2 positively and negatively regulate diverse types of alternative splicing events. RNA Biol. *6*, 546–562.

Waterman-Storer, C.M., Salmon, W.C., and Salmon, E.D. (2000). Feedback interactions between cell-cell adherens junctions and cytoskeletal dynamics in newt lung epithelial cells. Mol. Biol. Cell *11*, 2471–2483.

Weil, D., Blanchard, S., Kaplan, J., Guilford, P., Gibson, F., Walsh, J., Mburu, P., Varela, A., Levilliers, J., and Weston, M.D. (1995). Defective myosin VIIA gene responsible for Usher syndrome type 1B. Nature *374*, 60–61.

White, P.M., Doetzlhofer, A., Lee, Y.S., Groves, A.K., and Segil, N. (2006). Mammalian cochlear supporting cells can divide and trans-differentiate into hair cells. Nature *441*, 984–987.

Woods, C., Montcouquiol, M., and Kelley, M.W. (2004). Math1 regulates development of the sensory epithelium in the mammalian cochlea. Nat. Neurosci. *7*, 1310–1318.

Wright, T.J., and Mansour, S.L. (2003). Fgf3 and Fgf10 are required for mouse otic placode induction. Dev. Camb. Engl. *130*, 3379–3390.

Wu, J.Y., and Maniatis, T. (1993). Specific interactions between proteins implicated in splice site selection and regulated alternative splicing. Cell *75*, 1061–1070.

Xia, A., Kikuchi, T., Hozawa, K., Katori, Y., and Takasaka, T. (1999). Expression of connexin 26 and Na,K-ATPase in the developing mouse cochlear lateral wall: functional implications. Brain Res. *846*, 106–111.

Xiang, M., Gan, L., Li, D., Chen, Z.Y., Zhou, L., O'Malley, B.W., Klein, W., and Nathans, J. (1997). Essential role of POU-domain factor Brn-3c in auditory and vestibular hair cell development. Proc. Natl. Acad. Sci. U. S. A. *94*, 9445–9450.

Xiao, X., Tang, J.-J., Peng, C., Wang, Y., Fu, L., Qiu, Z.-P., Xiong, Y., Yang, L.-F., Cui, H.-W., He, X.-L., et al. (2017). Cholesterol Modification of Smoothened Is Required for Hedgehog Signaling. Mol. Cell *66*, 154–162.e10.

Xiong, H.Y., Alipanahi, B., Lee, L.J., Bretschneider, H., Merico, D., Yuen, R.K.C., Hua, Y., Gueroussov, S., Najafabadi, H.S., Hughes, T.R., et al. (2015). RNA splicing. The human splicing code reveals new insights into the genetic determinants of disease. Science *347*, 1254806.

Xu, P.X., Adams, J., Peters, H., Brown, M.C., Heaney, S., and Maas, R. (1999). Eya1-deficient mice lack ears and kidneys and show abnormal apoptosis of organ primordia. Nat. Genet. *23*, 113–117.

Yang, L., O'Neill, P., Martin, K., Maass, J.C., Vassilev, V., Ladher, R., and Groves, A.K. (2013). Analysis of FGF-dependent and FGF-independent pathways in otic placode induction. PloS One *8*, e55011.

Yang, S.-M., Chen, W., Guo, W.-W., Jia, S., Sun, J.-H., Liu, H.-Z., Young, W.-Y., and He, D.Z.Z. (2012). Regeneration of stereocilia of hair cells by forced Atoh1 expression in the adult mammalian cochlea. PloS One *7*, e46355.

Yang, Y., Park, J.W., Bebee, T.W., Warzecha, C.C., Guo, Y., Shang, X., Xing, Y., and Carstens, R.P. (2016). Determination of a Comprehensive Alternative Splicing Regulatory Network and Combinatorial Regulation by Key Factors during the Epithelial-to-Mesenchymal Transition. Mol. Cell. Biol. *36*, 1704–1719.

York, J.P., Ren, Y.A., Zeng, J., Bin Zhang, null, Wang, F., Chen, R., Liu, J., Xia, X., and Zhang, P. (2016). Growth Arrest Specific 2 (GAS2) is a Critical Mediator of Germ Cell Cyst Breakdown and Folliculogenesis in Mice. Sci. Rep. *6*, 34956.

Yu, K., Herr, A.B., Waksman, G., and Ornitz, D.M. (2000). Loss of fibroblast growth factor receptor 2 ligand-binding specificity in Apert syndrome. Proc. Natl. Acad. Sci. U. S. A. *97*, 14536–14541.

Zamore, P.D., and Green, M.R. (1989). Identification, purification, and biochemical characterization of U2 small nuclear ribonucleoprotein auxiliary factor. Proc. Natl. Acad. Sci. U. S. A. *86*, 9243–9247.

Zelarayan, L.C., Vendrell, V., Alvarez, Y., Domínguez-Frutos, E., Theil, T., Alonso, M.T., Maconochie, M., and Schimmang, T. (2007). Differential requirements for FGF3, FGF8 and FGF10 during inner ear development. Dev. Biol. *308*, 379–391.

Zetes, D.E., Tolomeo, J.A., and Holley, M.C. (2012). Structure and mechanics of supporting cells in the guinea pig organ of Corti. PloS One *7*, e49338.

Zhang, F., and Jetten, A.M. (2001). Genomic structure of the gene encoding the human GLI-related, Krüppel-like zinc finger protein GLIS2. Gene *280*, 49–57.

Zhang, T., Dayanandan, B., Rouiller, I., Lawrence, E.J., and Mandato, C.A. (2011). Growth-arrest-specific protein 2 inhibits cell division in Xenopus embryos. PloS One *6*, e24698.

Zhang, X., Ibrahimi, O.A., Olsen, S.K., Umemori, H., Mohammadi, M., and Ornitz, D.M. (2006). Receptor specificity of the fibroblast growth factor family. The complete mammalian FGF family. J. Biol. Chem. *281*, 15694–15700.

Zhang, X., Chen, M.H., Wu, X., Kodani, A., Fan, J., Doan, R., Ozawa, M., Ma, J., Yoshida, N., Reiter, J.F., et al. (2016). Cell-Type-Specific Alternative Splicing Governs Cell Fate in the Developing Cerebral Cortex. Cell *166*, 1147–1162.e15.

Zhang, X.M., Ramalho-Santos, M., and McMahon, A.P. (2001). Smoothened mutants reveal redundant roles for Shh and Ihh signaling including regulation of L/R asymmetry by the mouse node. Cell *105*, 781–792.

Zheng, J.L., and Gao, W.Q. (2000). Overexpression of Math1 induces robust production of extra hair cells in postnatal rat inner ears. Nat. Neurosci. *3*, 580–586.

Zheng, J.L., Shou, J., Guillemot, F., Kageyama, R., and Gao, W.Q. (2000). Hes1 is a negative regulator of inner ear hair cell differentiation. Dev. Camb. Engl. *127*, 4551–4560.

Zheng, W., Huang, L., Wei, Z.-B., Silvius, D., Tang, B., and Xu, P.-X. (2003). The role of Six1 in mammalian auditory system development. Dev. Camb. Engl. *130*, 3989–4000.

Zhou, H.-L., and Lou, H. (2008). Repression of prespliceosome complex formation at two distinct steps by Fox-1/Fox-2 proteins. Mol. Cell. Biol. *28*, 5507–5516.

Zine, A., and de Ribaupierre, F. (2002). Notch/Notch ligands and Math1 expression patterns in the organ of Corti of wild-type and Hes1 and Hes5 mutant mice. Hear. Res. *170*, 22–31.

Zine, A., Van De Water, T.R., and de Ribaupierre, F. (2000). Notch signaling regulates the pattern of auditory hair cell differentiation in mammals. Dev. Camb. Engl. *127*, 3373–3383.

Zine, A., Aubert, A., Qiu, J., Therianos, S., Guillemot, F., Kageyama, R., and de Ribaupierre, F. (2001). Hes1 and Hes5 activities are required for the normal development of the hair cells in the mammalian inner ear. J. Neurosci. Off. J. Soc. Neurosci. *21*, 4712–4720.

Zou, D., Silvius, D., Rodrigo-Blomqvist, S., Enerbäck, S., and Xu, P.-X. (2006). Eya1 regulates the growth of otic epithelium and interacts with Pax2 during the development of all sensory areas in the inner ear. Dev. Biol. *298*, 430–441.